Modulating and Monitoring Autonomic Nerves for Glycemic Control

by

Ahmad Asif A Jiman

A dissertation submitted in partial fulfillment
of the requirements for the degree of
Doctor of Philosophy
(Biomedical Engineering)
in the University of Michigan
2020

Doctoral Committee:

        Associate Professor Tim M. Bruns, Chair
        Associate Professor Cynthia A. Chestek
        Professor Malcolm J. Low
        Professor Randy J. Seeley

Ahmad Asif A Jiman

ajiman@umich.edu

ORCID iD: 0000-0001-8832-4672

Dedication

To my loving father, Asif: Thank you for guiding me through life, and allowing me to make my own mistakes. I will always aspire to acquire a portion of your wisdom.

To my adoring mother, Safiyah: Thank you for listening to my unusual opinions, and insisting on hearing them despite my mumbling voice. I am ever so grateful for your love and care.

To my beloved wife, Asmaa: Thank you for your endless love and support. I feel blessed to be with you every day of my life.

To my grandfather, Ahmad: I remember you each time I write my name. You are truly missed.

To my children, Amer, Maryam, and their brothers and sisters: I am so lucky to have you. You will always be the joy of my life.

To my friend, David: Working closely with you for 3 years has been an absolute honor. I could not have asked for a better research partner.

To my advisor, mentor, friend, and wiser brother, Tim: Thank you for being my family away from home. Our weekly meeting is what I will miss and treasure the most in my 7 years as a graduate student. I will always look up to you.

Acknowledgements

I would like to thank my dissertation committee members, Dr. Tim Bruns, Dr. Cindy Chestek, Dr. Malcolm Low, and Dr. Randy Seeley for mentoring and guiding me throughout this long PhD journey. Thank you Dr. Seeley for entering me in the intriguing world of diabetes and obesity. You are the reason I stayed in the field, and hope to never leave. Your vast knowledge, efficient way of thinking and humbleness are forces I will always admire. Dr. Low, thank you for allowing me to build on your renal nerve study. Your detailed and deliberate thinking is astonishing. The curiosity questions you raised immensely helped shape this dissertation. I am deeply thankful for that. Dr. Chestek, your enthusiasm, optimism and insights kept me going through the dark days of the microneedle project. I would have never achieved this much without you. I am ever so grateful for your support.

I have learned a lot from my collaborators in the renal nerve project. Thank you Dr. Paul Cederna for showing me the surgical approach for this study. I am still mesmerized by your surgical skills to this day. Dr. Alfor Lewis, thank you for fully developing and teaching me the renal surgeries. The knowledge, experience and friendship that I gained from and with you will be cherished for the rest of my life. Dr. Kavaljit Chhabra, I cannot thank you enough for mentoring me in my first years as a PhD student. I truly consider you as my brother.

The Michigan Microneedle team is the most active team I've been on by far. We started meeting every two weeks but that wasn't enough, so we met every week for two and a half years, and sometimes even that wasn't enough. Thank you Dr. John Seymour for leading this project and

providing a unique perspective that made everything we did better. Dongxiao Yan, I've always believed in you to figure it out, and you always did with your deep thinking and composure. Elissa Welle is a wonderful scientist that I am very fortunate to have worked with. Dr. Paras Patel has mentored me for many years since I was a master's student and continued to do so in this project. Thank you to all the members of this exciting team that I am extremely honored to be a part of.

The pNEURO Lab has been my second home for all these years. I am very grateful to have worked with caring members in a family atmosphere. Thank you Dr. Shani Ross for the many research and life skills that you have taught me. Eric Kennedy, you were vital in the research of this dissertation and I am thankful your patience with our many mistakes. My fellow graduate student siblings, Zach Sperry, Aileen Ouyang, Lauren Zimmerman, Elizabeth Bottorff, Jessica Xu, and Lauren Madden, sharing this journey with you has been an absolute honor. Zach, you brought a unique energy to the lab and you were always enthusiastically willing to help me and others. Aileen, I will always be grateful for the great lengths that you would go to in order to help us with anything. Elizabeth, it's been interesting watching you grow and develop, and I am certain that you will be a great leader and scientist. David Ratze has been instrumental in designing, performing and analyzing most of the experiments in this dissertation. I am blessed to have known you as a friend and worked with you as a research partner. To all members of the pNEURO Lab, it has been a pleasure knowing you all and I am looking forward to hearing about your great accomplishments.

The biggest sacrifice I had to make to achieve this goal was to live away from my family. My parents, Asif and Safiyah, my grandparents, Ahmad, Hasnah, Shafeey and Fatimah, my siblings, Ammar, Omamah, Hisham, Suhaib, Fidaa, Bilal, Alhasan, Ziyad, Salman, Mohammad and Maimoonah, and my wife's family, Mohammad, Zahdah, Amani, Adel, Arwa, Haitham,

Ahmad, Amnah, Abdulaziz, Omniah, Afnan, Mawaddah, and Abdulrasheed have always supported me and I am blessed to have you all in my life. I am lucky to have had my wife and children with me throughout this long journey. Asmaa, I feel extremely blessed to share every moment of my life with you. Thank you for your endless love and support. Amer and Mayram, you sprinkle me with joy and happiness every day. I am so lucky to have you.

King Abdulaziz University has provided me with a scholarship and unique opportunity to pursue my graduate studies. Thank you Dr. Nazeeh Alothmany, Dr. Abdulhameed Alkhateeb, Dr. Ali Morfeq, Dr. Adbullah Balamash, Prof. Ubaid Al-Saggaf, Prof. Mohammad Asif Hussain and Prof. Bahattin Karagozoglu for guiding me in making difficult decisions regarding my graduate studies. Thank you Dr. Sadedine Belarbi, Yasir Elbeshir and the Saudi Arabian Cultural Mission for assisting me throughout my times as a graduate student.

Thank you Dr. Tim Bruns for being there for me in every step of the way. We both came to the University of Michigan in 2013. You were the instructor for one of my first classes in the university where I started learning from you, and I continued to learn from you since then. When I first joined the lab in 2014, you really made me feel welcome. Whether it was walking me down to lab in my first days, teaching me surgical skills right away, or continuously asking about the progress my project, you always made sure that I had everything I needed to succeed. I always felt that you were looking out for me, whether it was related to work or not, and you doing everything you can for me to have a successful defense and solid dissertation are great examples for that. Your guidance on reading papers, critical thinking, designing experiments, attending conferences, giving presentations, and writing grants and papers are extremely valuable and I will continue to use them throughout my career. Thank you Dr. Bruns for everything!

Table of Contents

List of Tables

List of Figures

xii

List of Appendices

Abstract

Diabetic patients suffer from a long-term condition that results in high blood glucose levels (hyperglycemia). Many medications for diabetes lose their glycemic control effectiveness over time and patient compliance to these medications is a major challenge. Glycemic control is a vital continuous process and is innately regulated by the endocrine and autonomic nervous systems. There is an opportunity for developing an implantable and automated treatment for diabetic patients by accurately detecting and altering neural activity in autonomic nerves. Renal nerves provide neural control for glucose reabsorption in the kidneys, and the vagus nerve conveys important glucose regulation signals to and from the liver and pancreas. This dissertation investigated stimulation of renal nerves for glycemic control, assembled an implantation procedure for neural interface arrays designed for autonomic nerves, and recorded physiological action potential signals in the vagus nerve.

In a first study, stimulation of renal nerves in anesthetized, normal rats at kilohertz frequency (33 kHz) showed a notable average increase in urine glucose excretion (+24.5%). In contrast, low frequency (5 Hz) stimulation of renal nerves showed a substantial decrease in urine glucose excretion (−40.4%). However, these responses may be associated with urine flow rate.

In a second study, kilohertz frequency stimulation (50 kHz) of renal nerves in anesthetized, diabetic rats showed a significant average decrease (-168.4%) in blood glucose concentration rate, and an increase (+18.9%) in the overall average area under the curve for urine glucose concentration, with respect to values before stimulation.

In a third study, an innovative procedure was assembled for the chronic implantation of novel intraneural MIcroneedle Nerve Arrays (MINAs) in rat vagus nerves. Two array attachment approaches (fibrin sealant and rose-bengal bonding) were investigated to secure non-wired MINAs in nerves. The fibrin sealant approach was unsuccessful in securing the MINA-nerve interface for 4- and 8-week implant durations. The rose-bengal coated MINAs were in close proximity to axons ($\leq 50 \mu m$) in 75% of 1-week and 14% of 6-week implants with no significant harm to the implanted nerves or the overall health of the rats.

In a fourth study, physiological neural activity in the vagus nerve of anesthetized rats was recorded using Carbon Fiber Microelectrode Arrays (CFMAs). Neural activity was observed on 51% of inserted functional carbon fibers, and 1-2 neural clusters were sorted on each carbon fiber with activity. The mean peak-to-peak amplitudes of the sorted clusters were 15.1-91.7 µV with SNR of 2.0-7.0. Conducting signals were detected in the afferent direction (0.7-1.0 m/sec conduction velocities) and efferent direction (0.7-8.8 m/sec). These conduction velocities are within the conduction velocity range of unmyelinated and myelinated vagus fibers. Furthermore, changes in vagal nerve activity were monitored in breathing and blood glucose modulated conditions.

This dissertation, to our knowledge, was the first to demonstrate glucose regulation benefits by stimulation of renal nerves, chronically implant intraneural arrays in rat vagus nerves, and record physiological action potential in vagus nerves using multi-channel intraneural electrodes. Future work is needed to evaluate the long-term glucose regulation benefits of stimulation of renal nerves, and assess the tissue reactivity and recording integrity of implanted intraneural electrodes in autonomic nerves. This work supports the potential development of an alternative implantable

treatment modality for diabetic patients by modulating and monitoring neural activity in autonomic nerves.

Chapter 1: Introduction

1.1 Diabetes Mellitus

Diabetes mellitus is a chronic progressive disease that requires continuous monitoring and medical care to prevent severe complications associated with the disease (American Diabetes Association 2020). Over 450 million people around the world are affected by diabetes and the global healthcare expenditure is estimated to be more than $850 billion (Cho et al. 2018). Many diabetic patients struggle with glycemic control and are in high risk of morbidity and mortality. This worldwide disease is characterized by the impairment of insulin secretion (type-1 diabetes) or defective cell response to insulin (type-2 diabetes) (World Health Organization 2016). Insulin is a hormone produced by the pancreas and has a key-like function that facilitates the transport of glucose from blood into cells. Consequently, diabetic patients suffer from a long-term condition of high blood glucose levels (hyperglycemia) (Nathan 1993). The World Health Organization reported an estimate of 1.5 million deaths in 2012 caused by diabetes and an additional 2.2 million deaths caused by high blood glucose conditions (World Health Organization 2016).

1.1.1 Type-1 Diabetes

Patients with type-1 diabetes suffer from hyperglycemia due to environmental and/or genetic factors that lead to an autoimmune response that destroys insulin-secreting β-cells in the islets of Langerhans of the pancreas (Forbes and Cooper 2013). This autoimmune response is not fully understood and patients rely on the administration of insulin for their survival. Type-1

diabetes represent 5-15% of the diabetic population (Centers for Disease Control and Prevention 2020). The incidence rate of type-1 diabetes in children is annually increasing by 3-5%, which may be influenced by environmental triggers or the rising increase of insulin resistance (Harjutsalo, Sjöberg, and Tuomilehto 2008; Taplin et al. 2005).

1.1.2   Type-2 Diabetes

Type-2 diabetes is the most common form of diabetes and comprises over 85% of the diabetic population (Centers for Disease Control and Prevention 2020). Patients with type-2 diabetes have insulin resistance, which is a defective tissue cell response to insulin. The pancreas initially increases insulin secretion to compensate this insulin resistance, but eventually the secretion of insulin declines (Forbes and Cooper 2013; Lew and Wick 2015). Although insulin resistance of skeletal muscle, liver and adipose tissue impairs the glucose metabolism process, the reduction of insulin secretion is considered the final stage leading to hyperglycemia (Forbes and Cooper 2013; Kahn et al. 1993). The concerning increase in the prevalence of type-2 diabetes is believed to be mostly influenced by environmental factors and lifestyle changes that are associated with obesity (Henry, Chilton, and Garvey 2013; Wallenius and Maleckas 2015).

1.2   Physiology of Glucose Regulation

Glucose regulation is a vital continuous process for maintaining a healthy biological state. The body tightly regulates blood glucose levels at an average concentration of 90 mg/dL, peak concentration around 165 mg/dL after meals, and minimum of 55 mg/dL after exercise or fasting (Shrayyef and Gerich 2010). Glucose is the main metabolic fuel for the brain, which cannot synthesize or store glucose more than a few minutes of supply, and therefore, requires a continuous source of glucose from the blood (Shrayyef and Gerich 2010; Yi et al. 2010). This critical regulation requires complicated coordination between the endocrine and nervous systems

2

(Shrayyef and Gerich 2010; Niijima 1989; Thorens 2011). After meal consumption (absorptive state), the level of insulin secretion from the pancreas is increased to facilitate glucose uptake, and glucose is consumed by glycolysis or stored in the liver as glycogen. In the post-absorptive state, the breakdown of glycogen in the liver (glycogenolysis) is the main source for circulating glucose. This breakdown is promoted by glucagon, which is a hormone released from α-cells of the pancreas. When glycogen is depleted (12-18 hours of fasting), glucose production (gluconeogenesis) in the liver and kidney become the main source of blood glucose (Shrayyef and Gerich 2010; Tirone and Brunicardi 2001; El Bacha, Luz, and Da Poian 2010).

The nervous system has a major role in glucose regulation. Glucose sensors are present in the hepatic portal vein, gastrointestinal tract, carotid body and oral cavity, and trigger sensory signals through parasympathetic and sympathetic afferent neurons. Glucose sensors are also found in the hindbrain and hypothalamus of the brain (Watts and Donovan 2010; Verberne, Sabetghadam, and Korim 2014; Yi et al. 2010; Berthoud 2008; Soty et al. 2017). The liver is supplied by sympathetic splanchnic nerves that originate from celiac and superior mesenteric ganglia and are connected to the spinal cord. The liver is also supplied by parasympathetic nerves from the dorsal motor nucleus of the vagus (DMV) in the brainstem. (Yi et al. 2010; Mizuno and Ueno 2017). Decreased glucose levels in the portal vein of the liver activates vagal afferent neurons, which signal for the initiation of food intake (Yi et al. 2010; Mizuno and Ueno 2017). Stimulation of the splanchnic nerves increases blood glucose and decreases glycogen content in the liver (Shimazu and Fukuda 1965), while stimulation of the vagus nerve enhances glycogen synthesis (Shimazu 1967). The pancreas is also innervated by sympathetic and parasympathetic nerves. Activation of sympathetic nerves reduces insulin secretion and increases secretion of glucagon (Verberne, Sabetghadam, and Korim 2014), while excitation of parasympathetic nerves

increases the level of plasma insulin (Ionescu et al. 1983). Although many studies suggest the importance of the nervous system in glucose regulation, the physiological signaling and specific function of the nerves is somewhat controversial and far from well understood.

1.3   Management of Diabetes Mellitus

1.3.1   Insulin Replacement Therapy

The most effective treatment for patients with diabetes is insulin replacement therapy, which was first introduced in 1922 by Banting and Best (Lew and Wick 2015). Since β-cell function is absent or near-absent in type-1 diabetes, insulin administration is critical for the survival of these patients. Insulin is administered by multiple daily injections of rapid-acting and/or long-acting insulin, or by the continuous subcutaneous infusion of insulin with a pump (American Diabetes Association 2020). Insulin therapy is usually initiated for type-2 diabetic patients when hyperglycemia is severe ($\geq$ 300 mg/dL) (American Diabetes Association 2020; Wallia and Molitch 2014). The main risk associated with insulin therapy is hypoglycemia, which is the reduction of blood glucose levels. Hypoglycemia complications include nervousness and irritability at first, and may lead to more serious consequences, such as impaired cognitive function, coma or death if not treated within a few hours (Donovan and Watts 2014; Shrayyef and Gerich 2010). Studies on insulin-treated patients showed that type-1 diabetic patients have much higher incidents of hypoglycemia (91.0-136.8 episodes/person/year) than patients with type-2 diabetes (0.2-35.3 episodes/person/year) (Elliott et al. 2016).

1.3.2   Medications for Diabetes Mellitus

Medications for diabetic management are numerous and have various mechanisms of action (Lew and Wick 2015; Grempler et al. 2012; Matthaei et al. 2009; American Diabetes Association 2020). The first recommended therapy for diabetic patients today after diet and

exercise is metformin, which reduces glucose production in the liver. Sulfonylureas and Meglitinides bind to pancreatic cells to stimulate insulin secretion, while thiazolidinediones (TZDs) increase the sensitivity of skeletal muscle and adipose tissue to insulin. Glucagon-like peptide-1 (GLP-1) receptor agonists promote insulin secretion and increase satiety signals. A recently approved medication is sodium-glucose co-transporter 2 (SGLT-2) inhibitors, which prevent the activity of SGLT-2 transporters in proximal tubules of kidneys, reducing glucose reuptake by the kidneys and increasing glucose excretion into urine.

Despite the progress of medications for diabetes, many of these medications are associated with undesirable side effects, such as diarrhea in up to 50% of patients initiating therapy with metformin, urinary tract infections with SGLT-2 inhibitors, and risk of hypoglycemia with insulin-dependent medications (Lew and Wick 2015). Furthermore, many medications lose their glycemic control effectiveness over time and the combination of therapies is necessary for a large number of patients (Blak et al. 2012; Khunti et al. 2013; American Diabetes Association 2020). Consequently, almost half of adults with diabetes in the US did not meet the recommended goals for diabetic care (Ali et al. 2013). Moreover, sustained patient adherence to these diabetic medications in a lifelong therapy is a major challenge (García-Pérez et al. 2013; Ali et al. 2013). The World Health Organization reported that adherence to long-term therapies in developed countries is around 50% and is much lower in developing countries (Sabaté 2003). Therefore, there is a crucial need for alternative diabetic therapies that overcome these pharmaceutical limitations.

1.4 Diabetic Therapies that Target the Autonomic Nervous System

The autonomic nervous system has a major role in the regulation of unconscious functions that are essential to the body, such as breathing, blood pressure regulation, immune responses, digestion, bladder function and glucose regulation, among others (McCorry 2007; Browning,

Verheijden, and Boeckxstaens 2017; de Groat, Griffiths, and Yoshimura 2015; Niijima 1989). The system is divided into the sympathetic nervous system, which controls "fight-or-flight" responses, and the parasympathetic nervous system, which regulates "rest-and-digest" functions (McCorry 2007).

1.4.1 Renal Denervation

Overactivity of renal sympathetic nerves has been linked to the pathogenesis of hypertension (Esler et al. 2012). In recent years, a global interest has emerged for catheter-based renal denervation as a potential treatment for drug-resistant hypertension patients (Pan, Guo, and Teng 2015; Bhatt et al. 2014). Early renal denervation clinical trials showed significant blood pressure improvements (Esler et al. 2010; Krum et al. 2009). Interestingly, renal denervation also showed a significant decrease in blood glucose levels in pilot studies (Mahfoud et al. 2011; Witkowski et al. 2011). Renal denervation studies on animals align with the observed blood glucose control improvements reported in clinical trials (Rafiq et al. 2015; Iyer et al. 2016). However, a large, randomized, single-blinded, and sham-controlled clinical trial did not show significant improvements in blood pressure between treated and control patients (Bhatt et al. 2014). Furthermore, more recent studies did not show significant improvements in glucose regulation (Verloop et al. 2015; Matous et al. 2015).

1.4.2 Bioelectronic Medicine

An emerging class of therapies that rely on targeted detection and modulation of neural activity in autonomic nerves is bioelectronic medicine (Tracey 2014; Birmingham et al. 2014; Pavlov and Tracey 2019). A variety of bioelectronic medicine applications target the vagus nerve, which innervates many critical visceral organs (e.g. heart, lungs, stomach, liver, pancreas and intestines) (Agostoni et al. 1957; Andrews 1986). Clinical studies on vagus nerve stimulation

(VNS) have shown improvements in patients with epilepsy (Ben-Menachem 2002), stroke (Dawson et al. 2016), depression (Spindler et al. 2019), rheumatoid arthritis (Koopman et al. 2016) and impaired glucose tolerance (Huang et al. 2016). Vagal nerve block (vBloc) therapy was approved in 2015 by the Food and Drug Administration (FDA) for certain patients with morbid obesity (Ikramuddin et al. 2014). Interestingly, clinical trials on vBloc therapy reported improvements in blood glucose control for patients with obesity and type-2 diabetes (Shikora et al. 2013) but were not sustained after 24 months (Shikora et al. 2015).

1.4.2.1 Renal Nerves

Renal nerves are predominantly efferent sympathetic nerves that form axonal junctions on renal arterioles, juxtaglomerular renin-secreting cells and epithelial cells of proximal tubules, the glucose reabsorption region in the kidney nephron (Gattone, Marfurt, and Dallie 1986; Luff et al. 1992; Muller and Barajas 1972; DeFronzo, Davidson, and Del Prato 2012). A recent study reported that mutant (neuronal POMC-deficient) mice showed improved capability for tolerating high blood glucose levels by exaggerating urine glucose excretion (glycosuria) compared to wild-type mice at similar induced blood glucose concentrations (Chhabra et al. 2016). A following study determined that the observed glycosuria and improved glucose tolerance were a result of reduced activity in renal sympathetic nerves (Chhabra et al. 2017). Therefore, a treatment that reduces renal nerve activity may provide glycemic control benefits for diabetic patients.

1.4.2.2 The Vagus Nerve

The vagus nerve is a main parasympathetic nerve that innervates many visceral organs, such as the heart, lungs, stomach, intestines liver and pancreas (Agostoni et al. 1957; Andrews 1986), and contributes in the regulation of numerous autonomic functions, which include breathing, immune responses, digestion, and glucose regulation, among others (Berthoud and

Neuhuber 2000; Borovikova et al. 2000; Browning, Verheijden, and Boeckxstaens 2017; Berthoud 2008; Waise, Dranse, and Lam 2018). The fibers in the vagus nerve predominantly convey afferent (sensory) signals from the innervated organs to the central nervous system (Foley and DuBois 1937). The vagus nerve conveys important neural signals for glucose regulation. Neural signals in the hepatic branch of the vagus nerve are important in the regulation of glucose uptake, storage and production in the liver (Matsuhisa et al. 2000; López-Soldado et al. 2017; Masi, Valdés-Ferrer, and Steinberg 2018). Neurons that originate in the dorsal motor nucleus of the vagus (DMV) were found to innervate the pancreas (Jansen, Hoffman, and Loewy 1997), and excitation of these neurons increased the level of plasma insulin (Ionescu et al. 1983). Hence, the vagus nerve is a potential nerve target for the development of an effective bioelectronic medicine for diabetic patients by monitoring and controlling glucose regulation signals.

1.5 Opportunity for Bioelectronic Medicine for Diabetic Patients

Although clinical trials on VNS therapies have shown improvements in glucose regulation (Shikora et al. 2015; Huang et al. 2016), to our knowledge, no clinical studies have investigated organ-targeted bioelectronic medicine as a treatment approach for diabetes. Furthermore, bioelectronic medicine stimulation patterns are generally selected by experimenting with different parameters without monitoring the physiological signaling in the nerve. Recording neural activity from autonomic nerves is very challenging due to the small nature of these nerves and the low-amplitude waveforms generated from unmyelinated C-fibers that dominate autonomic nerves (Jones 1937; DiBona, Sawin, and Jones 1996). Another difficult challenge is the chronic implantation of intraneural electrodes that penetrate a nerve, and maintaining recording sites closely to axons for high-fidelity long-term recordings while enduring the foreign body response (de la Oliva, Navarro, and del Valle 2018; Wurth et al. 2017).

Bioelectronic medicine therapies are becoming more accepted by patients and healthcare practitioners due to their effectiveness, reversibility and automation of treatment (Johnson 2014; Kumar et al. 2007). Developing a bioelectronic medicine for diabetic patients that can accurately detect and alter neural signals for effective glycemic control will assist patients overcome therapeutic limitations with current medications. The renal and vagus nerves are potential targets for this bioelectronic medicine treatment. Effective glycemic control will help diabetic patients avoid complications associated with the disease, such as blindness, cardiovascular events, kidney failure and limb amputations (World Health Organization 2016; Inzucchi et al. 2012).

1.6   Research Specific Aims

Diabetic medications are critical for the treatment of current patients with diabetes (American Diabetes Association 2020). However, many patients fail to achieve the recommended glycemic control goals (Hoerger, Segel, and Gregg 2008) and sustained patient adherence to these medications in a continuing therapy is an ongoing major challenge (García-Pérez et al. 2013). Our long-term goal is to develop a reversible, automated and effective treatment that will assist patients and healthcare providers in the commitment of a lifelong therapy for diabetes. The objective of this dissertation is to demonstrate bioelectronic medicine as a potential treatment approach for diabetic patients. We hypothesized that alteration of renal nerve activity by electrical stimulation would regulate blood glucose levels, and newly developed intraneural electrodes would cause minimal tissue damage and obtain high-fidelity physiological recordings in autonomic nerves. The Specific Aims of this dissertation are:

1.6.1 Determine Effective Stimulation Parameters for the Modulation of Urine Glucose by Stimulation of Renal Nerves in Normal Rats

In this aim study, we stimulated renal nerves at kilohertz frequencies (1-50 kHz) or low frequencies (2-5 Hz), and observed the response on urine glucose excretion and urine flow rate. We hypothesized that stimulation of renal nerves at kilohertz frequencies, which can block propagation of action potentials, would increase urine glucose excretion. Conversely, we hypothesized that low frequency stimulation, which has been shown to increase renal nerve activity, would decrease urine glucose excretion. Our experimental results showed that stimulation of renal nerves may modulate urine glucose excretion, however, this response may be associated with urine flow rate. This aim is covered in Chapter 2 and has been published (Jiman et al. 2018).

1.6.2 Evaluate Impact of Kilohertz Frequency Stimulation of Renal Nerves on Blood Glucose Concentration in Diabetic Rats

In this research, we hypothesized that kilohertz frequency stimulation of renal nerves would reduce blood glucose concentration levels in diabetic animals by increasing urinary glucose excretion. We applied bilateral kilohertz frequency stimulation (50 kHz) of renal nerves in diabetic streptozotocin (STZ)-induced rats. Our results showed that kilohertz frequency stimulation of renal nerves is a possible approach for the modulation of blood glucose concentration and may introduce an alternative treatment modality for glycemic control in patients with diabetes. This research aim is covered in Chapter 3 and has been published (Jiman et al. 2019).

1.6.3 Develop Surgical Procedure for the Chronic Implantation of Microneedle Nerve Arrays in Rat Vagus Nerves

We assembled an innovative chronic implantation procedure for novel intraneural MIcroneedle Nerve Arrays (MINAs). We investigated two array attachment approaches (fibrin

sealant and rose-bengal bonding) to secure non-wired MINAs in rat vagus nerves. We assessed the approaches by determining the proximity of the MINA to the nerve and evaluated the nerve condition by electrophysiology testing. Our results suggest that a future functional rose bengal-bonded MINA will have excellent promise for yielding high-fidelity neural signals through one week of implant and may provide novel insights in neural signaling of autonomic nerves. This aim is covered in Chapter 4 and is in the process for submission as a publication.

1.6.4 Demonstrate Intraneural Recordings in Rat Vagus Nerves Using Carbon Fiber Microelectrode Arrays

We hypothesized that Carbon Fiber Microelectrode Arrays (CFMAs), which have shown excellent intracortical recordings with minimal impact on neural tissue, would obtain intraneural physiological recordings in an autonomic nerve. We inserted CFMA in rat cervical vagus nerves, recorded physiological neural activity on multiple channels in spontaneous and triggered conditions, and determined propagation direction and conduction velocity of vagal signals. Our experiments demonstrated CFMA as a viable multi-channel intraneural electrode for recording neural activity in an autonomic nerve. This work is a milestone towards the comprehensive understanding of physiological signaling in autonomic nerves, which may lead to the development of innovative treatment modalities for restoring autonomic regulatory functions. This specific aim is covered in Chapter 5 and is in preparation for publication.

These specific aims, to our knowledge, were the first to demonstrate stimulation of renal nerves as a potential treatment modality for glycemic control, assemble a chronic implantation procedure for novel intraneural arrays in small autonomic nerves and record physiological signals in vagus nerves using multi-channel intraneural arrays. Future work is needed to evaluate the long-term glycemic control benefits of stimulation of renal nerves, and assess the tissue reactivity and

recording integrity of implanted intraneural arrays in small autonomic nerves. The development of a reversible, automated and effective treatment for glycemic control will assist many patients suffering from diabetes in the commitment of a lifelong therapy. The findings of all the specific aims, impact on the field and future directions are summarized in Chapter 6.

Chapter 2: Electrical Stimulation of Renal Nerves for Modulating Urine Glucose Excretion in Rats

2.1   Abstract

The role of the kidney in glucose homeostasis has gained global interest. Kidneys are innervated by renal nerves, and renal denervation animal models have shown improved glucose regulation. We hypothesized that stimulation of renal nerves at kilohertz frequencies, which can block propagation of action potentials, would increase urine glucose excretion. Conversely, we hypothesized that low frequency stimulation, which has been shown to increase renal nerve activity, would decrease urine glucose excretion.

We performed non-survival experiments on male rats under thiobutabarbital anesthesia. A cuff electrode was placed around the left renal artery, encircling the renal nerves. Ureters were cannulated bilaterally to obtain urine samples from each kidney independently for comparison. Renal nerves were stimulated at kilohertz frequencies (1-50 kHz) or low frequencies (2-5 Hz), with intravenous administration of a glucose bolus shortly into the 25-40-minute stimulation

period. Urine samples were collected at 5-10-minute intervals, and colorimetric assays were used to quantify glucose excretion and concentration between stimulated and non-stimulated kidneys. A Kruskal-Wallis test was performed across all stimulation frequencies ($\alpha = 0.05$), followed by a post-hoc Wilcoxon rank sum test with Bonferroni correction ($\alpha = 0.005$).

For kilohertz frequency trials, the stimulated kidney yielded a higher average total urine glucose excretion at 33 kHz (+24.5%; n=9) than 1 kHz (-5.9%; n=6) and 50 kHz (+2.3%; n=14). In low frequency stimulation trials, 5 Hz stimulation led to a lower average total urine glucose excretion (-40.4%; n=6) than 2 Hz (-27.2%; n=5). The average total urine glucose excretion between 33 kHz and 5 Hz was statistically significant ($p < 0.005$). Similar outcomes were observed for urine flow rate, which may suggest an associated response. No trends or statistical significance were observed for urine glucose concentrations.

To our knowledge, this is the first study to investigate electrical stimulation of renal nerves to modulate urine glucose excretion. Our experimental results show that stimulation of renal nerves may modulate urine glucose excretion, however, this response may be associated with urine flow rate. Future work is needed to examine the underlying mechanisms and identify approaches for enhancing regulation of glucose excretion.

2.2   Introduction

Diabetes mellitus is a chronic progressive disease that requires continuous monitoring and medical care to prevent the development of severe complications (American Diabetes Association (ADA) 2018). Medications for diabetic management are numerous and have different mechanisms of action (Chatterjee and Davies 2015). Recently, sodium-glucose co-transporter 2 (SGLT-2) inhibitors were approved by the US Food and Drug Administration (FDA) for patients with type 2 diabetes. SGLT-2 inhibitors prevent the activity of SGLT-2 transporters in the renal proximal

tubule, thereby reducing glucose reuptake by the kidneys and increasing glucose excretion into urine (Lew and Wick 2015). Despite the progress in the development of diabetic medications, many lose their effectiveness over time, which makes achieving blood glucose control targets difficult for many diabetic patients (Blak et al. 2012; Khunti et al. 2013; Ali et al. 2013). Furthermore, sustained patient adherence to these diabetic medications in a lifelong therapy is a major challenge (García-Pérez et al. 2013; Sabaté 2003). Therefore, there is a crucial need for alternative diabetic therapies that overcome these pharmaceutical limitations.

In recent years, a global interest has emerged for catheter-based renal denervation as a potential treatment for drug-resistant hypertension (Pan, Guo, and Teng 2015; Bhatt et al. 2014). Early clinical trials of renal denervation showed significant blood pressure improvements (Esler et al. 2010; Krum et al. 2009). Interestingly, renal denervation was also associated with significant decreases in blood glucose levels (Mahfoud et al. 2011; Witkowski et al. 2011). Renal denervation studies in animals align with the observed blood glucose control improvements reported in clinical trials (Rafiq et al. 2015; Iyer et al. 2016). Furthermore, a recent study reported that mutant (neuronal POMC-deficient) mice showed improved capability for tolerating high blood glucose levels by exaggerating urine glucose excretion (glycosuria) compared to wild-type mice at similar induced blood glucose concentrations (Chhabra et al. 2016). A following study determined that the observed glycosuria and improved glucose tolerance were a result of reduced activity in renal sympathetic nerves (Chhabra et al. 2017). A non-pharmaceutical and reversible approach that has emerged in recent years for reducing nerve activity is kilohertz frequency stimulation, which has demonstrated nerve conduction block on multiple types of nerves (Kilgore and Bhadra 2014; Joseph and Butera 2009; 2011). We hypothesized that kilohertz frequency stimulation (1-50 kHz) on renal nerves would attain similar results to renal denervation and induce urine glucose

excretion.

Several studies have successfully influenced renal nerve activity in humans and animals by applying electrical stimulation. Electrical stimulation of renal nerves with an intra-arterial catheter electrode demonstrated increased blood pressure, and was considered as a method for locating suitable renal denervation targets for the treatment of drug-resistant hypertensive patients (Chinushi et al. 2013; Madhavan et al. 2014; Gal et al. 2015). Direct stimulation of renal nerves in rats using wire hook electrodes at low frequencies (0.5-10 Hz) showed increased renin secretion and water reabsorption, and decreased renal blood flow and sodium excretion responses (DiBona and Kopp 1997; DiBona and Sawin 1982; Bello-Reuss, Trevino, and Gottschalk 1976; Hermansson et al. 1981; Van Vliet, Smith, and Guyton 1991). Sodium and glucose reabsorption are partially associated due to the presence of sodium-glucose co-transporters (SGLTs) in the renal proximal tubule (Mather and Pollock 2011). Our hypothesis was that direct stimulation of renal nerves at low frequencies (0.5-10 Hz) would decrease urine glucose excretion.

Therapies that directly alter neural activity (neuromodulation) are commonly prescribed as treatments for a variety of conditions (Krames, Peckham, and Rezai 2009; Famm et al. 2013). Gastric electrical stimulation is used to help patients with delayed stomach-emptying of solid foods (gastroparesis), which is commonly observed in patients with diabetes (Abell et al. 2003). Vagal nerve block (vBloc) therapy was recently approved by the FDA for certain patients with morbid obesity (Apovian et al. 2017). Clinical trials on vBloc therapy reported improvements in blood glucose control for patients with obesity and type 2 diabetes but were not sustained after 24 months (Herrera et al. 2017). Despite the success of neuromodulation therapies, to our knowledge, no clinical studies have investigated organ-targeted neuromodulation as a treatment approach for diabetes. In this study, we investigated modulation of urine glucose excretion with kilohertz and

low frequency stimulation on renal nerves.

2.3 Methods

All experimental procedures were approved by the University of Michigan Institutional Animal Care and Use Committee (IACUC).

2.3.1 Animals and Housing

Rats have a similar urinary system to humans and rat renal nerves have been visualized by several research groups (Stocker and Muntzel 2013; Miki, Kosho, and Hayashida 2002). Non-survival, anesthetized experiments were performed on 24 male 290-550 g Long-Evans and Sprague-Dawley rats (Charles Rivers Laboratories, Wilmington, MA, USA). All animals were housed in ventilated cages under controlled temperature, humidity and photoperiod (12-h light/dark cycle). The animals were provided with laboratory chow (5L0D, LabDiet, St. Louis, MO, USA) and tap water ad libitum.

2.3.2 Experimental Preparation

For anesthesia, a single dose of thiobutabarbital sodium salt hydrate (Inactin, T133-1G, Sigma-Aldrich Corp., St. Louis, MO, USA) was injected intraperitoneally (110 mg/kg BW). Thiobutabarbital is commonly used in renal studies and is known to preserve renal function during anesthesia (Walter, Zewde, and Shirley 1989; Sohtell, Karlmark, and Ulfendahl 1983). Rats were placed on a heating pad (ReptiTherm, Zoo Med Laboratories Inc., San Luis Obispo, CA, USA) and temperature was monitored through a rectal temperature sensor (SurgiVet, Smiths Medical, Norwell, MA, USA). Under a dissection microscope (Lynx EVO, Vision Engineering Inc., New Milford, CT, USA), a midline cervical incision was made and the jugular vein was cannulated with polyethylene tubing (BTPE-50, Instech Laboratories Inc., Plymouth Meeting, PA, USA). Through

the jugular vein, 0.9% NaCl (saline), equivalent to 10% body weight, was infused over 30 minutes, and then followed by a continuous infusion of 0.2 mL/min using a syringe pump (NE-1000, New Era Pump Systems Inc., Farmingdale, NY, USA) (Bello-Reuss, Trevino, and Gottschalk 1976). A tracheotomy was performed to ensure a clear airway. Ureters were cannulated bilaterally with polyethylene tubing (BTPE-10, Instech Laboratories Inc., Plymouth Meeting, PA, USA) to obtain urine samples from each kidney independently. The left kidney was exposed through a midline abdominal incision. Fat and connective tissue surrounding the kidney were separated using cotton-tipped applicators to further expose the kidney and renal artery. A bipolar nerve cuff electrode (1.00 mm inner-diameter, 100 µm platinum contacts, Microprobes for Life Science, Gaithersburg, MD, USA) was placed around the renal artery, encircling renal nerves that run along the artery (Miki, Kosho, and Hayashida 2002; Stocker and Muntzel 2013). Care was taken not to damage the renal nerve branches and not to occlude blood flow in the renal artery. To ensure that the renal nerves were intact, biphasic stimulation pulses at 10 Hz, 10 V were applied for approximately 1 minute through the nerve cuff electrode. This resulted in temporary kidney ischemia, which was confirmed by the observation of kidney surface blanching (Hermansson et al. 1981). This stimulation-driven ischemia occurred in all the experiments in which we performed the test (n=18). Prior to implant, electrode impedance measurements (4.77 ± 1.53 kΩ) were taken using an impedance tester (nanoZ, White Matter LLC, Seattle, WA, USA) at 1 kHz in saline to confirm functionality of the nerve cuff electrode.

2.3.3   Electrical Stimulation

The nerve cuff electrode placed on the renal nerves was connected to an isolated pulse stimulator (Model 4100, A-M Systems, Loop Sequim, WA, USA). For kilohertz frequency stimulation, a function generator (33220A, Agilent Technologies, Santa Clara, CA, USA) was

connected to the isolated pulse stimulator to generate sinusoidal waveforms at 1, 33 or 50 kHz. The stimulation amplitude was fixed at 15 V, which has been shown to provide nerve conduction block for all selected frequencies on unmyelinated nerves (Joseph and Butera 2009; 2011). For low frequency stimulation, the isolated pulse stimulator generated biphasic pulses at 2 or 5 Hz. The stimulation amplitude and pulse width was fixed at 10 V and 0.5 msec, respectively, which is above the activation threshold for rat C-fibers using cuff electrodes (Woodbury and Woodbury 1990). The stimulation frequencies were randomly ordered between trials across all experiments to mitigate sequential effects.

2.3.4 Experimental Protocol

After completion of surgery, a stabilization period of 10-60 minutes was provided. In each experiment, 1-3 trials with different stimulation frequencies were applied on the nerve cuff electrode. Stimulation was applied at the start of a trial and remained on for 25-40 minutes. To elevate blood glucose levels beyond the expected renal threshold for glucose excretion (400 mg/dL) (Liang et al. 2012), a 0.30-1.00 g bolus dose of glucose (50% Dextrose Injection USP, Hospira Inc., Lake Forest, IL, USA) was delivered through the jugular vein at 2-16 minutes into each trial. To confirm blood glucose increase and to monitor blood glucose levels over time, drops of blood (< 0.1 mL) from a tail cut were used to obtain blood glucose concentration measurements using a glucometer (AlphaTRAK 2, Abbott, Abbott Park, IL, USA) before glucose infusion and every 5-10 minutes after glucose infusion. Urine samples from each kidney were collected in pre-weighed sampling tubes (3448, Thermo Fisher Scientific, Waltham, WA, USA) at 5-10-minute intervals. Ten minutes after the end of a trial, blood glucose measurements were expected to be around baseline levels. If not, a longer washout period was provided to the rat before proceeding to the next experimental trial. The collected urine samples were weighed on a scale (AE 160,

Mettler Toledo, Columbus, OH, USA) for volume estimations (1 μL/mg). Urine glucose

concentrations were measured using colorimetric assays (10009582, Cayman Chemical, Ann

Arbor, MI, USA). The experimental setup and protocol timeline are summarized in Figure 2.1.
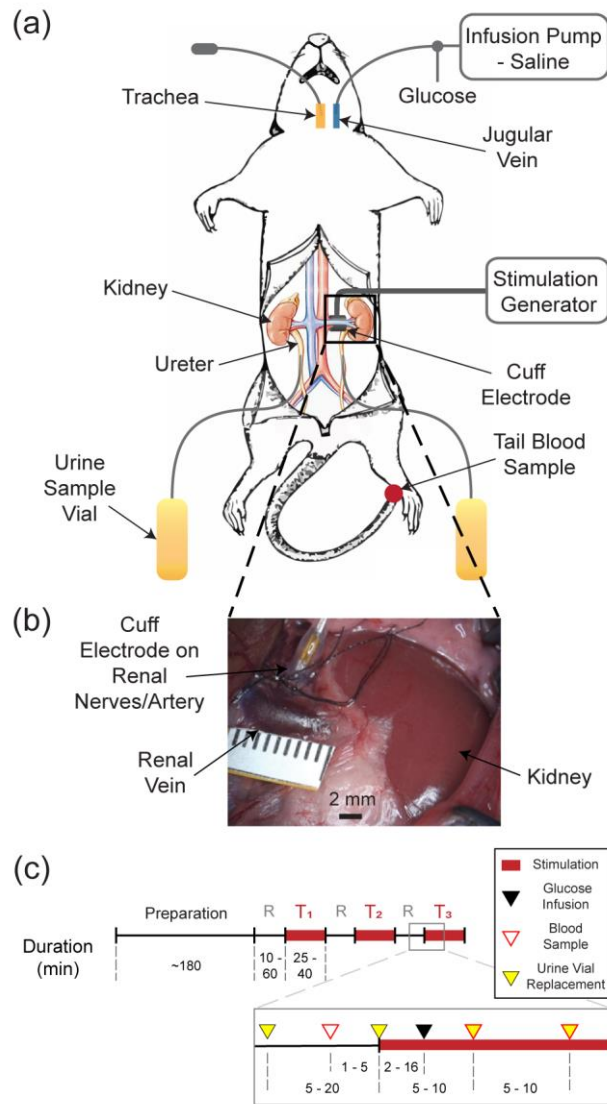
Figure 2.1 Experimental setup diagram and protocol timeline. (a) Experimental setup: Jugular vein was cannulated for saline and glucose infusion. Nerve cuff electrode was placed on renal nerves of the left kidney and connected to a stimulation generator. Ureters were cannulated bilaterally, and urine samples were collected in sampling vials. (b) Nerve cuff electrode was placed around the renal artery, encapsulating the renal nerve branches that run along the renal artery. (c) Timeline for experimental protocol: Each experiment consisted of 1-3 stimulation trials (T1-T3), with a rest period (R) before each trial. A glucose bolus was infused in each trial. Blood glucose measurements and urine samples were obtained periodically throughout the trials.

From the urine sample volumes and glucose concentration measurements, the total urine glucose excretion (UGE) was calculated and compared between the stimulated and non-stimulated kidney [$\Delta UGE = (UGE_{stimulated} - UGE_{non\text{-}stimulated})/UGE_{non\text{-}stimulated} \times 100$] for each trial. For urine glucose concentration (UGC) and urine flow rate (UFR), the area under the curve (AUC) was calculated for each trial by trapezoidal numerical integration and compared between the kidneys in a similar manner as UGE. From blood glucose concentration (BGC) values, a BGC decrease rate (BGCDR) was obtained by calculating the linear regression slope of BGC values starting approximately 10 minutes after the glucose bolus infusion and ending with the final value in the trial. The glucometer was unable to read blood glucose concentrations above 750 mg/dL, which occasionally occurred during the first 10 minutes after a glucose bolus infusion. Therefore, BGC values within 10 minutes after a glucose bolus infusion were excluded in BGCDR calculations for all stimulation trials.

2.3.5 Statistical Analysis

Across all experiments, data sets did not follow a normal distribution (confirmed by one-sample Kolmogorov-Smirnov test). Therefore, a non-parametric Kruskal-Wallis test was performed to measure statistical significance across stimulation frequencies. Statistical significance was considered at $p < 0.05$. A two-sided Wilcoxon rank sum test was then applied between pairs of stimulation frequencies. The significance level (α) was adjusted according to a Bonferroni correction, where α was divided by the number of stimulation pairs (10). Thus, statistical significance for the Wilcoxon rank sum test was considered at $p < 0.005$. All data analysis and statistical tests were performed using MATLAB software (R2014b, MathWorks, Natick, MA, USA).

2.4 Results

Across the 24 experiments on male rats, we performed stimulation trials at kilohertz frequencies (1 kHz [n = 6], 33 kHz [n = 9] and 50 kHz [n = 14]) and low frequencies (2 Hz [n = 5] and 5 Hz [n = 6]). We obtained measurements of urine glucose excretion, urine glucose concentration, urine flow rate, and blood glucose concentration in each trial.

2.4.1 Urine Glucose Excretion

Glucose excretion was analyzed and compared between the urine samples obtained from the stimulated and non-stimulated kidneys. The percentage difference of urine glucose excretion (ΔUGE) between the stimulated and non-stimulated kidneys for all stimulation frequencies are shown in Figure 2.2a. Overall, stimulation frequency had a statistically significant effect on ΔUGE (Kruskal-Wallis test, $p < 0.05$). In kilohertz frequency trials, 33 kHz yielded a higher average ΔUGE (+24.5%; n = 9) than 1 kHz (-5.9%; n = 6) and 50 kHz (+2.3%; n = 14). In low frequency trials, 5 Hz stimulation led to a lower average ΔUGE (-40.4%; n = 6) than 2 Hz (-27.2%; n = 5). Statistical significance only occurred between the ΔUGE of 33 kHz and 5 Hz trials (Wilcoxon rank sum test, $p < 0.005$). Stimulation at kilohertz frequencies met our hypothesis of increased UGE in 14 trials (48.2%), had no apparent effect (|ΔUGE| < 5%) in 10 trials (34.5%), and showed a decrease in UGE in 5 trials (17.2%) out of the 29 total kilohertz frequency trials. In low frequency stimulation trials, we observed a decrease of UGE in 9 trials (81.8%), no apparent effect in 1 trial (9.1%), and an increase of UGE in 1 trial (9.1%) out of 11 trials in total. Examples of stimulation trials at 33 kHz that displayed an increase, no apparent effect, or a decrease in UGE are shown in Figure 2.2b-d.
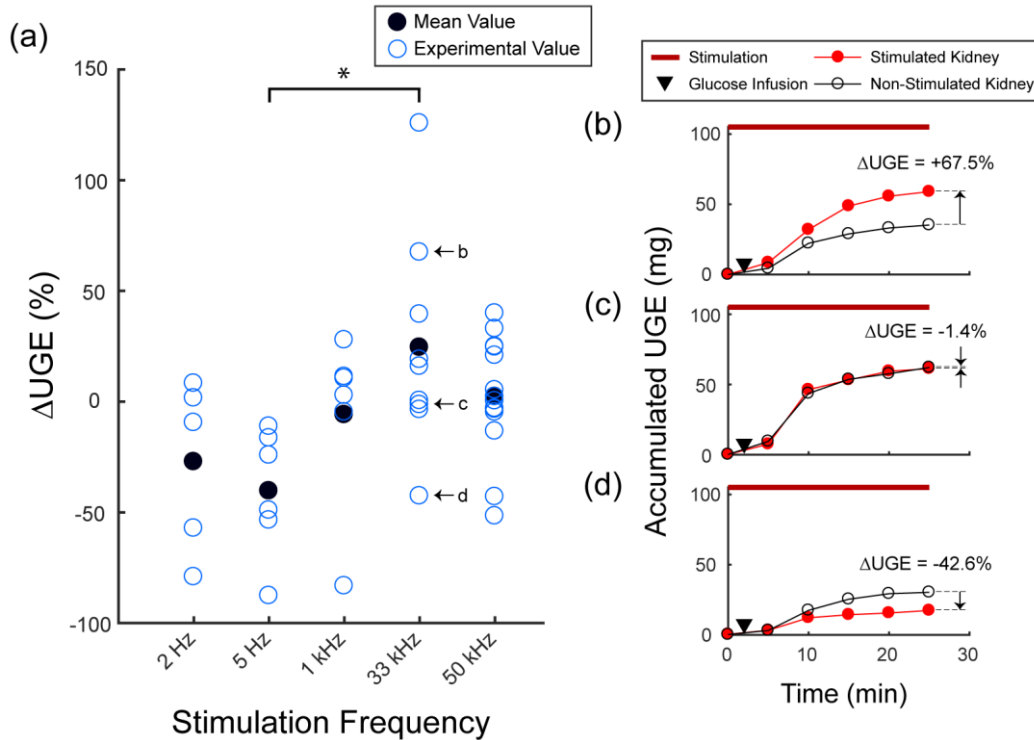
Figure 2.2 Changes in urine glucose excretion. (a) The percentage difference in urine glucose excretion between the stimulated and non-stimulated kidney (ΔUGE) at the applied stimulation frequencies. Stimulation frequency had a statistically significant main effect (Kruskal-Wallis test, $p < 0.05$), with one within-frequency comparison being significant (5 Hz and 33 kHz; post-hoc Wilcoxon rank sum test, $* = p < 0.005$). (b) Representative stimulation trial at 33 kHz that showed an increase in UGE. (c) Representative stimulation trial at 33 kHz that showed no apparent effect on UGE. (d) Representative stimulation trial at 33 kHz that showed a decrease in UGE.

2.4.2 Urine Glucose Concentration

The urine glucose concentration (UGC) differences between the urine samples obtained from the stimulated and non-stimulated kidneys at all stimulation frequencies are shown in Figure 2.3a. The average UGC difference was +5.9% at 2 Hz (n = 5), +12.6% at 5 Hz (n = 6), +3.7% at 1 kHz (n = 6), +3.7% at 33 kHz (n = 9), and -6.2% at 50 kHz (n = 14). Stimulation frequency did not have an overall significant effect on UGC (Kruskal-Wallis test, $p = 0.2365$).
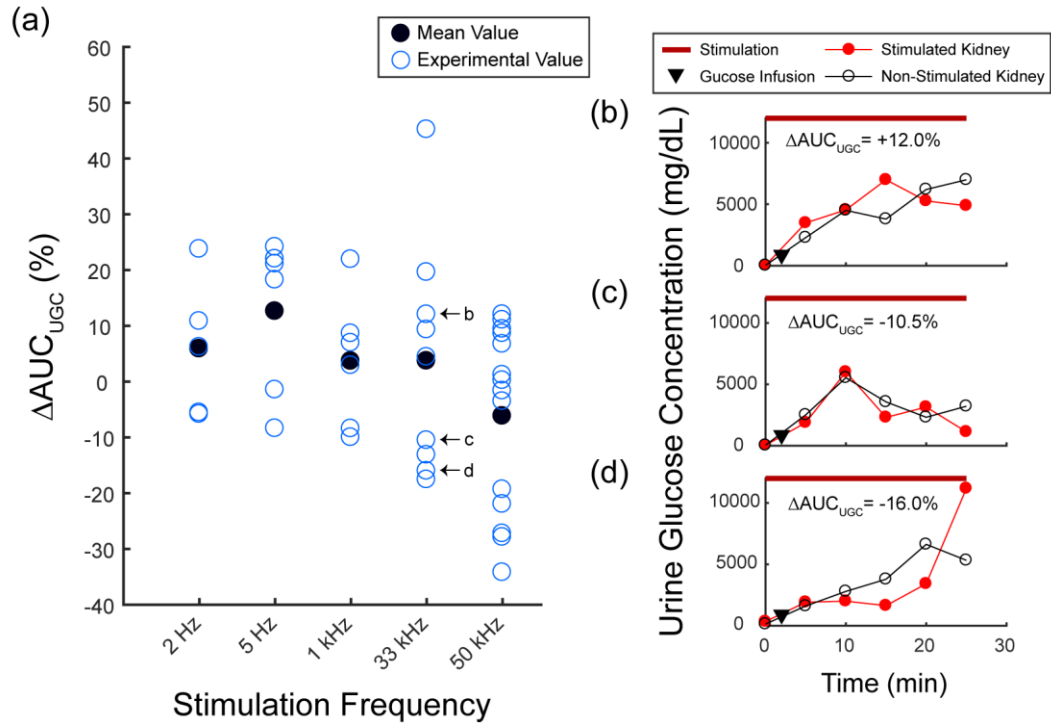
Figure 2.3 Changes in urine glucose concentration. (a) The percentage difference between the area under the curve for urine glucose concentration of the stimulated and non-stimulated kidney (ΔAUC_{UGC}) at the applied stimulation frequencies. (b) Urine glucose concentration (UGC) measurements for the trial shown in Figure 2.2b. (c) UGC measurements for the trial shown in Figure 2.2c. (d) UGC measurements for the trial shown in Figure 2.2d.

2.4.3   Urine Flow Rate

The urine flow rate (UFR) differences between the urine samples obtained from the stimulated and non-stimulated kidneys at all stimulation frequencies are shown in Figure 2.4a. The average UFR difference was -27.7% at 2 Hz (n = 5), -40.6% at 5 Hz (n = 6), -6.0% at 1 kHz (n = 6), +14.6% at 33 kHz (n = 9), and +9.8% at 50 kHz (n = 14). Stimulation frequency had a statistically significant main effect on UFR (Kruskal-Wallis test, $p < 0.05$), with trials at 33 kHz and 5 Hz significantly different from one another (post-hoc Wilcoxon rank sum test, $p < 0.005$).
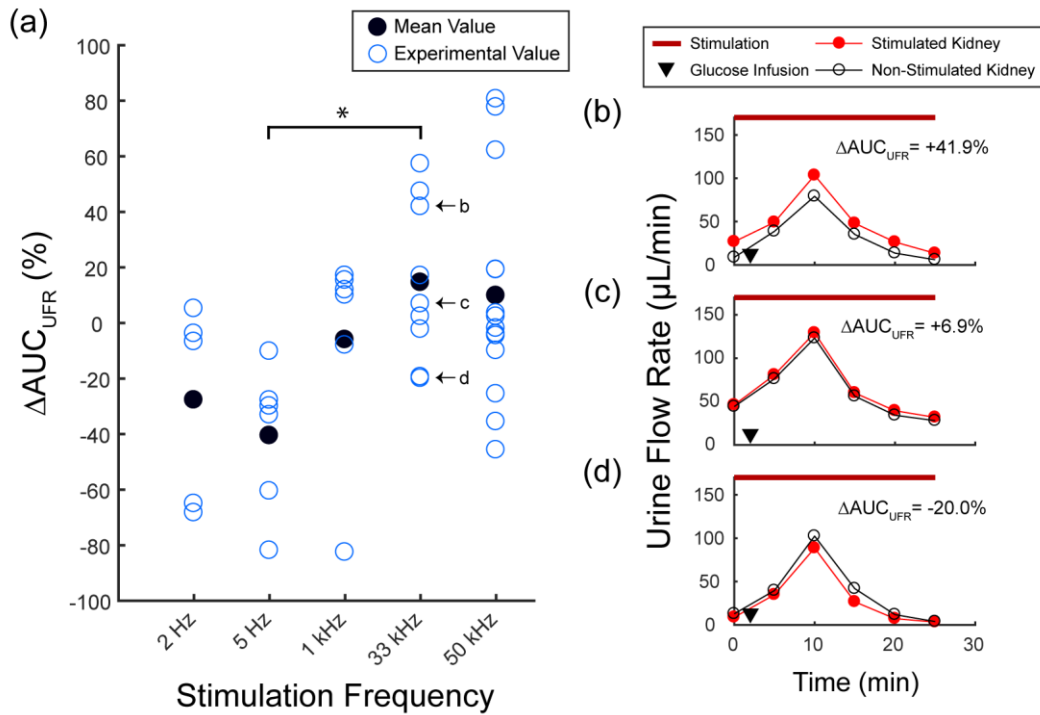
Figure 2.4 Changes in urine flow. (a) The percentage difference between the area under the curve for urine flow rate of the stimulated and non-stimulated kidney (ΔAUC_{UFR}) at the applied stimulation frequencies. Stimulation frequency had a significant main effect (Kruskal-Wallis test, $p < 0.05$), with 5 Hz and 33 kHz trials significantly different from each other (post-hoc Wilcoxon rank sum test, $* = p < 0.005$). (b) Urine flow rate (UFR) measurements for the trial shown in Figure 2.2b. (c) UFR measurements for the trial shown in Figure 2.2c. (d) UFR measurements for the trial shown in Figure 2.2d.

2.4.4 Blood Glucose Concentration

The blood glucose concentration decrease rates (BGCDRs) during stimulation at all frequencies are shown in Figure 2.5a. The average BGCDR was -9.1 mg/dL/min at 2 Hz (n = 4), -13.5 mg/dL/min at 5 Hz (n = 5), -13.5 mg/dL/min at 1 kHz (n = 6), -12.0 mg/dL/min at 33 kHz (n = 9), and -12.5 mg/dL/min at 50 kHz (n = 13). No statistically significant main effect occurred across all stimulation frequencies (Kruskal-Wallis test, $p = 0.4708$). BGCDR at some stimulation trials [2 Hz (n = 1), 5 Hz (n = 1) and 50 kHz (n = 1)] were not calculated due to insufficient BGC values.
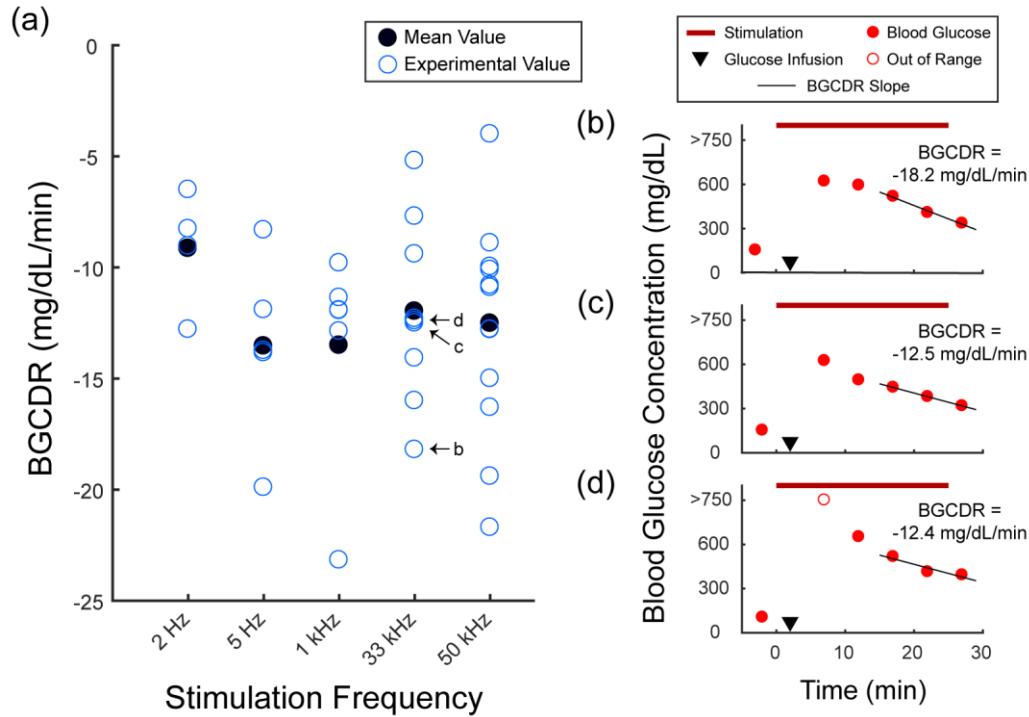
Figure 2.5 Changes in blood glucose concentration. (a) The blood glucose concentration decrease rate (BGCDR) at the applied stimulation frequencies. (b) Blood glucose concentration (BGC) measurements and BGCDR (slope) for the trial shown in Figure 2.2b. (c) BGC and BGCDR measurements for the trial shown in Figure 2.2c. (d) BGC and BGCDR measurements for the trial shown in Figure 2.2d. BGC measurements above 750 mg/dL were not available due to the limitations of the glucometer.

2.5 Discussion

The aim of this study was to investigate modulation of urine glucose excretion by electrical stimulation of renal nerves. We hypothesized that stimulation of renal nerves at kilohertz frequencies (1-50 kHz) would increase urine glucose excretion (UGE), while low frequency stimulation (2-5 Hz) would decrease UGE. Although stimulation at kilohertz frequencies did not always lead to an increase in UGE, 33 kHz showed a notable average increase in UGE in accordance with our hypothesis. In contrast, low frequency stimulation typically showed a decrease in UGE, with the strongest effect observed at 5 Hz stimulation (Figure 2.2). To our knowledge, this study is the first to demonstrate influence of electrical stimulation of renal nerves

26

on glucose excretion.

The average differences in UGE were similar to the average differences observed in urine flow rate (UFR), as shown in Figure 2.4. This associated response may suggest that either UGE or UFR was the primary effect of stimulation, while the other was a secondary response. Previous studies that applied stimulation of renal nerves at low frequencies observed a 25-52% reduction in UFR (Bello-Reuss, Trevino, and Gottschalk 1976; Pontes et al. 2015). Those percentages align with the average reduction of UFR we observed at low frequency stimulation (28% at 2 Hz, 41% at 5 Hz), suggesting that UFR may be the primary response of stimulation at low frequencies. On the other hand, we observed an increase in UFR at 33 and 50 kHz stimulation. To our knowledge, no studies have reported an increase in UFR by stimulation of renal nerves. Although it is possible that changes in UFR may have directly led to corresponding changes in UGE, the primary response of UFR or UGE to stimulation at kilohertz frequencies cannot be determined in this study. UFR and UGE are normally associated, as increased urination is a common adverse event in diabetic patients treated with sodium-glucose co-transporter 2 (SGLT2) inhibitors that primarily increase urine glucose excretion (Seufert 2015; Wilding 2014). Additional studies are required to distinguish the glucose excretion and urine flow effects for stimulation of renal nerves.

Stimulation of renal nerves did not have a clear effect on urine glucose concentration (UGC), as no statistical significance occurred across stimulation frequencies (Figure 2.3). Furthermore, we did not observe a clear difference between kilohertz or low frequency stimulation on the decrease rate for blood glucose concentration (BGC) after infusion of an artificial glucose bolus (Figure 2.5). Typically, BGC would reach a peak value within the first 10 minutes after glucose bolus infusion. Then, BGC values would gradually decrease and return to around baseline values at 30-40 minutes after the glucose infusion, regardless of the stimulation parameters. The variation in

the sample size of the stimulation frequency groups may have also contributed to these unclear responses. Modifications and improvements in experimental design may be necessary to capture clear and consistent responses to stimulation of renal nerves.

Renal nerve branches are distributed around the renal artery in a plexus form. Ultrastructural studies using electron microscopy techniques have shown that renal nerve fibers innervate epithelial cells of proximal tubules, the glucose reabsorption region of the kidney (Muller and Barajas 1972; Luff et al. 1992; Mather and Pollock 2011). Although studies have examined the distribution of renal nerves around the renal artery (Maeda et al. 2014; Sakakura et al. 2014; van Amsterdam et al. 2016), we could not determine the renal nerve branches that innervate the proximal tubules in this study. Therefore, we utilized a cuff electrode with the purpose of encircling all the renal nerve branches surrounding the renal artery. In order to place a cuff electrode, the renal artery was isolated by removing adjacent connective tissue that may have contained fine renal nerve branches. Although we ensured that the renal nerves were moderately intact by observing temporary kidney surface blanching at 10 Hz stimulation (Hermansson et al. 1981; Yao et al. 2014), the variations in connective tissue removal and relative shifts in the electrode placement along the renal artery across experiments may have contributed to the variability of our outcome results. This inconsistency in outcomes has also been observed in renal denervation studies, where conflicting results were reported in clinical studies (Mahfoud et al. 2011; Bhatt et al. 2014; Witkowski et al. 2011). The reported variability is suspected to be from variations in ablation locations across renal denervation procedures performed in multiple centers (Mahfoud, Edelman, and Böhm 2014). Experimental improvements in electrode placement and the plexus-electrode interface may be required to obtain more consistent results.

An anatomical analysis in rats showed that 96% of renal nerve axons are unmyelinated C-

fibers (DiBona, Sawin, and Jones 1996). Although nerve conduction block experiments using kilohertz frequency stimulation were typically performed using cuff electrodes encircling myelinated motor neurons while monitoring muscle tension for block validation (Kilgore and Bhadra 2014; Bhadra and Kilgore 2005), nerve block has also been demonstrated on purely unmyelinated fibers using suction electrodes and confirmed by direct recordings of action potential propagation (Joseph and Butera 2009). In this study, the amplitude of sinusoidal kilohertz frequency stimulation was fixed at 15 V, which is expected to be above the threshold for nerve conduction block at the selected frequencies (Joseph and Butera 2011; Y. A. Patel and Butera 2015; Bhadra and Kilgore 2005). On the other hand, previous studies increased renal nerve activity by low frequency stimulation (Bello-Reuss, Trevino, and Gottschalk 1976; DiBona 2000). The stimulation amplitude and pulse width in this study at low frequencies was consistent at 10 V and 0.5 msec, respectively, which is above the activation threshold for rat C-fibers using cuff electrodes (Woodbury and Woodbury 1990). However, to validate the true presence of nerve conduction block or increased neural activity, multiple recording and stimulating electrodes must be placed along the renal nerves. Unfortunately, this was difficult to accomplish in this study due to our limited ability to expose and isolate the renal nerves (~2-4 mm), in addition to the anticipated noise contamination issues between adjacent stimulating and recording electrodes (Kilgore and Bhadra 2014). Additional experiments are required to examine the mechanism of action for stimulation of renal nerves.

The work presented here was a feasibility study to investigate glucose excretion modulation by stimulation of renal nerves. There are numerous limitations to this study. Although changes in UGE were observed in response to stimulation of renal nerves, this study does not provide any evidence on the underlying mechanisms for these changes. It is unknown if the observed changes

29

in UGE were a consequence of changes in UFR, or directly related to the gluconeogenesis process or the glucose transport pathways in the proximal tubules that are innervated by renal nerves (Mather and Pollock 2011; Muller and Barajas 1972; Luff et al. 1992). Measurements of renal function, such as glomerular filtration rate, renal plasma flow and sodium excretion (Toto 1995; Phillips and Hamilton 1948) were not obtained in this feasibility study. The assessment of renal function is an absolute necessity for the progression of this research. The large variation in the results of this study may have been due to multiple reasons. In addition to the variability in electrode placement, the unilateral stimulation approach in this study may have provoked reno-renal reflexes, where the non-stimulated kidney modifies its activity based on changes in the stimulated kidney (Zanchetti et al. 1984). The possible presence of these reflexes may have altered the outcomes of this study. Further experiments with reno-renal reflex elimination procedures, such as bilateral stimulation or denervation of non-stimulated kidneys, may be necessary to obtain unhindered stimulation outcomes.

Although further experiments are required to examine the underlying mechanisms for stimulation of renal nerves, this study may introduce a new approach for regulation of glucose excretion. Recently approved medications for patients with type 2 diabetes are SGLT-2 inhibitors, which prevent the activity of glucose transporters in the kidney and lead to increased glucose excretion into urine (Lew and Wick 2015). Stimulation of renal nerves may provide an alternative treatment approach for glycemic control that avoids patient compliance issues typically seen with medications (Polonsky and Henry 2016).

2.6 Conclusion

To our knowledge, this is the first study to investigate electrical stimulation of renal nerves to modulate urine glucose excretion. Our experimental results show that stimulation of renal nerves

may modulate urine glucose excretion, however, this outcome may be associated with urine flow rate. Future work is needed to examine the underlying mechanisms and identify approaches for enhancing regulation of glucose excretion.

2.7   Acknowledgements

Chapter 3: Kilohertz Frequency Stimulation of Renal Nerves for Modulating Blood Glucose Concentration in Diabetic Rats

This chapter has been published:

3.1 Abstract

In recent years, the role of the kidney in glucose homeostasis has gained global interest. The kidneys are innervated by renal nerves, and renal denervation studies to control hypertension have shown improved glucose regulation. We hypothesized that kilohertz frequency stimulation, which can block propagation of action potentials, applied to renal nerves would reduce blood glucose concentration levels by increasing urinary glucose excretion.

We performed experiments (n = 8) on anesthetized, diabetic streptozotocin-induced male Long-Evans rats. The renal nerves of each kidney were encircled by a nerve cuff electrode. Blood samples were obtained from the tail for blood glucose concentration measurements. Ureters were cannulated bilaterally for collection of urine samples, and colorimetric assays were used to measure urine glucose concentrations. Electrical stimulation (sinusoidal, 50 kHz, 15 V) of the renal nerves was applied for 60 minutes.

The average blood glucose concentration rate (BGCR) was lower during kilohertz frequency stimulation (-0.78 ± 1.20 mg/dL/min; mean ± standard deviation), compared to BGCR before stimulation (+1.14 ± 1.83 mg/dL/min; $p < 0.05$) and after stimulation (+0.63 ± 1.32 mg/dL/min). The average area under the curve for urine glucose concentration over the time period (AUC_{UGC}/t) was higher during kilohertz frequency stimulation (7687.4 ± 4006.1 mg/dL), compared to AUC_{UGC}/t before stimulation (6466.9 ± 2772.8 mg/dL) and after stimulation (5277.2 ± 3381.5 mg/dL).

Overall, our results show that kilohertz frequency stimulation of renal nerves is a possible approach for the modulation of blood glucose concentration and may introduce an alternative treatment modality for glycemic control in patients with diabetes.

3.2 Introduction

Diabetes is a chronic progressive disease that affects the lives of millions of people around the world (Cho et al. 2018). Many diabetic patients struggle with glycemic control and are at high risk of severe disease complications (American Diabetes Association (ADA) 2018). In recent years, the role of the kidney in glucose homeostasis has gained considerable interest (DeFronzo, Davidson, and Del Prato 2012). The kidneys are innervated by renal nerves that form axonal junctions on epithelial cells of proximal tubules, the glucose reabsorption region in the kidney nephron (DeFronzo, Davidson, and Del Prato 2012; Luff et al. 1992). Early clinical trials of renal denervation on patients with drug-resistant hypertension showed significant improvements in blood glucose control (Mahfoud et al. 2011), and subsequent animal studies of renal denervation supported this observation (Chhabra et al. 2017). A reversible approach that has demonstrated nerve conduction block on various types of nerves is kilohertz frequency stimulation (Kilgore and Bhadra 2014). Our previous study showed that electrical stimulation of renal nerves may modulate

urinary glucose excretion in glucose-bolus infusion experiments (Jiman et al. 2018). In this study, we hypothesized that kilohertz frequency stimulation of renal nerves would reduce blood glucose concentration levels in diabetic animals by increasing urinary glucose excretion.

3.3 Methods

All experimental procedures were approved by the University of Michigan Institutional Animal Care and Use Committee (IACUC).

3.3.1 Animals and Housing

We performed non-survival, anesthetized experiments on 8 male 310-420 g Long-Evans rats (Charles Rivers Laboratories, Wilmington, MA, USA). The animals were housed in ventilated cages under controlled temperature, humidity and photoperiod (12-h light/dark cycle), and were provided with laboratory chow (5L0D, LabDiet, St. Louis, MO, USA) and tap water ad libitum. The animals were injected with streptozotocin (S0130-1G, Sigma-Aldrich Corp., St. Louis, MO, USA) intravenously through the tail vein (50 mg/kg BW), which is a common research approach for developing an animal model for diabetes (Wei et al. 2003). A period of 2-4 weeks was allowed between streptozotocin administration and the experimental procedure in order to obtain stable non-fasting blood glucose concentration levels above 400 mg/dL.

3.3.2 Experimental Preparation

For anesthesia, a single intraperitoneal injection of thiobutabarbital sodium salt hydrate (Inactin, T133-1G, Sigma-Aldrich Corp., St. Louis, MO, USA) was administered (110 mg/kg BW), which is commonly used in renal studies to preserve renal function (Walter, Zewde, and Shirley 1989). Animal temperature was maintained using a heating pad (ReptiTherm, Zoo Med Laboratories Inc., San Luis Obispo, CA, USA) and was monitored through a rectal temperature

34

sensor (SurgiVet, Smiths Medical, Norwell, MA, USA). Under a dissection microscope (Lynx EVO, Vision Engineering Inc., New Milford, CT, USA), a midline cervical incision was made and the jugular vein was cannulated with polyethylene tubing (BTPE-50, Instech Laboratories Inc., Plymouth Meeting, PA, USA) to continuously infuse 0.9% NaCl (saline) through the jugular vein at 0.2 mL/min using a syringe pump (NE-1000, New Era Pump Systems Inc., Farmingdale, NY, USA). A tracheotomy was performed to ensure a clear airway. Through a midline abdominal incision, ureters were cannulated bilaterally with polyethylene tubing (BTPE-10, Instech Laboratories Inc., Plymouth Meeting, PA, USA). The kidneys and renal arteries were exposed by removing surrounding fat and connective tissue. A bipolar nerve cuff electrode (1.00 mm inner-diameter, 100 µm platinum contacts, Microprobes for Life Science, Gaithersburg, MD, USA) was placed around each renal artery, encircling renal nerves that run along the artery. Care was taken to not damage the renal nerve branches and to not occlude blood flow in the renal artery. To ensure that the cuff electrodes were in contact with intact renal nerves, biphasic stimulation pulses at 10 Hz, 10 V were applied for approximately 1 minute through the nerve cuff electrode. This resulted in temporary kidney ischemia, which was confirmed by the observation of kidney surface blanching (Hermansson et al. 1981). Before surgery, electrode impedance measurements (5.75 ± 2.81 kΩ) were obtained using an impedance tester (nanoZ, White Matter LLC, Seattle, WA, USA) at 1 kHz in saline to confirm functionality of the nerve cuff electrode.

3.3.3   Electrical Stimulation

Each nerve cuff electrode was connected to a stimulus isolation unit (Model 4100 or Model 2200, A-M Systems, Loop Sequim, WA, USA). A function generator (33220A, Agilent Technologies, Santa Clara, CA, USA) was connected to each stimulus isolation unit to generate sinusoidal waveforms at 50 kHz, 15 V.

3.3.4 Experimental Protocol

After completion of the experimental preparation, a stabilization period of at least 10 minutes was allowed before obtaining blood and urine samples. Blood samples were acquired from a tail cut every 10-25 minutes for blood glucose concentration measurements using a glucometer (AlphaTRAK 2, Abbott, Abbott Park, IL, USA). Urine samples from each kidney were collected in pre-weighed sampling tubes (3448, Thermo Fisher Scientific, Waltham, WA, USA) at 10-minute intervals. The collected urine samples were weighed on a scale (AE 160, Mettler Toledo, Columbus, OH, USA) for volume estimations (1 µL/mg), and urine glucose concentration measurements were obtained using colorimetric assays (10009582, Cayman Chemical, Ann Arbor, MI, USA). Blood and urine samples were obtained before stimulation for 30-40 minutes, during kilohertz frequency stimulation that continued for 60 minutes, and after stimulation for another 30-40 minutes. A diagram of the experimental setup is shown in Figure 3.1.
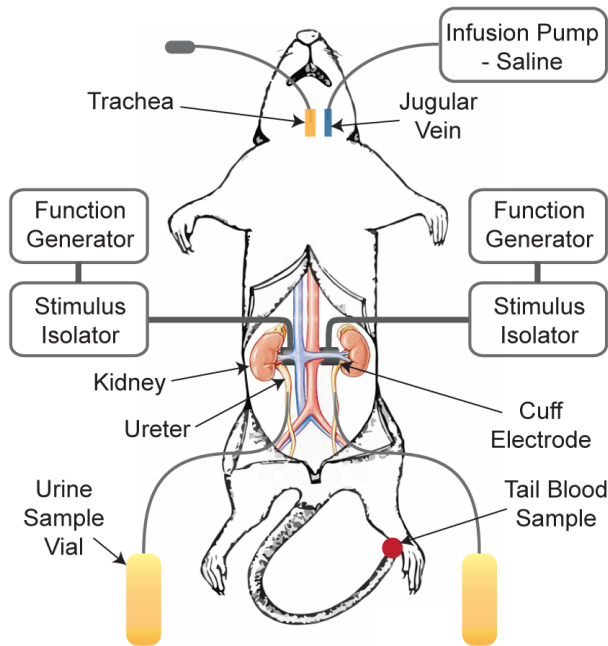
Figure 3.1 Diagram of the experimental setup. Electrical stimulation was applied to renal nerves bilaterally in streptozotocin-induced diabetic rats, with the ureters cannulated bilaterally.

3.3.5 Data Analysis

The blood glucose concentration rate (BGCR) was obtained by calculating the linear regression slope of blood glucose concentration measurements over the time periods before, during, and after stimulation. The total amount of glucose excreted was calculated from the urine glucose concentration measurements and the urine sample volumes of each kidney. The total amount of glucose excreted was divided by the total volume of the urine samples to obtain the average urine glucose concentration value between the two kidneys. The average area under the curve for urine glucose concentration (AUC_{UGC}) over the time period (t) before, during, and after stimulation was calculated by the trapezoidal numerical integration method. To test statistical significance for the BGCR data set, a one-way analysis of variance (ANOVA) was performed across all periods (before, during, and after stimulation), followed by a Tukey-Kramer multiple comparison post-hoc test. The AUC_{UGC}/t data set did not follow a normal distribution (confirmed by one-sample Kolmogorov-Smirnov test). Therefore, a non-parametric Kruskal-Wallis test was performed to assess statistical significance across all periods. Statistical significance was considered at $p < 0.05$. Values are presented as mean ± standard deviation. All data analysis and statistical tests were performed using MATLAB software (R2014b, MathWorks, Natick, MA, USA).

3.4 Results

We performed 8 experiments on streptozotocin-induced diabetic rats and applied bilateral kilohertz frequency stimulation of renal nerves. Measurements of blood and urine glucose concentrations were obtained before, during, and after stimulation. An example of an experiment is shown in Figure 3.2.
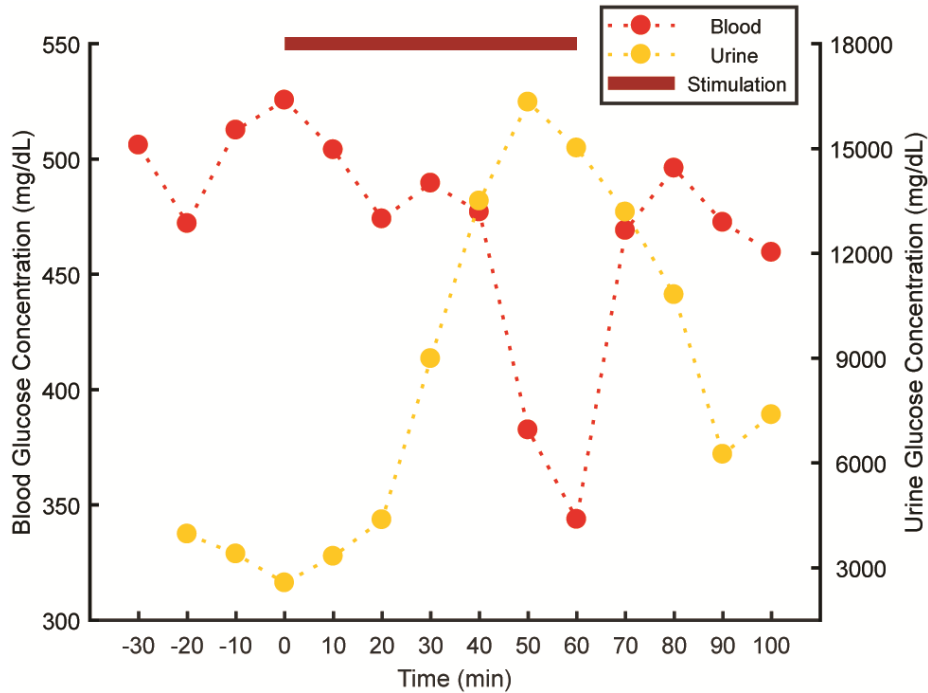
Figure 3.2 Blood and urine glucose concentration measurements in an example experiment. Here, the blood glucose concentration rate (BGCR) was +0.99 mg/dL/min before stimulation, -2.81 mg/dL/min during stimulation, and +2.35 mg/dL/min after stimulation. The area under the curve for urine glucose concentration over the time period (AUC$_{UGC}$/t) was 3329.2 mg/dL before stimulation, 9215.5 mg/dL during stimulation, and 10359.2 mg/dL after stimulation.

3.4.1   Blood Glucose Concentration

The blood glucose concentration rate (BGCR) was calculated for the periods before, during, and after stimulation. The mean BGCR was lower during kilohertz frequency stimulation (-0.78 ± 1.20 mg/dL/min), compared to the mean BGCR before stimulation (+1.14 ± 1.83 mg/dL/min), and after stimulation (+0.63 ± 1.32 mg/dL/min), as shown in Figure 3.3. Statistical significance occurred across all periods (ANOVA test, $p < 0.05$), and between the BGCR values before and during stimulation (Tukey-Kramer test, $p < 0.05$).
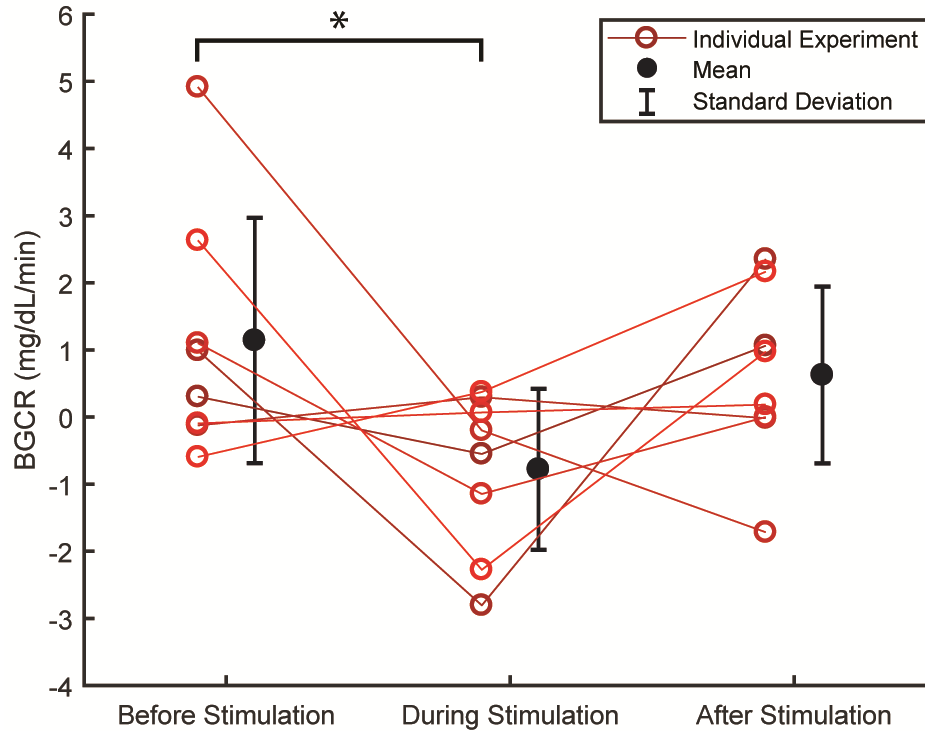
Figure 3.3 Blood Glucose Concentration Rates (BGCRs) before, during and after stimulation for all individual experiments. Statistical significance occurred across all periods (ANOVA test, $p < 0.05$), and between the BGCR values before and during stimulation (Tukey-Kramer test, $* = p < 0.05$).

3.4.2 Urine Glucose Concentration

The average area under the curve was calculated for urine glucose concentrations over the time period (AUC_{UGC}/t) before, during, and after stimulation. The mean AUC_{UGC}/t was higher during kilohertz frequency stimulation (7687.4 ± 4006.1 mg/dL), compared to the mean AUC_{UGC}/t before stimulation (6466.9 ± 2772.8 mg/dL), and after stimulation (5277.2 ± 3381.5 mg/dL), as shown in Fig. 3.4. In one of the experiments, urine glucose concentrations before stimulation were not obtained. No statistical significance occurred across all the periods (Kruskal-Wallis test, $p = 0.46$).
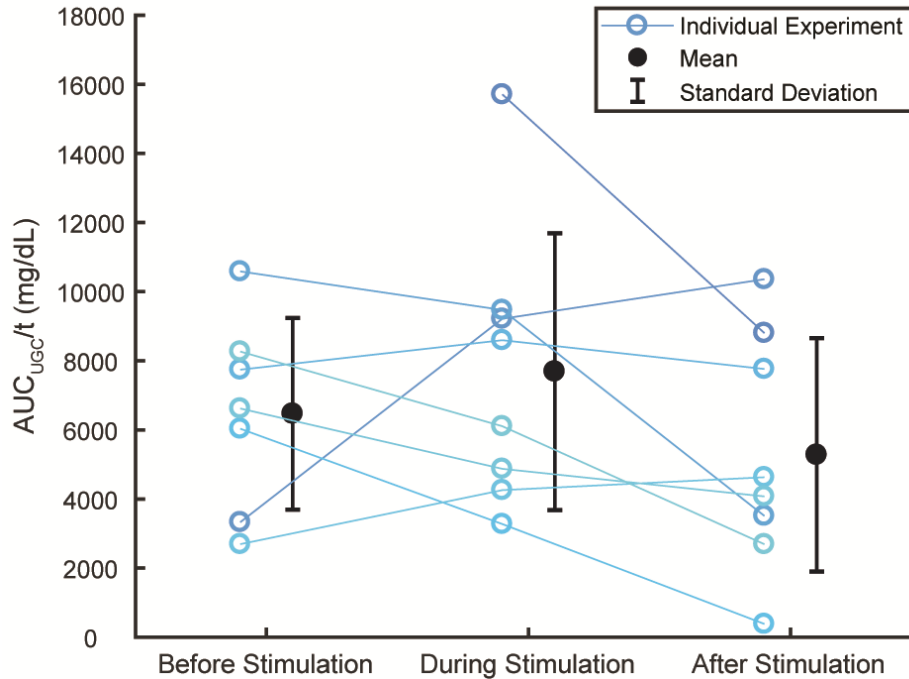
Figure 3.4 Area under the curve for urine glucose concentration over the time period (AUC$_{UGC}$/t) before, during, and after stimulation for all individual experiments. An AUC$_{UGC}$/t value was not obtained in one of the experiments before stimulation. No statistical significance occurred across all the periods (Kruskal-Wallis test, $p = 0.46$).

3.5   Discussion

The objective of this study was to investigate modulation of blood glucose concentration and urinary glucose excretion in diabetic rats in response to bilateral kilohertz frequency stimulation of renal nerves. We hypothesized that kilohertz frequency stimulation of renal nerves would reduce blood glucose concentration levels by increasing urinary glucose excretion. Kilohertz frequency stimulation of renal nerves showed a significant decrease (-168.4%) in blood glucose concentration rate (BGCR), and an increase (+18.9%) in the overall average area under the curve for urine glucose concentration (AUC$_{UGC}$/t), with respect to values before stimulation, as shown in Figure 3.3 and Figure 3.4, respectively. The experimental results of this study suggest that kilohertz

frequency stimulation of renal nerves is a potential approach for glycemic control in diabetic conditions.

Renal nerves are distributed around the renal artery in a plexus form. Therefore, we placed a cuff electrode around the renal artery to encircle the renal nerves that surround the artery. It is possible that stimulation may have disrupted blood flow in the renal artery. However, the selected stimulation parameters in this study (50 kHz, 15 V, sinusoidal) showed minimal effect on renal blood flow measured by a perivascular flow meter system and kidney perfusion (Appendix A). Further studies are needed to examine the safety of kilohertz frequency stimulation and explore the optimal effective stimulation parameters for reducing blood glucose concentration levels.

Although changes in blood glucose concentrations were observed in response to kilohertz frequency stimulation of renal nerves, it is unknown if these changes were directly related to the glucose reabsorption pathways in the renal proximal tubules that are innervated by renal nerves (DeFronzo, Davidson, and Del Prato 2012; Luff et al. 1992). Renal function measurements, such as glomerular filtration rate and renal plasma flow (Toto 1995), were not evaluated in this study. The variation in the results of this study may be due to the dissimilarities in the process of removing connective tissue around the renal artery, which may have contained fine renal nerve branches. Improvements in the electrode interface may be necessary to obtain more consistent results.

In recent years, there is an emerging interest in the development of bioelectronic medicine that directly modulates neural activity to alleviate various diseases (Tracey 2014). Clinical trials on vagal nerve stimulation and gastric electrical stimulation have reported improvements in glycemic control for patients with obesity and type 2 diabetes (Herrera et al. 2017; Lebovitz et al. 2015). Although further experiments are necessary to examine the underlying mechanisms for kilohertz frequency stimulation of renal nerves, this study and our prior work (Jiman et al. 2018)

may introduce a novel approach for glycemic control in diabetic patients through glucose regulation at the kidneys, which occupy a vital role in glucose homeostasis (DeFronzo, Davidson, and Del Prato 2012).

3.6 Conclusion

This study investigates the modulation of blood glucose concentration and urinary glucose excretion in diabetic rats by kilohertz frequency stimulation of renal nerves. Our experimental results show that kilohertz frequency stimulation of renal nerves may reduce blood glucose concentration levels in diabetic conditions. This study suggests that kilohertz frequency stimulation of renal nerves is a potential treatment modality for glycemic control.

3.7 Acknowledgment

Chapter 4: Development and Assessment of Surgical Procedure for the Chronic Implantation of Intraneural Microneedle Nerve Arrays in Rat Vagus Nerves

4.1 Abstract

Autonomic nerves of the peripheral nervous system conduct essential neural signals that regulate vital body functions, such as breathing, metabolism and immune responses. Interfacing with autonomic nerves to detect physiological neural signaling will help researchers identify potential stimulation patterns to restore regulatory functions. Among electrodes that interface with peripheral nerves, intraneural electrodes provide a balance between selectivity and invasiveness. Intraneural electrode arrays have been chronically implanted in various peripheral nerves but not in fine autonomic nerves (diameter ≤ 0.5 mm), due to challenges associated with the small size of these nerves. We developed a novel intraneural Microneedle Nerve Array (MINA) for fine autonomic nerves, and assembled an innovative implantation procedure. We investigated two array attachment approaches (fibrin sealant and rose-bengal bonding) to secure non-wired MINAs in rat vagus nerves (diameter of 300-500 µm), and assessed the approaches by determining the proximity of the MINA to the nerve. Furthermore, we evaluated the nerve condition by electrophysiology testing. The fibrin sealant approach was unsuccessful in maintaining the MINA-nerve interface for 4- and 8-week implant durations. The rose-bengal coated MINAs were in close proximity to axons (≤ 50 µm) in 75% of 1-week and 14% of 6-week implants. The electrophysiology testing showed evoked neural responses in MINA-implanted nerves. No statistical significance occurred for body

weight, blood glucose concentration, or stimulation threshold values between MINA-implanted and sham-implant animals. Further work is needed to implement and demonstrate recording-capabilities of functional MINA. Overall, we demonstrated a new chronic implantation procedure for a novel intraneural array in a fine autonomic nerve. The complete development of this intraneural array may provide novel insights in neural signaling of autonomic nerves and may assist in the development of innovative treatments to restore vital regulatory functions.

4.2   Introduction

The peripheral nervous system conveys sensory and motor information between the central nervous system and the organs of the body. Peripheral nerves are classified as somatic nerves, which control conscious voluntary movements, or autonomic nerves, that regulate essential unconscious bodily functions, such as breathing, blood pressure regulation, immune responses, digestion and bladder function, among others (McCorry 2007; Browning, Verheijden, and Boeckxstaens 2017; de Groat, Griffiths, and Yoshimura 2015). Irregular activity in these autonomic nerves may lead to chronic disorders (e.g. hypertension, diabetes, obesity and bladder dysfunction) that likely require a lifelong therapy (Mathias and Bannister 2013; Goldstein et al. 2002). Existing treatments may have undesirable side effects or limited efficacy, and many patients struggle with managing these disorders (Mahfoud et al. 2011; Ali et al. 2013; Gaunt and Prochazka 2006). An alternative treatment modality is a direct electrode interface with autonomic nerves to detect and alter neural activity. An emerging class of therapies that revolve around this targeted interface concept to restore regulatory functions is bioelectronic medicine (Tracey 2014; Pavlov and Tracey 2019; Birmingham et al. 2014).

Interfacing electrodes for peripheral nerves are categorized into three main types: extraneural, intraneural, and regenerative electrodes (Micera and Navarro 2009; Larson and Meng

2019). Extraneural electrodes (Silverman et al. 2018; Ward et al. 2015; Lee et al. 2017; González-González et al. 2018; Shikano et al. 2019) are the most commonly used and least invasive among the three main electrode types. However, the main disadvantage for these electrodes is the lack of spatial selectivity, as these electrodes are positioned outside of the nerve and cannot detect or alter individual or local axon activity through the protective, highly-resistive epineurium layer that surrounds the nerve, and the perineurium layer that surrounds the bundle of axons (Garai et al. 2017; Weerasuriya et al. 1984). In contrast, regenerative electrodes (Srinivasan et al. 2016; Ramachandran et al. 2006; Spearman et al. 2018) may provide high selectivity but require transection of a nerve, and depend on the possibility of the nerve to regenerate and reconnect through the electrode. This transection may lead to severe permanent nerve damage, and these electrodes are more suitable for neuroprosthetic applications with severed nerves in amputee limbs. Intraneural electrodes, such as microelectrode arrays (Wark et al. 2014; Mathews et al. 2014; Byun et al. 2017) and intrafascicular electrodes (Wurth et al. 2017; de la Oliva, Navarro, and del Valle 2018; Badia et al. 2011), provide a balance between selectivity and invasiveness, and have demonstrated chronic interface stability on peripheral nerves with a diameter of 1 mm or larger. A research group has developed intrafascicular carbon nanotube (CNT) electrodes that were chronically implanted in fine autonomic nerves (diameter ≤ 0.5 mm) (McCallum et al. 2017). They obtained excellent signal-to-noise ratio recordings (SNR > 10 dB) for 10 weeks by implanting two single-channel CNT electrodes in a nerve target. Although the CNT electrode was 10 μm in diameter, a large tungsten needle (outer diameter ≥ 75 μm) was used to insert each CNT electrode. Another research group developed a 4-channel carbon fiber microelectrode array (electrode diameter ≤ 15 μm) that was directly inserted in fine autonomic nerves (Gillis et al. 2018). However, to our knowledge, these carbon fiber arrays have not yet been chronically implanted in autonomic

nerves. Chronically implanting an intraneural electrode in fine autonomic nerves is extremely challenging due to the difficulty of handling sub-millimeter nerves, the precision necessary to insert an electrode through the protective epineurium layer of the nerve, and the difficulty of securing the electrode without causing damage to the nerve.

We have developed an intraneural, multi-channel Microneedle Nerve Array (MINA) with ultra-miniaturized needles (average diameter of 11.6 μm). The individual MINA needles are silicon-based to provide sufficient robustness to penetrate the epineurium layer of a nerve, and the needles are connected together with a highly compliant, biocompatible polydimethylsiloxane (PDMS) substrate (Park et al. 2014) that allows the MINA to conform and reduce the mechanical mismatch with a nerve. We hypothesize that a chronically-implanted MINA with ultra-miniaturized needles would cause minimal damage and tissue response in fine autonomic nerves. Carbon fiber electrodes with similar dimensions as MINA microneedles were successfully implanted in the rat cerebral cortex with minimal to no tissue reactivity around these electrodes (Kozai et al. 2012; P. R. Patel et al. 2016). This was achieved after removing the dura, which is equivalent to the epineurium, and securing the electrode position by anchoring it to the skull. Studies have shown that tissue reactivity in the rat cerebral cortex is significantly diminished as the dimensions of a neural probe are reduced (Seymour and Kipke 2007).

The objective of this study was to develop a reliable procedure to chronically implant MINA arrays in fine autonomic nerves and evaluate the nerve condition. We implanted non-wired MINAs in rat vagus nerves to evaluate the tissue response to the MINA itself and eliminate any accompanying factors, such as connector and wire tethering forces. We investigated two attachment approaches to secure the implanted MINA: 1) fibrin sealant and 2) rose-bengal coating. Fibrin sealant is a biocompatible and biodegradable tissue adhesive that is commonly used in

surgical practice (Jackson 2001). The sealant requires the mixture of fibrinogen and thrombin compounds to activate a coagulation cascade that forms the fibrin sealant (Tse and Ko 2012). Rose-bengal is a photochemical tissue bonding technique used in tissue adhesion applications, such as skin closure (Chan, Kochevar, and Redmond 2002) and nerve repair (Sliow et al. 2019; Barton et al. 2013; Fairbairn et al. 2015). The technique involves using a green laser beam to activate the rose-bengal solution applied between two tissue surfaces and form crosslink bonding of collagen fibers with minimal heat production (Lauto et al. 2011). We assessed the fibrin sealant and rose-bengal attachment approaches by determining the proximity of the MINA to the implanted vagus nerve at the terminal procedure, and evaluated the nerve condition by testing for stimulation-evoked neural responses.

4.3   Methods

We chronically implanted MINAs in rat cervical vagus nerves using two attachment approaches: 1) fibrin sealant and 2) rose-bengal coating. The implanted rats were regularly monitored and terminated after 1-8 weeks to evaluate the nerve condition and MINA proximity to the nerve using electrophysiology testing and microscopic computed tomography imaging.

4.3.1   Fabrication of Microneedle Nerve Array (MINA)

The MINAs were fabricated at the Lurie Nanofabrication Facility (LNF) at the University of Michigan, and described in detail in Appendix B (D. Yan et al. 2019) with modifications on needle configuration and dimensions. Briefly, the base of the MINA was a silicon-on-insulator (SOI) wafer, and the needles were fabricated through masking, depositing and etching techniques. High-quality insulation of the silicon was provided by thermal oxidation. A polydimethylsiloxane (PDMS) substrate with a thickness of 80 μm was formed at the base of the needles. The exposed needles had an average length, overall diameter, tip diameter and pitch of 140 μm, 11.6 μm, 6.3

µm and 150 µm, respectively. A MINA had 24 needles in total. The needle configuration for MINAs implanted with the fibrin sealant approach was 3x8 (Figure 4.1a). However, we noticed that the width of the needle-region (239 µm) was very close to the diameter of a typical rat vagus nerve (300 µm). Therefore, the needle-region width was reduced in half by adjusting the needle configuration to 2x12 for rose-bengal coated MINAs (Figure 4.2a).

4.3.2   Rose-Bengal Coated MINA

A set of MINAs were coated with a solution of rose-bengal to adhere the MINA to a nerve. The rose-bengal coating process is described in detail in Appendix B (D. Yan et al. 2019). Briefly, collagen and rose-bengal were dissolved separately in 30% ethanol. The collagen and rose-bengal ethanol solutions were mixed at a 10:1 ratio. The MINA surface was treated with oxygen plasma to allow bonding of the MINA surface to the applied rose-bengal solution. The MINAs were then dried at 50°C to allow evaporation of the solution and form the rose-bengal coating on the MINA surface. The individual MINAs were cut with a scalpel blade under a microscope as narrow as possible (~0.5x3.0 mm) with slight extensions on the edges of the needle region to allow handling of the MINA with fine forceps, as shown in Figure 4.2a. The rose-bengal coated MINAs were sterilized at low temperature (37°C) ethylene oxide (EtO) in preparation for implantation.

4.3.3   Design of Vacuum Suction Adaptor

To handle the MINA, a vacuum suction pen (71894-01, Electron Microscopy Sciences, Hatfield, PA, USA) was used with a custom designed 3D-printed tip adaptor, shown in Figure 4.2b. Between the vacuum suction pen and the tip adaptor was a blunt needle (22G, SAI Infusion Technologies, Lake Villa, IL, USA). Suction was provided by an aspirator machine (S430A, Schuco, Bielefeld, Germany) at a pressure of 100-200 psi. The tip adaptor was designed with a computer-aided design (CAD) software (Fusion 360, Autodesk, San Rafael, CA, USA) and

fabricated using a 3D-printer with clear resin (Form 2, Formlabs, Somerville, MA, USA). The suction surface had two suction holes with a diameter of 0.5 mm, which was the smallest printable hollow diameter with the 3D printer. The vacuum suction adaptor was coated with mineral oil (S25439, Fisher Scientific, Hampton, NH, USA) to eliminate the residual adhesiveness from the resin-printing process. The MINA was centered on the suction surface using fine forceps under a microscope. A center-post on the side of the adaptor was designed to assist the MINA-centering process (Figure 4.2a) and aligning the centered MINA with a vagus nerve before insertion (Figure 4.2f). The detailed CAD design of the vacuum suction adaptor is shown in Appendix C Figure C.1.

4.3.4   Nerve-Holder Design

Inserting the MINA directly into the vagus nerve without a nerve-holder was challenging due to the movement of the vagus nerve when applying insertion force, fluid and breathing motion of the cervical cavity, and the difficulty of positioning a camera at the same level as the MINA-nerve interface to visualize the alignment and insertion of MINA needles. To address these challenges, we designed a custom nerve-holder that secures the nerve in place during insertion, elevates the nerve away from fluids and breathing motions of the cervical cavity, and enables accurate positioning of a small camera to visualize the MINA needles during insertion. Multiple design iterations were developed using the same CAD software and 3D printer as the vacuum suction adaptor.

The nerve-holder for the fibrin sealant attachment approach was designed to allow fibrin to form around the implanted MINA region on the vagus nerve, as shown in Figure 4.1b. The nerve-holder had slots at the edges to secure the nerve in place. The center of the holder provided a contained space for a ~3.5 mm-diameter encapsulation of fibrin to form around the MINA-implanted region of the nerve. The detailed CAD design is shown in the Appendix C (Figure C.2).

49

The design of the nerve-holder for rose-bengal coated MINAs had a solid surface at the bottom of nerve trench to firmly secure the nerve in place, as shown in Figure 4.2c. A lens flap was added to the design to distribute the intensity of a laser beam across the surface area of the rose-bengal coated MINA. The holder contained circular magnets to secure the flap in an open or closed position. A flat surface that was perpendicular to the bottom surface of the nerve trench was designed to provide a benchmark surface for aligning the nerve-holder with the vacuum suction adaptor. This allowed accurate insertion of the MINA at the appropriate transverse and longitudinal angles along the vagus nerve. The dimensions of the nerve-holder (Figure C.3) and lens flap (Figure C.4) designs are shown in Appendix C.

4.3.5 Design of Nerve-Release Tool

The process of releasing a MINA-implanted vagus nerve from the nerve-holder required extremely accurate handling and could result in applying excess tension on the nerve that led to a MINA detaching from the nerve. Thus, a nerve-release tool that could be controlled precisely with a micromanipulator (KITE-R, World Precision Instruments, Sarasota, FL, USA) was designed to facilitate the release process, as shown in Figure 4.2d. The nerve-release tool has two extended rods that hold the MINA-implanted vagus nerve while the nerve-holder is separated and removed away from the nerve by accurately controlling a manipulator arm (51600, Stoelting Co., Wood Dale, IL, USA) that is connected to the nerve-holder. The dimensions of the nerve-release tool are shown in Appendix C Figure C.5.

4.3.6 Animal Surgery

All experimental procedures were approved by the University of Michigan Institutional Animal Care and Use Committee (IACUC). Experiments were performed on male (0.45-0.64 kg) and female (0.21-0.24 kg) Sprague-Dawley rats (Charles Rivers Laboratories, Wilmington, MA,

USA). One day prior to surgery, animals were injected subcutaneously with dexamethasone (0.2 mg/kg, VetOne, Boise, ID, USA). On the day of the procedure, a blood sample was obtained from a cut at the tip of the tail to measure blood glucose concentration with a glucometer (AlphaTRAK 2, Abbott, Abbott Park, IL, USA). Animals were anesthetized with isoflurane (1-5%, Fluriso, VetOne, Boise, ID, USA) and injected subcutaneously with carprofen (5 mg/kg, Rimadyl, Zoetis Animal Health, Parsippany, NJ, USA), lidocaine (0.4%, VetOne, Boise, ID, USA), and dexamethasone (0.2 mg/kg, VetOne, Boise, ID, USA). Rats were placed on a heating pad (ReptiTherm, Zoo Med Laboratories Inc., San Luis Obispo, CA, USA). Temperature and oxygen saturation (SpO2) were measured with a vitals-monitor (SurgiVet, Smiths Medical, Norwell, MA, USA). A midline cervical incision was made to access the cervical vagus nerve. Under a dissection microscope (Lynx EVO, Vision Engineering Inc., New Milford, CT, USA), the vagus nerve (8-10 mm in length) was isolated from the carotid artery and surrounding tissue. Using the dissection microscope camera, an image of the isolated vagus nerve next to a scale-bar ruler was captured in some experiments for later nerve strain calculations (described below).

4.3.7   Implantation of MINA with Fibrin Sealant

The MINA arrays for the fibrin sealant approach were cut to a dimension of 2x3 mm that provided sufficient surface area for fibrin to form on top of the MINA. In the animal procedure, the right cervical vagus nerve was lifted on the nerve-holder designed for the fibrin sealant approach. The MINA was held on a vacuum suction pen, which was accurately controlled by a micromanipulator (KITE-R, World Precision Instruments, Sarasota, FL, USA). A small pen-shaped camera (MS100, Teslong, Shenzhen, China) was positioned in the surgical opening to visualize alignment of the MINA needles with the vagus nerve. Once aligned, the MINA was inserted into the vagus nerve. Fibrin sealant (Evicel, Ethicon Inc., Somerville, NJ, USA) was

applied to surround the MINA-nerve interface. The fibrin sealant compounds of fibrinogen and thrombin were mixed at a 2:1 ratio (60-80 µL fibrinogen, 30-40 µL thrombin) using pipettes (Finnpipette F2, Thermo Fisher Scientific, Waltham, WA, USA) due to our desire for a stronger sealant than the recommended fibrin sealant formed at a 1:1 ratio mixture of fibrinogen and thrombin (Tse and Ko 2012). A duration of at least 5 minutes was provided for the fibrin sealant to form. The fibrin sealant was released from the suction adaptor and nerve-holder using fine forceps. The nerve, MINA and fibrin sealant encapsulation was encircled in most experiments by a nerve protector (~5 x 10 mm, AxoGuard, AxoGen, Alachua, FL, USA) made of porcine small intestinal submucosa (SIS), which is commonly used for tissue repair (Papatheodorou, Williams, and Sotereanos 2015; Mosala Nezhad et al. 2016). The purpose of the nerve protector (Figure 4.1d) was to promote connective tissue encapsulation, and stabilize the MINA on the nerve as the fibrin sealant gradually degraded. The encircling nerve protector was fastened with a suture knot (7-0 vicryl, Ethicon Inc., Somerville, NJ, USA). The cervical skin incision was closed with surgical clips (AutoClip, MikRon Precision Inc., Gardena, CA, USA) and triple antibiotic topical ointment (Actavis, Parsippany-Troy Hills, NJ, USA) was applied on the closed incision. A subcutaneous injection of carprofen (5 mg/kg) and dexamethasone (0.2-0.05 mg/kg) were administered daily after surgery for 2-3 days, and the animal's health was checked regularly. One week after the implant procedure, the incision clips were removed under isoflurane anesthesia. Body weight and blood glucose concentration were measured on a weekly basis.
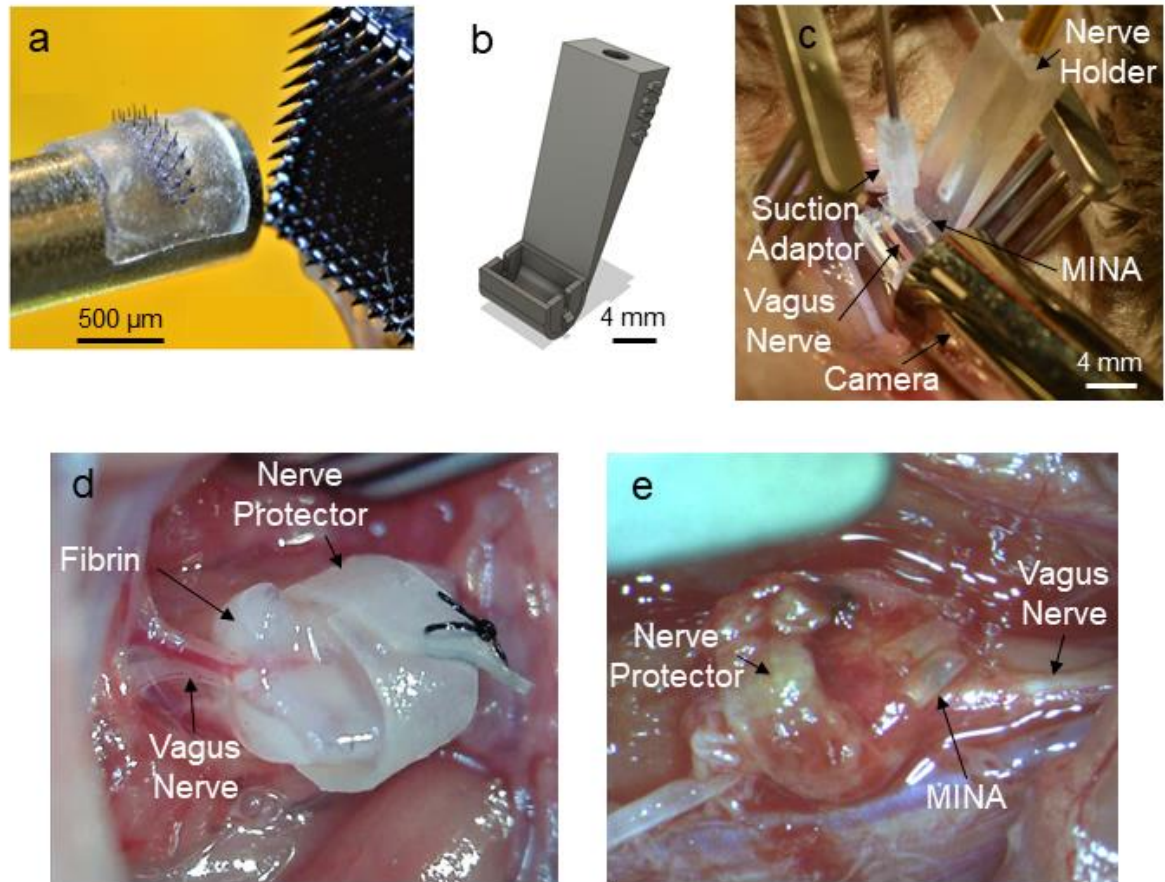
Figure 4.1 Implantation of microneedle nerve array (MINA) with fibrin sealant approach. (a) MINA with 3x8 needle configuration next to a high-density Utah slanted electrode array. (b) Nerve-holder design for fibrin sealant approach. Design dimensions are shown in Appendix C Figure C.2. (c) Surgical setup for implantation of MINA. (d) MINA-implanted vagus nerve surrounded by fibrin and a nerve protector at the implant procedure of rat FA. (e) MINA-implanted vagus nerve at the terminal procedure of rat FA.

4.3.8 Implantation of Rose-Bengal Coated MINA

Similarly to the fibrin sealant approach, the MINA was held on a vacuum suction adaptor that was controlled by a micromanipulator. The left cervical vagus nerve was placed in the nerve trench of a rose-bengal nerve-holder, which was connected to a manipulator arm (51600, Stoelting Co., Wood Dale, IL, USA). The left vagus nerve was targeted in these animals to facilitate a modified implantation setup, which was secured on an optical breadboard (MB1218, Thorlabs Inc., Newton, NJ, USA), as shown in Figure 4.2e. The vacuum suction adaptor and nerve-holder were

aligned together. The MINA was accurately aligned and aimed towards the nerve using a pen-camera (Figure 4.2e, f). The nerve was rinsed with saline (0.9% NaCl, Nurse Assist Inc., Haltom City, TX, USA), and the excess fluid around the nerve was removed with an absorbent triangle (18105-03, Fine Science Tools Inc., Foster City, CA, USA). The initial temperature of the nerve was measured with an infrared sensor (IRT0421, Kintrex, Vienna, VA, USA). The MINA was inserted in the vagus nerve (Figure 4.2g) and the lens flap of the nerve-holder was closed on the MINA-nerve interface. The rose-bengal adhesion coating was activated by applying a green laser beam (532 nm, 85 mW, 0.8 mm beam-diameter, Civil Laser, Hangzhou, China) for 6 minutes on the lens, which distributed the intensity of the beam across the MINA (Figure 4.2h). The lens flap was removed and the temperature of the nerve was measured again with the infrared sensor to calculate the difference in nerve temperature [Δ Nerve Temperature = Nerve Temperature (Post-Laser) – Nerve Temperature (Pre-Laser)]. The vagus nerve was released from the nerve holder using the nerve-release tool (Figure 4.2i). In experiments with a captured image of the nerve immediately after the isolation process, another image was captured of the MINA-implanted vagus nerve to assess the nerve strain caused by the implantation procedure. The length of the whole isolated nerve was measured using an image analysis software (ImageJ, National Institute of Health, Bethesda, MD, USA) and the nerve strain was calculated with the following equation: Nerve Strain = [Nerve Length (Post-Implant) – Nerve Length (Pre-Implant)] / Nerve Length (Pre-Implant) x100. The cervical skin incision was closed with surgical clips and triple antibiotic topical ointment was applied along the closed incision. A subcutaneous injection of carprofen (5 mg/kg) and dexamethasone (0.2-0.05 mg/kg) were administered daily after surgery for 2-3 days, and the animal's health was checked regularly. One week after the implant procedure, body weight and blood glucose concentration were measured, and the surgical clips were removed from the incision

under isoflurane anesthesia. Sham animals underwent procedures that were identical to the implantation procedure but without a MINA. No implantation procedures were performed on the control animals.
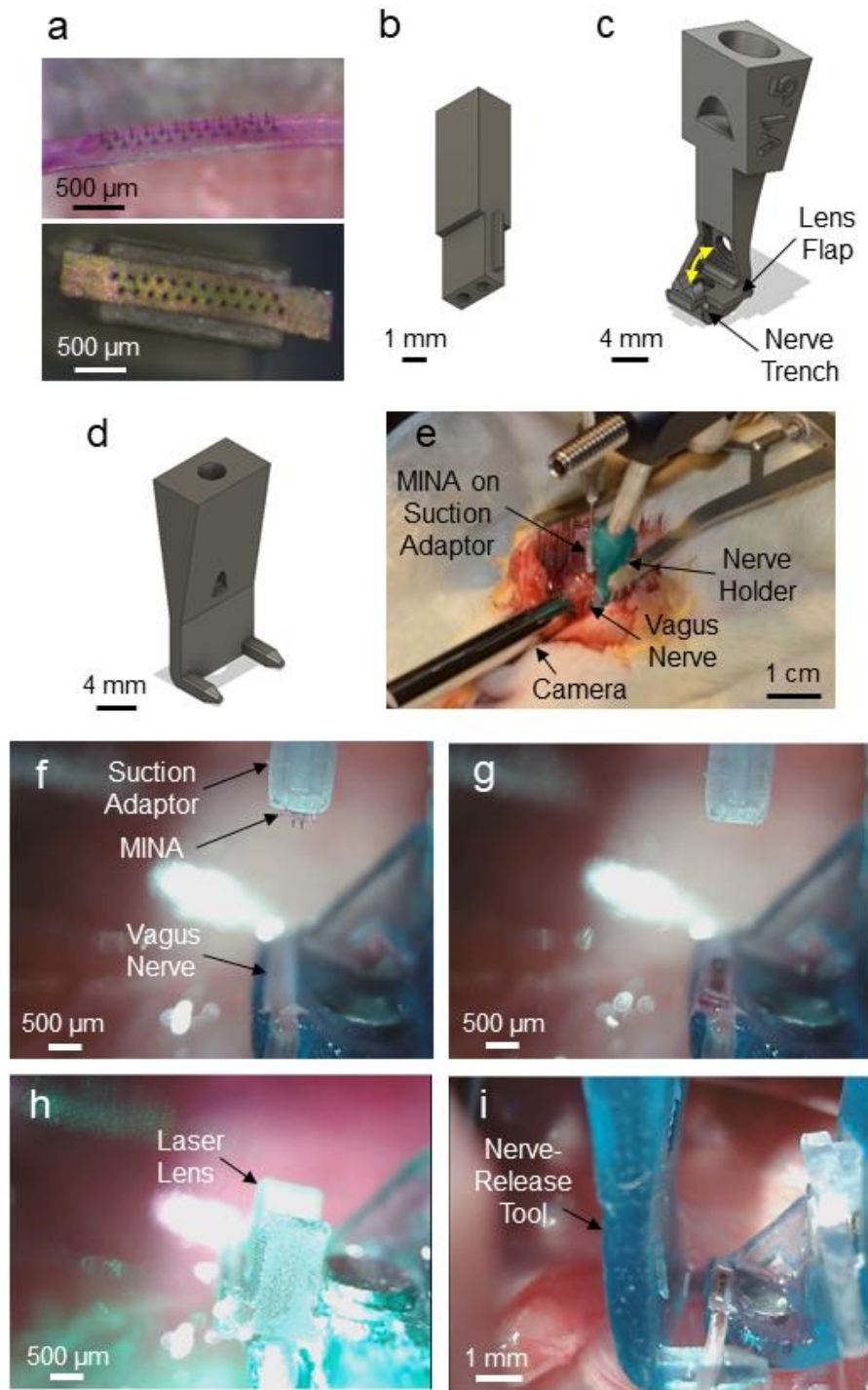
Figure 4.2 Implantation of rose-bengal coated MINA. (a) Rose-Bengal coated MINA with 2x12 needle configuration. MINA centered on vacuum suction adaptor (bottom). (b) Design of vacuum suction adaptor. Design dimensions are shown in Appendix C Figure C.1. (c) Nerve-holder design for rose-bengal coated MINA. Yellow arrow shows movement path of lens flap. Dimensions of the design are shown in Appendix C Figure C.3 and 4. (d) Design of nerve-release tool. Dimensions of the design are in Appendix C Figure C.5. (e) Surgical setup for implantation. (f) View from pen-shaped camera for aligning MINA with the vagus nerve. (g) MINA inserted in the vagus nerve. (h) Placement of lens flap and activation of rose-bengal coating with green laser. (i) Release of MINA-implanted vagus nerve from the nerve-holder using the nerve-release tool.

4.3.9 Terminal Procedure

Terminal procedures were performed on all animals to assess nerve condition and extract the vagus nerve. The cervical vagus nerve was accessed similarly to the implant procedure. To assess nerve condition, an electrophysiology test was performed (Figure 4.3a and b). A stimulation probe (017509, Natus Neuro, Middleton, WI, USA) was placed on the vagus nerve proximal to the implant region and connected to an isolated pulse generator (Model 2100, A-M Systems, Loop Sequim, WA, USA). Electrical stimulation (1-10 mA, 2 Hz, 200 μs pulse-width) was applied to evoke neural activity that was recorded with a data acquisition system (PowerLab, ADInstruments, Sydney, Australia) through a bipolar cuff electrode (0.75 mm inner-diameter, 0.5 mm contact separation, Microprobes for Life Science, Gaithersburg, MD, USA) that was placed on the nerve distal to the implant region. The neural recordings were analyzed using MATLAB (R2014b, MathWorks, Natick, MA, USA) to determine the stimulation amplitude threshold, and the conduction velocity for each peak of the evoked responses.

Animals were euthanized with an overdose of sodium pentobarbital (400 mg/kg, Euthanasia Solution, VetOne, Boise, ID, USA). The vagus nerve was extracted and soaked in 3% glutaraldehyde overnight (12-20 hours) and stored in 0.15 M cacodylic acid for at least 24 hours. The body weight, blood glucose concentration, and electrophysiology stimulation threshold values for each group did not follow a normal distribution (confirmed with Kolmogorov-Smirnov test). To test for statistical significance, two-sided Wilcoxon rank sum tests were performed between the data set values of MINA-implanted and sham animals using MATLAB. Statistical significance was considered at $p < 0.05$. Summary data are presented as mean ± standard deviation (SD).
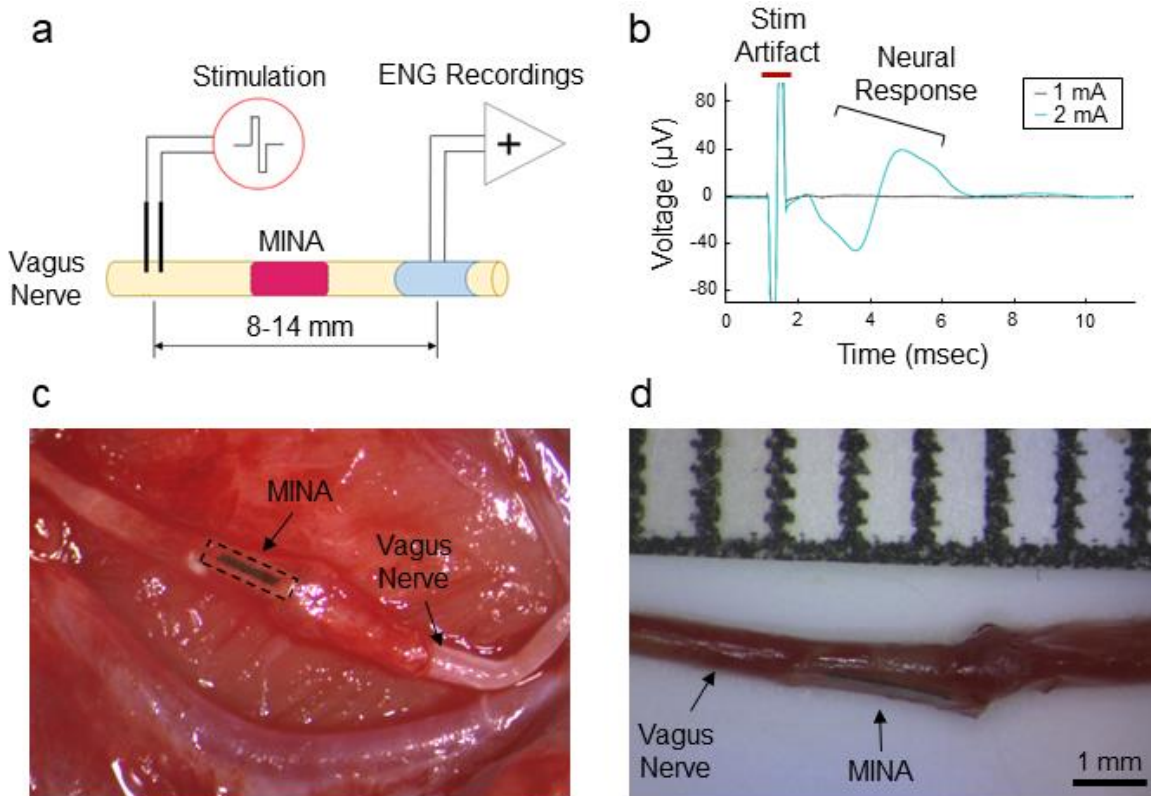
Figure 4.3 Electrophysiology testing and nerve extraction at a terminal procedure. (a) Setup diagram for electrophysiology testing. (b) Stimulation-evoked neural responses in Rat FB. (c) Isolation (top-down view) and (d) extraction (side view) of MINA-implanted vagus nerve at the 1-week terminal procedure of rat RC.

4.3.10 3D Microscopic Computed Tomography Imaging

The vagus nerve samples were stained with osmium-tetroxide and imaged using a 3D microscopic computed tomography (micro-CT) scanner (Xradia 520 Versa, Zeiss, Oberkochen, Germany) at the Michigan Center for Materials Characterization at the University of Michigan. The samples were prepared in pipette tips (10 μL barrier tip, Thomas Scientific, Swedesboro, NJ, USA) filled with phosphate-buffered saline (PBS), sealed with laboratory parafilm (Parafilm M, Bemis Company Inc., Oshkosh, WI, USA), and placed on a rotating platform. The micro-CT device scanned the nerve samples at 30 kV, 2 W, with an exposure time of 1.8-3.0 sec for a single scan, and resolution of 1.7-5.5 μm/pixel. The total number of scans for each sample was 1601

projections with a 360° platform rotation. The images were visualized with a 3D-analysis software (Dragonfly Pro, Objective Research Systems Inc., Montreal, Canada) and 2D cross-section segmentations along the nerve were exported with an image thickness of 1.7-5.5 μm. From these segmentation images and using an image analysis software (FIJI, ImageJ, National Institute of Health, Bethesda, MD, USA) (Schindelin et al. 2012), the perimeter of the nerve fascicle (bundle of axons) was specified from the micro-CT image (L. Yan et al. 2017) for the software to compute the fascicle area. Additionally, the shortest distance of each MINA needle tip to the fascicle region was determined.

4.4   Results

We performed a total of 32 experiments: 7 animals were implanted with MINAs using the fibrin sealant approach, 16 animals were implanted with rose-bengal coated MINAs, 6 animals had sham rose-bengal procedures, and 3 were control animals.

4.4.1   Implantation of MINA with Fibrin Sealant

We implanted 7 animals with MINA arrays using the fibrin sealant approach (Table 4.1). The animals were terminated at either 4 weeks (n=5) or 8 weeks (n=2). The MINAs were mostly found away from the nerve (e.g. Figure 4.1e) but the animals recovered well from the implantation procedures based on body weight and blood glucose concentration measurements. The electrophysiology testing on the MINA-implanted nerves confirmed that the nerves were relatively healthy, based on the observed stimulation-evoked neural responses.

Table 4.1 Summary of animals implanted with the fibrin sealant approach.

Rat ID	Implant			Terminal			Electrophys. Test	
	Weight (kg)	Blood Gluc. (mg/dL)	Nerve Protector	Weight (kg)	Blood Gluc. (mg/dL)	MINA Substrate	Stim. Thres. (mA)	Cond. Vel. (m/s)
4-Week Implant								
FA	0.24	150	Yes	0.28	115	On nerve but away from nerve protector	Not performed	
FB	0.21	111	Yes	0.28	124	Within nerve protector encapsulation	2	2.4-8.2
FC	0.25	150	No	0.28	124	Away from nerve	Not performed	
FD	0.23	121	No	0.25	118	Within fibrin encapsulation but away from nerve	1	2.1-4.3
FE	0.24	126	Yes	0.29	98	Within nerve protector encapsulation but away from nerve	2	2.8-3.7
Mean ± SD	0.23 ± 0.02	131.6 ± 17.6	-	0.28 ± 0.02	115.8 ± 10.7	-	1.7 ± 0.6	-
8-Week Implant								
FF	0.24	112	Yes	0.29	98	Within nerve protector encapsulation. Micro-CT showed needles were close but not in fascicle	1	2.1-7.6
FG	0.24	151	Yes	0.33	112	Within nerve protector encapsulation	2	3.2-6.5
Mean ± SD	0.24 ± 0.00	131.5 ± 27.6	-	0.31 ± 0.03	105.0 ± 9.9	-	1.5 ± 0.7	-

4.4.2 Implantation of Rose-Bengal Coated MINA

We implanted 16 animals with rose-bengal coated MINAs. The animals were terminated at either 1 week (n=8; e.g. Figure 4.3c and d; Table 4.2) or 6 weeks (n=8; Table 4.3). One of the 6-week implanted animals expired unexpectedly at 4.5 weeks (rat RY), and was not included in further analysis. Sham implant procedures were performed on animals which were terminated at 1 week (n=5) or 6 weeks (n=3), and terminal procedures were performed on control animals (n=3; Table 4.4). No statistical significance occurred between the MINA-implanted and sham animals for body weight, blood glucose concentration and stimulation threshold values.

Table 4.2 Summary of 1-week rose-bengal coated MINA-implanted and sham procedure animals.

Rat ID	Implant				Terminal			Electrophys. Test	
	Weight (kg)	Blood Gluc. (mg/dL)	Δ Nerve Temp (°C)	Nerve Strain (%)	Weight (kg)	Blood Gluc. (mg/dL)	MINA Substrate	Stim. Thres. (mA)	Cond. Vel. (m/s)
1-Week Implant									
RA	0.44	137	NR	NR	0.45	97	Attached to nerve	2	4.0-7.0
RB	0.44	102	NR	NR	0.40	107	Attached to nerve	2	1.8-11.0
RC	0.55	100	0.4	NR	0.50	104	Attached to nerve	2	3.8-9.1
RD	0.57	118	-0.1	NR	0.54	NR	Attached to nerve	3	3.1-4.9
RE	0.58	101	1.1	NR	0.54	NR	Attached to nerve	2	2.6-4.1
RQ	0.53	155	1.5	9.5	0.51	105	Partially attached to nerve	5	2.4-4.7
RS	0.56	162	1.9	4.7	0.51	114	Attached to nerve	4	2.6-3.3
RZ	0.64	166	4.4	3.5	0.58	140	Detached from nerve	10	2.1-7.4
Mean ± SD	0.54 ± 0.07	130.1 ± 28.4	1.5 ± 1.6	5.9 ± 3.2	0.50 ± 0.06	111.2 ± 15.1	-	3.8 ± 2.8	-
1-Week Sham									
RF	0.60	148	2.7	NR	0.54	109	–	1	2.3-7.0
RH	0.45	97	1.2	NR	0.42	NR	–	high noise	
RR	0.53	142	1.4	8.9	0.51	92	–	2	3.2-9.2
RT	0.56	104	0.7	2.7	0.53	141	–	1	2.3-4.7
RU	0.58	138	2.3	1.1	0.54	112	–	2	3.2-3.6
Mean ± SD	0.54 ± 0.06	125.8 ± 23.5	1.7 ± 0.8	4.2 ± 4.1	0.51 ± 0.05	113.5 ± 20.3	–	1.5 ± 0.6	-
Implant vs Sham									
p	0.76	0.83	-	-	0.80	0.76	-	0.06	-

NR: the value was not recorded.

Table 4.3 Summary of 6-week rose-bengal coated MINA-implanted and sham procedure animals.

Rat ID	Implant				Terminal			Electrophys. Test	
	Weight (kg)	Blood Gluc. (mg/dL)	Δ Nerve Temp (°C)	Nerve Strain (%)	Weight (kg)	Blood Gluc. (mg/dL)	MINA Substrate	Stim. Thres. (mA)	Cond. Vel. (m/s)
6-Week Implant									
RG	0.45	103	0.8	NR	0.62	99	Attached to nerve	1	3.4-5.7
RI	0.45	146	1.0	NR	0.53	109	Attached to nerve	high noise	
RK	0.45	112	-0.3	NR	0.58	109	Attached to nerve	2	3.9-10.0
RL	0.43	111	0.3	NR	0.55	109	Detached from nerve	1	2.3-6.7
RO	0.59	113	0.2	8.3	0.62	137	Detached from nerve	4	2.6-7.8
RW	0.49	109	1.7	6.2	0.62	91	Detached from nerve	2	3.8-7.4
RX	0.54	150	1.1	3.4	0.63	130	Attached to nerve	2	3.0-8.8
RY*	0.57*	125*	4.9*	2.8*	0.64*	-	Attached to nerve but expired early at 4.5 weeks	-	-
Mean ± SD	0.49 ± 0.06	120.6 ± 19.1	0.7 ± 0.7	5.9 ± 2.4	0.59 ± 0.04	112.0 ± 16.3	-	2.0 ± 1.1	-
6-Week Sham									
RM	0.46	137	1.1	NR	0.55	NR	-	2	1.6-5.0
RN	0.60	132	1.2	1.7	0.66	118	-	1	3.5-4.8
RP	0.47	151	-0.7	1.5	0.55	119	-	3	3.1-10.6
Mean ± SD	0.51 ± 0.08	140.0 ± 9.8	0.5 ± 1.0	1.6 ± 0.1	0.59 ± 0.06	118.5 ± 0.7	-	2.0 ± 1.0	-
Implant vs Sham									
p	0.50	0.13	-	-	0.95	0.50	-	1.00	-

NR: the value was not recorded.

* Animal expired early (4.5 weeks) and values are not included in summary statistics.

Table 4.4 Summary of control animals.

Rat ID	Weight (kg)	Blood Gluc. (mg/dL)	Electrophys. Test	
			Stim. Thres. (mA)	Cond. Vel. (m/s)
RJ	0.45	NR	high artifacts	
RV	0.59	104	3	5.7
RAA	0.58	125	2	3.6-8.9
Mean ± SD	0.54 ± 0.08	114.5 ± 14.9	2.5 ± 0.7	-

NR: the value was not recorded.

4.4.3 3D Microscopic Computed Tomography Imaging

From the segmentation micro-CT images of animals implanted with rose-bengal coated MINAs, the distance between the tip of each needle and the nerve fascicle was determined. The rose-bengal coated MINAs had a needle configuration of 2 columns, with 12 needles in each column. We noticed that typically one column was longitudinally centered with the nerve (e.g. Figure 4.4b) while the other column was misaligned (e.g. Figure 4.4c). Therefore, the average distance for the aligned and misaligned columns of each animal were separately determined (Figure 4.4d). At least one column was in close proximity ($\leq$ 50 µm) to the nerve fascicle in 75% of the animals terminated at 1 week and 14% of the animals terminated at 6 weeks. The average fascicle area for the MINA-implanted, sham and control nerves are shown in Figure 4.4e.

4.5 Discussion

We developed a novel intraneural Microneedle Nerve Array (MINA), and formed an innovative procedure for the chronic implantation of the array in small-diameter (300-500 µm) rat vagus nerves. We investigated two attachment approaches to secure the implanted MINA (fibrin sealant and rose-bengal bonding), assessed the attachment approaches by determining the proximity of the MINA to the nerve, and evaluated the nerve condition by testing for stimulation-evoked neural responses. Our results suggest that a future functional rose bengal-bonded MINA will have excellent promise for yielding high-fidelity neural signals through one week of implant and near-nerve signals through six weeks. The chronic implantation of fully-functional intraneural arrays in autonomic nerves will provide novel insights in physiological neural signaling that regulate autonomic functions, which may assist in the development of new treatment modalities to restore these vital functions.
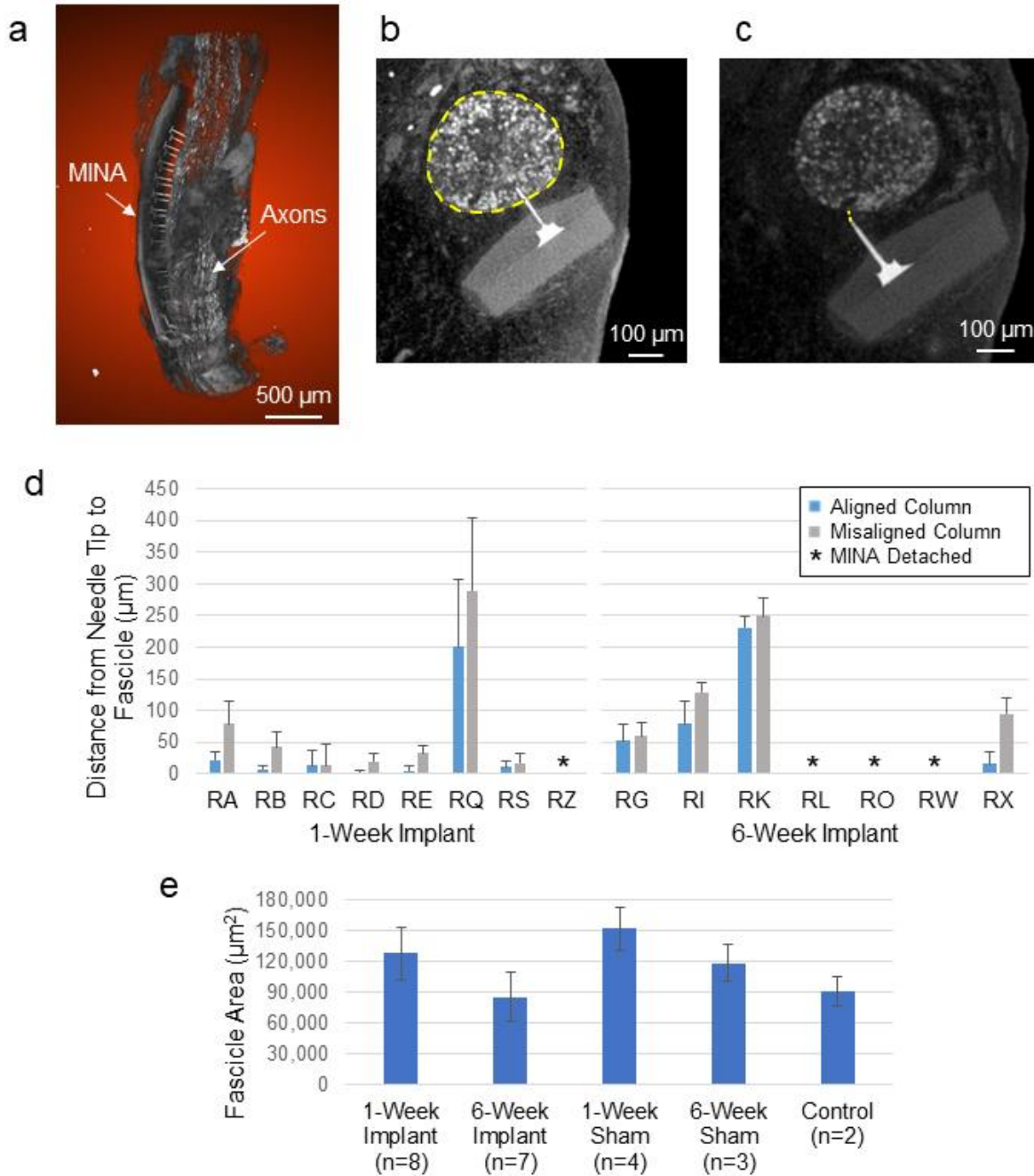
Figure 4.4 Microscopic Computed Tomography (Micro-CT) imaging of MINA-implanted, sham and control vagus nerves. (a) Reconstructed 3D image of 1-week implanted MINA attached to the vagus nerve in rat RB. (b) Cross-section segmentation image of MINA needle in the vagus nerve fascicle of rat RD. Highlighted in yellow is the perimeter of the fascicle (fascicle area = 107314.4 μm^2). (c) Segmentation image of MINA needle from a misaligned column, which was 21.1 μm from the nerve fascicle in rat RD. (d) Average distance to nerve fascicle for aligned and misaligned needle columns in each MINA-implanted animal. Each rose-bengal coated MINA has 2 columns, with 12 needles in each column. Error bars show standard deviation. (e) Average fascicle area for MINA-implanted, sham and control nerves. Error bars show standard deviation.

Animals were implanted with non-wired MINA arrays with fibrin sealant to secure the interface, or MINAs with an innovative adhesive rose-bengal coating. The fibrin sealant approach failed to secure the MINA-nerve interface for 4- and 8-week implant durations. The rose-bengal coating approach was successful in maintaining MINA needles with close proximity to the axons ($\leq 50\,\mu m$) for 1-week and 6-week implants in 75% and 14% of the implanted animals, respectively (Figure 4.4d). We monitored the body weight, blood glucose concentration and performed electrophysiology testing for rose-bengal MINA-implanted and sham (implant procedure with no MINA) animals to assess the animal and nerve condition. The body weight changes ($-6.3 \pm 4.0\%$ at 1 week, $+22.9 \pm 10.6\%$ at 6 weeks) and blood glucose concentration measurements (111.2 ± 15.1 mg/dL at 1 week, 112.0 ± 16.3 mg/dL at 6 weeks) were within previously reported ranges for vagus nerve sham procedures (Hao et al. 2014; Chambers et al. 2011), and there was no statistical difference between the MINA-implanted and sham animals (Table 4.2 and Table 4.3). The conduction velocities of the evoked responses were within the range of myelinated Aδ and B fibers, and unmyelinated C fibers, which are all present in the rat cervical vagus nerve (Qing et al. 2018; Waataja, Tweden, and Honda 2011).

Intraneural electrodes for peripheral nerves provide superior selectivity than extraneural electrodes, and are considerably less invasive than regenerative electrodes (Micera and Navarro 2009; Spearman et al. 2018). We demonstrated the chronic implantation of a non-wired intraneural electrode array in a fine autonomic nerve (diameter ≤ 0.5 mm). Multiple intraneural electrodes have been implanted in somatic or large autonomic nerves (diameter ≥ 1 mm) (Wark et al. 2014; Mathews et al. 2014; Byun et al. 2017), but only a few were developed for fine autonomic nerves. Carbon nanotube (CNT) electrodes (McCallum et al. 2017) were chronically implanted in fine autonomic nerves (diameter of 100-300 µm), but a relatively-large tungsten needle (diameter ≥ 75

µm) was used to insert each of the two single-channel CNT electrodes in a nerve target. A carbon fiber array (Gillis et al. 2018) was directly inserted in a fine autonomic nerve (diameter of 125 µm), but was only demonstrated in an acute setup. Securing a multi-channel array in a small-diameter autonomic nerve is extremely challenging due to the fine structure of autonomic nerves. We assembled a new implantation procedure that involved the design of a vacuum suction adaptor to handle the array, nerve-holder to facilitate the array insertion process, and nerve-release tool to accurately relocate the implanted nerve. The MINA array was inserted directly into a rat vagus nerve (diameter of 300-500 µm) with a manual micromanipulator, without a shuttle or high-pressure insertion tool (e.g. tungsten needle for CNT electrode, pneumatic inserter for Utah array). The procedure also incorporated an innovative attachment approach to secure the array interface by applying a rose-bengal coating on the MINA, which promotes crosslink bonding between collagen fibers in the MINA coating and nerve once activated with a laser (Figure 4.2). These implantation components are easily adjustable and may be useful for implanting other electrodes in or on various nerves across the peripheral nervous system or to attach devices to other locations such as on organ surfaces.

The rose-bengal coated MINAs remained attached to the vagus nerve in 47% of the overall implanted animals. However, there was a clear discrepancy in the attachment success rate (needle proximity ≤ 50 µm) of 1-week (75%) and 6-week (14%) rose-bengal MINA implanted animals. The close proximity of the MINA needles to axons at 1 week was highly encouraging. A previous study followed the tissue response (infiltration of microphages and tissue encapsulation) to longitudinal-intrafascicular electrode (LIFE) implants in rat sciatic nerves from 1 day to 8 months, and reported that the tissue response gradually increased and reached a peak at 2 weeks (de la Oliva, Navarro, and del Valle 2018). Therefore, we anticipated the MINA-implants that endured

the tissue response for 1 week would overcome the peak tissue response and appear stable at 6 weeks. However, the difference in the MINA design may have led to a different outcome than the LIFE electrode implants. Another study investigated the implantation of a non-wired high-density Utah slanted electrode array (HD-USEA) in rat sciatic nerves for 4 and 8 weeks (Wark et al. 2014). Although the majority (80%) of the implanted arrays had electrodes with close proximity ($\leq$ 100 µm) to axons, sensorimotor deficits were observed in most of the rats and "waffle-like" tissue damage was clearly visible on the extracted nerves. This was likely due to the large size of these electrodes (shank diameter of ~70 µm at 50% from the tip) compared to the axon diameters (1-11 µm) in the implanted sciatic nerves (Wark et al. 2013; 2014). The HD-USEA was implanted in a relatively large sciatic nerve (overall diameter of 1-2 mm) and also encircled with a nerve protector that attracted encapsulation tissue to secure the implanted array, which may explain their excellent attachment success rate. Encircling this nerve protector around a rose-bengal coated MINA, or coating the outer surface of a MINA with the same material as the nerve protector may lead to improved outcomes for long-term MINA implants.

Modifications to the implantation procedure of rose-bengal coated MINAs also may lead to an improved success rate. First, refinement of the alignment process between the MINA and nerve would provide more interface surface area for rose-bengal adhesion to occur and firmly secure the MINA. The difference in the proximity-distance of aligned and misaligned needle-columns (Figure 4.4d) shows the need for this adjustment. The alignment may be improved by using higher-resolution cameras from multiple angles but must overcome the limited space in the rat cervical cavity. Second, developing an advanced nerve-holder integrated with a precise MINA insertion process may eliminate the need for elevating the nerve and would reduce the observed strain on the nerve (Table 4.2 and Table 4.3). Although the strain in nerves implanted with rose-

bengal coated MINAs (5.9 ± 2.5%) was within the tolerable limit (~12%) for peripheral nerve function (Wall et al. 1992), this may have compromised the structure of the nerve and reduced our chronic attachment success. The nerve-holder designed in this study was necessary to position a camera and visualize the MINA-nerve interface during insertion but could be upgraded with further design advancements. Third, the MINA had a substrate layer of polydimethylsiloxane (PDMS), which was selected for its biocompatible and flexible features (Park et al. 2014). We observed in later benchtop testing (data not shown) that a polyurethane (PU) substrate, which could be formed to have similar biocompatible and flexible features as PDMS (Singhal et al. 2012), enhanced rose-bengal bonding strength to a nerve. However, replacing the PDMS substrate with PU would require substantial modifications in the MINA fabrication process.

Although the chronically-implanted MINAs in this study were not functional and had no connection wires, the close proximity of the MINA needles to the axons is highly encouraging. A study in the rat hippocampus showed that neural recordings from an electrode that had a distance of 50 μm or less from a neuron were detectable and separable from the activity of other nearby neurons (Henze et al. 2000). Although the source of neural signals in the hippocampus are mainly from neuron cell bodies, which generate larger-amplitude waveforms than axons in peripheral nerves, a close proximity with functional intraneural MINAs may provide novel insights into axonal recordings from the vagus nerve. The motor and sensory fibers of the vagus nerve innervate multiple critical organs, such as the heart, lungs, liver, stomach and pancreas, and convey neural signals that regulate numerous essential autonomic bodily functions (Berthoud and Neuhuber 2000; Browning, Verheijden, and Boeckxstaens 2017; Waise, Dranse, and Lam 2018; Masi et al. 2019). This information would likely help us better understand physiological vagal signaling, and may allow us to study the changes in signaling as certain diseases progress, which may help us

provide improved treatments for patients suffering from these diseases. Furthermore, the vagus nerve is an important target in bioelectronic medicine (Pavlov and Tracey 2019), and an improved electrode interface with this nerve would immensely benefit this emerging class of therapies.

This work demonstrated the chronic implantation of an intraneural array in a small-diameter autonomic nerve, but had numerous limitations. The implanted MINAs were non-functional devices and were not fabricated with a connection setup for signal recording. While connection components will be necessary for neural recording studies, a primary objective of this study was to evaluate the nerve condition in response to the array itself, similar to studies that evaluated the tissue response to other electrodes (de la Oliva, Navarro, and del Valle 2018; Wark et al. 2014). Further work is needed to demonstrate the fabrication and recording-capabilities of fully functional MINAs as well as to assess the progression of the tissue response in chronic implants over time. The fibrin sealant approach was unsuccessful in maintaining the MINA attachment to the nerve. A possible reason for this failure is the large width of the MINA substrate (2 mm) in the fibrin sealant implants, compared to the small diameter of the vagus nerve (300-500 µm). This may have facilitated the migration of the MINA as the fibrin degraded and connective tissue formed between the MINA and nerve. Reducing the width of the MINA substrate closer to the nerve diameter, as we did with the rose-bengal coated MINA, may lead to better array attachment outcomes with the fibrin sealant approach. Another limitation was the recorded temperature increase at the surface of nerves implanted with rose-bengal coated MINAs (1.1 ± 1.2°C) due to the laser exposure. To mitigate this issue, we designed the nerve-holder lens flap (Figure 4.2c) to distribute the laser beam and dissipate the generated heat. Despite this residual increase in nerve temperature, all the nerve temperature measurements before and after the laser exposure (26-35°C) were within a functional range for peripheral nerves (over 50% of normal

conduction velocity at 24-37°C) (Paintal 1965; Rasminsky 1973). An additional limitation was the termination of animals implanted with rose-bengal coated MINAs at only two timepoints (1 week and 6 weeks). As mentioned earlier, we anticipated the peak tissue response to occur at 2 weeks and aimed to assess the implant condition before and after this peak response. Further studies of chronic implants with multiple terminal timepoints and thorough histological analysis are needed to evaluate the progression of tissue reactivity surrounding this novel MINA array.

The complete development of a multi-channel intraneural array suitable for chronic implantation in fine autonomic nerves will provide a valuable research tool for the advancement of neuroscience. Monitoring neural signals in autonomic nerves will help us better understand the physiological communication between the nervous system and innervated organs to regulate essential bodily functions. This may assist in identifying signal patterns that can potentially restore these regulatory functions, and provide an innovative treatment modality for patients with neurological deficiencies.

4.6   Conclusion

We developed a novel intraneural, multi-channel Microneedle Nerve Array (MINA), and assembled an innovative approach for the chronic implantation of the array in the rat vagus nerve. We are, to the best of our knowledge, the first to chronically implant an intraneural electrode array in a fine autonomic nerve (diameter ≤ 0.5 mm). The complete development of such array will provide a valuable research tool for studying the neural signaling in autonomic nerves, which regulate a variety of essential bodily functions. Further work is needed to demonstrate the neural recording capabilities of functional MINA and to evaluate the chronic tissue reactivity surrounding this novel intraneural array at different timepoints.

4.7 Acknowledgements

Chapter 5: Intraneural Recordings in Rat Vagus Nerves Using Carbon Fiber Microelectrode Arrays

5.1 Abstract

Autonomic nerves are essential in the regulation of many vital organs in the body. Recording physiological neural signals from autonomic nerves is very challenging due to the small nature of these nerves and the low-amplitude signals from their small axons. Our research group has developed a multi-channel, intraneural carbon fiber microelectrode array (CFMA), which has demonstrated high signal-to-noise ratio (SNR) recordings in the brain. We hypothesized that CFMA can obtain physiological recordings with high SNR in a small, peripheral autonomic nerve. In this study, we inserted CFMA in the cervical vagus nerve of 22 isoflurane-anesthetized rats. We recorded physiological neural activity, determined propagation direction and conduction velocity of vagal signals, and monitored changes in vagal activity in breathing and blood glucose modulated conditions. We observed neural activity on 167 out of 326 inserted functional carbon fibers, and sorted 1-2 neural clusters on each carbon fiber with activity. The mean peak-to-peak amplitudes of the sorted clusters were 15.1-91.7 µV with SNR of 2.0-7.0. We detected propagation of vagal signals in the afferent direction at conduction velocities of 0.7-1.0 m/sec (n=10), and efferent signals at 0.7-8.8 m/sec (n=5), which are within the conduction velocity range of myelinated and unmyelinated vagus fibers. We observed vagal signals with periodic firing-burst behavior at an average repetition rate of 39.4 ± 10.8 cycles/min, which was similar to the measured average

breathing rate of 39.3 ± 9.9 breaths/min (n=6). We modulated breathing rates by increasing anesthesia depth (n=3) and observed reduced firing-burst behavior at repetition rates (19.1 ± 10.3 cycles/min) similar to the reduced breathing rates (20.0 ± 8.0 breaths/min). Recorded neural activity were sorted into 174 clusters. The firing rates of these clusters showed moderate or high correlation coefficients ($|\rho| \geq 0.3$) with one (n=16), two (n=35), or all three (n=95) of the measured physiological parameters (blood glucose concentrations, breathing rate, and heart rate). Overall, our experiments demonstrated CFMA as a viable multi-channel intraneural electrode array for autonomic nerves. Further work is needed to refine the selectivity of CFMA and validate CFMA recordings in various autonomic nerves. This work is a milestone towards the comprehensive understanding of physiological signaling in autonomic nerves, which may lead to the development of innovative treatment modalities for restoring autonomic functions.

5.2 Introduction

The autonomic nervous system has a major role in the regulation of unconscious functions that are essential to the body. The system is divided into the sympathetic nervous system, which controls "fight-or-flight" responses, and the parasympathetic nervous system, which regulates "rest-and-digest" functions (McCorry 2007). A main parasympathetic nerve is the vagus nerve, which innervates many visceral organs, such as the heart, lungs, stomach, liver, pancreas and intestines (Agostoni et al. 1957; Andrews 1986), and contributes to the regulation of numerous autonomic functions, which include breathing, immune responses, digestion, glucose metabolism and others (Berthoud and Neuhuber 2000; Borovikova et al. 2000; Browning, Verheijden, and Boeckxstaens 2017; Berthoud 2008; Waise, Dranse, and Lam 2018). The vagus nerve at the cervical level is partially composed of myelinated Aδ and B fibers (Qing et al. 2018; Kajekar et al. 1999), but the great majority of axons (over 80%) are unmyelinated C-fibers (Hoffman and

73

Schnitzlein 1961; Evans and Murray 1954; Agostoni et al. 1957). These fibers predominantly convey afferent (sensory) signals from the innervated organs to the central nervous system (Foley and DuBois 1937).

A class of therapies that has gained considerable interest in recent years is bioelectronic medicine, which targets autonomic nerves to detect and alter neural activity for restoring autonomic functions (Tracey 2014; Birmingham et al. 2014; Pavlov and Tracey 2019). The variety of bioelectronic medicine applications that target the vagus nerve have led to clinical trials on vagus nerve stimulation (VNS) for patients with epilepsy (Ben-Menachem 2002), stroke (Dawson et al. 2016), depression (Spindler et al. 2019), rheumatoid arthritis (Koopman et al. 2016), obesity (Apovian et al. 2017), and type-2 diabetes (Shikora et al. 2015), among others. Despite the therapeutic benefits of VNS and bioelectronic medicine, stimulation patterns are generally selected by experimenting with different parameters without monitoring the physiological signaling in the nerve. A key element that is needed to achieve the full potential of bioelectronic medicine is a better understanding of neural signaling in normal and triggered physiological conditions.

Recording neural activity from autonomic nerves is very challenging due to the often sub-millimeter nature of these nerves and the low-amplitude waveforms generated from small unmyelinated C-fibers that dominate autonomic nerves. Studies have applied electrical stimulation on autonomic nerves to record evoked neural activity using extraneural electrodes, which record from outside the nerve (Qing et al. 2018; Ward et al. 2015), and intraneural electrodes, which penetrate the nerve (Gillis et al. 2018). Although evoked responses like these can be useful in determining the type of activated fibers, these responses do not represent physiological neural signaling. Research groups have obtained physiological neural recordings from autonomic nerves using extraneural cuff electrodes (Silverman et al. 2018; Zanos et al. 2018; Shikano et al. 2019;

González-González et al. 2018). A study decoded vagal signals using cuff electrodes to predict blood glucose levels at hypoglycemic (reduced blood glucose) conditions (Masi et al. 2019). However, extraneural electrodes lack spatial selectivity, as these electrodes record the compound activity of hundreds to thousands of axons from outside the nerve. Intraneural electrodes penetrate the nerve to be closer to axons and provide better selectivity and higher signal-to-noise ratio (SNR) recordings than extraneural electrodes (Micera and Navarro 2009; Larson and Meng 2019). Intraneural high-density Utah slanted electrode arrays (HD-USEAs) have been used to record signals in cat pudendal nerves, which have an approximate diameter of 1 mm, (Mathews et al. 2014). The silicon-based HD-USEA is considered large (1x2 mm) and rigid for smaller autonomic nerves. For recording from fine autonomic nerves (diameter $\leq$ 0.5 mm), carbon nanotube (CNT) electrodes have demonstrated high SNR recordings (> 10 dB) in rat glossopharyngeal and vagus nerves (diameter of 100-300 µm) by inserting two single-channel CNT electrodes in a nerve target (McCallum et al. 2017). Another research group inserted 4-channel carbon fiber arrays in tracheosyringeal nerves (diameter of 125 µm) of zebra finch birds (Gillis et al. 2018) and recorded spontaneous and stimulation-evoked compound neural responses. However, a need remains for an intraneural array that can record physiological single-neuron activity in fine autonomic nerves.

Our research group has developed a multi-channel, intraneural carbon fiber microelectrode array (CFMA), which has ultra-small recording electrodes (8-9 µm in diameter). The CFMA has demonstrated high SNR recordings with minimal tissue damage in the cerebral cortex of rats (Kozai et al. 2012; P. R. Patel et al. 2015; 2016). We hypothesized that CFMA would obtain physiological recordings with high SNR in a small autonomic nerve. In this study, we inserted CFMA in rat cervical vagus nerves (diameter of 300-500 µm), recorded physiological neural

activity in spontaneous and triggered conditions, and determined propagation direction and conduction velocity of vagal signals.

5.3 Methods

We performed 22 non-survival rat experiments to obtain and analyze intraneural CFMA recordings of vagal nerve activity in spontaneous and modulated conditions.

5.3.1 Fabrication of Carbon Fiber Microelectrode Array

The CFMA arrays were fabricated at the Cortical Neural Prosthetics Lab at the University of Michigan (P. R. Patel et al. 2015; 2016; Welle et al. 2020). Briefly, a printed circuit board (PCB) was custom manufactured (MicroConnex, Snoqualmie, WA, USA). A connector (A79024-001, Omnetics Connector Corp., Minneapolis, MN, USA) was soldered on one end of the PCB with epoxy. On the other end, 16 bare carbon fibers (T-650/35 3 K, Cytec Industries, Woodland Park, NJ, USA) with a length of 2-3 mm were attached to the PCB in a 2x8 configuration and a pitch of 132 µm. The array was coated with approximately 800 nm of parylene-c (PDS 2035, Specialty Coating Systems Inc., Indianapolis, IN, USA) for insulation. The insulated carbon fibers had a diameter of 8-9 µm and were cut down to 150-250 µm in length. The carbon fiber tips were sharpened with a microtorch (MT-51, Master Appliance Corp., Racine, WI, USA) while the base of the fibers were submerged in water (Gillis et al. 2018). The exposed carbon on the sharpened tips (135-160 µm) were electrodeposited with poly(3,4-ethylene-dioxythiophene):sodium p-toluenesulfonate (PEDOT:pTS). A fabricated CFMA is shown in Figure 5.1.
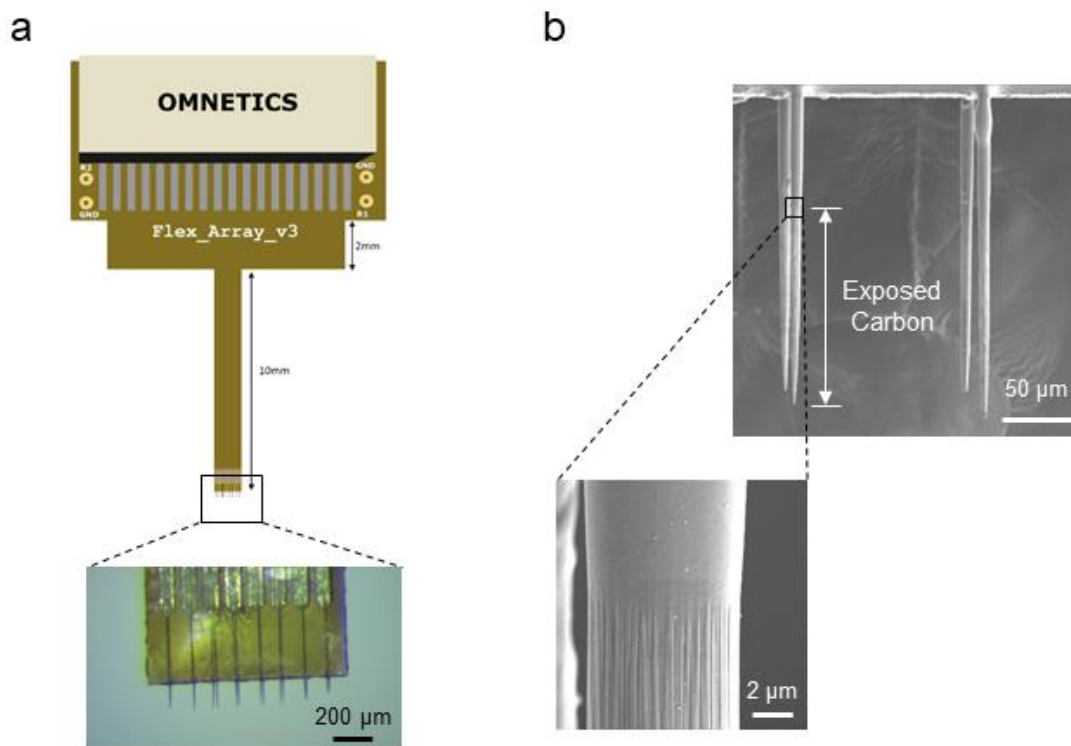
Figure 5.1 Carbon Fiber Microelectrode Array (CFMA). (a) CFMA with 16 blowtorch-sharpened carbon fibers in a 2x8 configuration. (b) Scanning Electron Microscopy (SEM) images of sharpened carbon fibers. Arrows indicate an exposed (non-insulated) carbon fiber region with a length of ~140 µm from the tip.

5.3.2 Design of Nerve-Holder

To facilitate the insertion of a CFMA in a vagus nerve, we designed a nerve-holder to secure and elevate the vagus nerve away from fluid and breathing motions of the cervical cavity, and allow accurate positioning of a small camera to visualize the CFMA-nerve interface during insertion (Figure 5.2a). The nerve-holder had a hollow center to allow insertion of carbon fibers without breakage, and to drain excess fluid around the nerve which may obscure the camera view. To handle the nerve-holder, a circular threaded rod (21YN67, Grainger Inc., Lake Forest, IL, USA) was inserted in the holder and was connected to a soldering arm (900-015, Eclipse, Amelia Court House, VA, USA). The nerve-holder was designed using a computer-aided design (CAD) software

77

(Fusion 360, Autodesk, San Rafael, CA, USA) and 3D-printed with clear resin (Form 2, Formlabs. Somerville, MA, USA). The dimensions of the design are shown in the Appendix C (Figure C.6).

5.3.3 Animal Surgery

All experimental procedures were approved by the University of Michigan Institutional Animal Care and Use Committee (IACUC). Non-survival experiments were performed on male (0.48-0.83 kg) and female (0.36-0.42 kg) Sprague-Dawley rats (Charles Rivers Laboratories, Wilmington, MA, USA). The animals were housed in ventilated cages under controlled temperature, humidity, and photoperiod (12-h light/dark cycle), and provided with laboratory chow (5L0D, LabDiet, St. Louis, MO, USA) and tap water ad libitum. The rats were fasted for 3 hours before the procedure. Anesthesia was induced by 5% isoflurane (Fluriso, VetOne, Boise, ID, USA) and maintained at 2-3% isoflurane. Rats were placed on a heating pad (ReptiTherm, Zoo Med Laboratories Inc., San Luis Obispo, CA, USA). A vitals-monitor (SurgiVet, Smiths Medical, Norwell, MA, USA) was used to monitor heart rate with an oxygen saturation (SpO_2) sensor. A midline ventral cervical incision was made, and retractors (17009-07, Fine Science Tools Inc., Foster City, CA, USA) were used to maintain the cervical opening. Using a dissection microscope (Lynx EVO, Vision Engineering Inc., New Milford, CT, USA), the left cervical vagus nerve (9-12 mm in length) was isolated from the carotid artery and surrounding tissue using fine forceps (00632-11, Fine Science Tools Inc., Foster City, CA, USA). The vagus nerve was lifted (~2 mm) and placed on the nerve-holder to facilitate CFMA insertion. The heating pad and dissection microscope were disconnected to reduce electrical noise.

5.3.4 CFMA Insertion

The CFMA was accurately controlled by a micromanipulator (KITE-R, World Precision Instruments, Sarasota, FL, USA) that was secured on an optical breadboard (MB1218, Thorlabs

Inc., Newton, NJ, USA) under the animal. A small pen-shaped camera (MS100, Teslong Shenzhen, China) was placed in the cervical opening to visualize and align the CFMA fibers for insertion. The nerve was rinsed with saline (0.9% NaCl, Baxter International Inc., Deerfield, IL, USA) and the CFMA was inserted in the vagus nerve. The experimental setup is shown in Figure 5.2b.

The CFMA was connected to a neural interface processor (Grapevine, Ripple LLC, Salt Lake City, UT, USA) that recorded signals at a sampling rate of 30 kHz on a linked desktop computer. Impedances were measured with the neural interface processor at 1 kHz in saline before the procedure, and in the nerve immediately after insertion and at the end of the experiment.

5.3.5 Experimental Protocol

After completion of surgery and insertion of the CFMA, a baseline recording period of at least 5 minutes was obtained. A dose of glucose (n=6; 1 g, Dextrose 50%, Hospira, Lake Forest, IL, USA), insulin (n=6; 20 U, Vetsulin, Merck Animal Health, Madison, NJ, USA), 2-deoxy-D-glucose (2-DG, n=6; 60 mg, D8375-1G, Sigma-Aldrich, St. Louis, MO, USA), or saline (n=4; 0.9% NaCl, Baxter International Inc., Deerfield, IL, USA) was injected intraperitoneally (IP). Recordings from the CFMA were continued for 60 minutes after the injection. Measurements of blood glucose concentration with a glucometer (AlphaTRAK 2, Abbott, Abbott Park, IL, USA), heart rate with the SpO_2 sensor, and breathing rate with a timer were obtained every 5 minutes. The glucometer was unable to measure blood glucose concentrations above 750 mg/dL in one experiment due to the limitations of the glucometer. The experimental protocol is summarized in Figure 5.2c. In experiments with observed breathing-related neural signals (n=3), a recording period of 1 minute was obtained at 2% isoflurane, followed by a 5-minute recording at 5%

79

isoflurane. At the end of the experiment, animals were euthanized with an overdose of sodium

pentobarbital (400 mg/kg, Euthanasia Solution, VetOne, Boise, ID, USA).
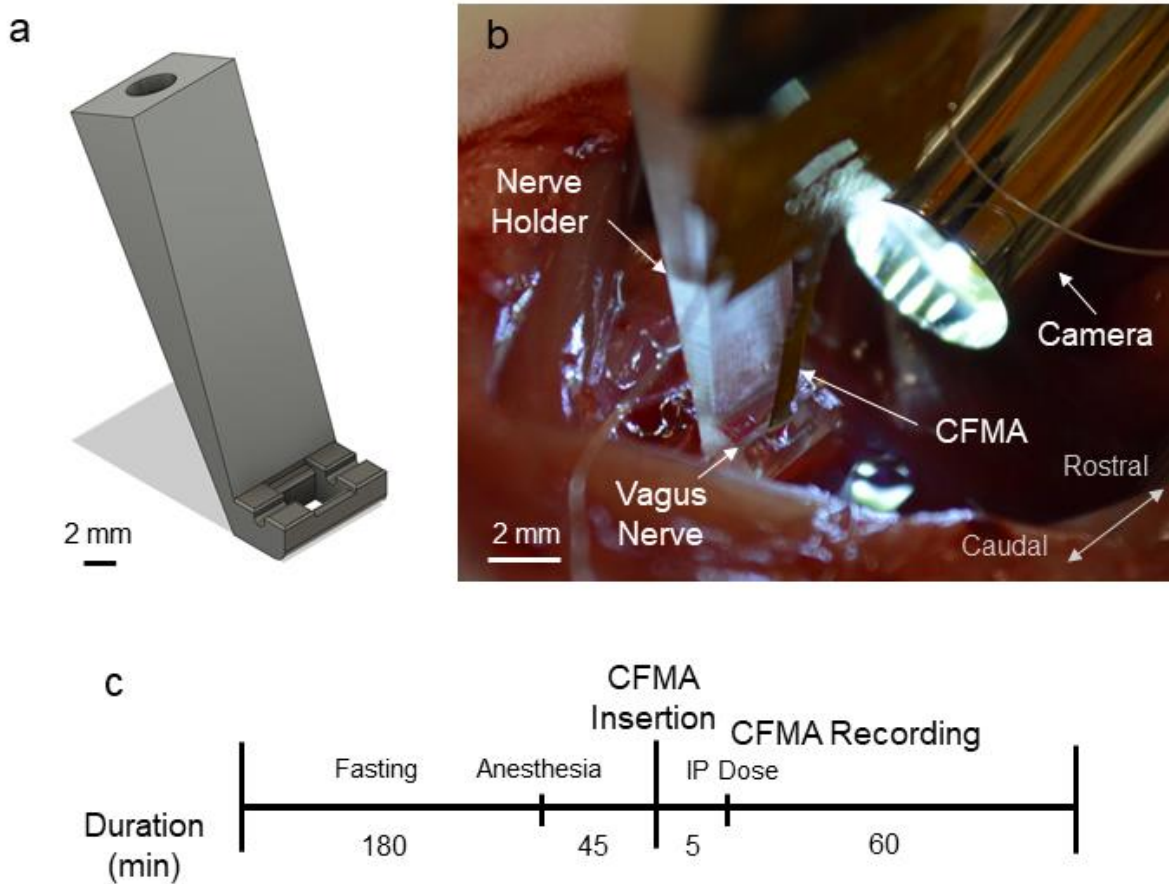
Figure 5.2 Experimental setup and protocol. (a) Design of the nerve-holder. Dimensions of the design are shown in Appendix C Figure C.6. (b) Surgical setup for CFMA insertion. (c) Timeline for the experimental protocol.

5.3.6 Analysis of Neural Recordings

The recorded signals were sorted into clusters using Wave_clus (Chaure, Rey, and Quian

Quiroga 2018), which is a spike-sorting MATLAB-based algorithm that uses wavelet

decomposition to extract waveform features and superparamagnetic clustering to cluster the

spikes. The signals were filtered with a band-pass filter at 300-10,000 Hz. The spike detection

threshold was set between 3.3 and 10.1σ [σ = median(|filtered signal| / 0.6745)] (Chaure, Rey, and Quian Quiroga 2018). The sorted clusters were exported to MATLAB (R2014b, MathWorks, Natick, MA, USA) for analysis. Firing rates were calculated with a bin duration of 1 sec. To calculate signal-to-noise ratio (SNR), the mean peak-to-peak amplitude (Vpp) of a sorted cluster was determined and noise intervals with a total duration of at least 7 sec were specified at periods with no occurring spikes or artifacts [SNR = Vpp / (2 x standard deviation of noise)] (Kozai et al. 2012; P. R. Patel et al. 2016). Cross-correlation was performed between the sorted clusters across all the recording carbon fibers of a CFMA to inspect the latency of spikes along the CFMA. Latencies with high occurrences (count >> mean occurrence) were determined, and conduction velocity and signal propagation direction were computed for those latencies. The bin-size for the latency counts was set at 0.2 msec, except for one experiment that had multiple high counts at zero latency with this 0.2 msec bin-size resolution. For this experiment only (experiment 10), the bin-size was set at 0.01 msec to provide latency counts with higher resolution. The correlation coefficient (ρ) was calculated for all sorted clusters between the firing rate of each cluster and the measured physiological parameters (breathing rate, heart rate and blood glucose concentration) for that experiment. Since the physiological measurements were much less frequent (every 5 minutes) than cluster firing rates (every second), the average cluster firing rate for 1 minute, centered at the time of each physiological measurement, was determined and used for the correlation coefficient computations. When appropriate, data are presented as mean ± standard deviation (SD).

5.4 Results

We inserted 6 CFMA arrays in the left cervical vagus nerve of 22 rats. We observed neural activity on 167 out of 326 inserted functional carbon fibers (impedance < 1 MΩ). The neural activity on each carbon fiber was sorted into 1 neural cluster (n=160) or 2 neural clusters (n=7).

The functional carbon fibers had an average impedance of 31.2 ± 42.0 kΩ in saline before an experiment, 70.8 ± 81.9 kΩ in the nerve immediately after insertion, and 94.7 ± 146.7 kΩ in the nerve at the end of the experiment. Three of the CFMAs were used in more than one experiment (4-8 experiments per CFMA), which initially had a total of 48 functional carbon fibers (16 carbon fibers per CFMA) with an average impedance of 52.8 ± 36.8 kΩ after insertion in the first experiment. After insertion in the fourth experiment, 45 of the functional carbon fibers on these three CFMAs (14-16 carbon fibers per CFMA) remained with an average impedance of 92.6 ± 149.5 kΩ. On average for a single experiment, we made 2.3 ± 2.9 attempts to insert a CFMA with 14.9 ± 1.8 functional carbon fibers and observed neural activity on 7.7 ± 5.9 carbon fibers. There were no distinctive differences among the recordings of rats with different gender or sizes.

5.4.1 Multi-Channel Recordings of Vagal Nerve Activity

We observed physiological neural activity in the vagus nerve on at least one recording carbon fiber in 19 of the total 22 experiments. The recorded neural activity was sorted into clusters and the mean peak-to-peak amplitudes of the sorted clusters were between 15.1 and 91.7 µV with SNR of 2.0-7.0. An example of vagal nerve activity on multiple recording carbon fibers from the same experiment is shown in Figure 5.3.
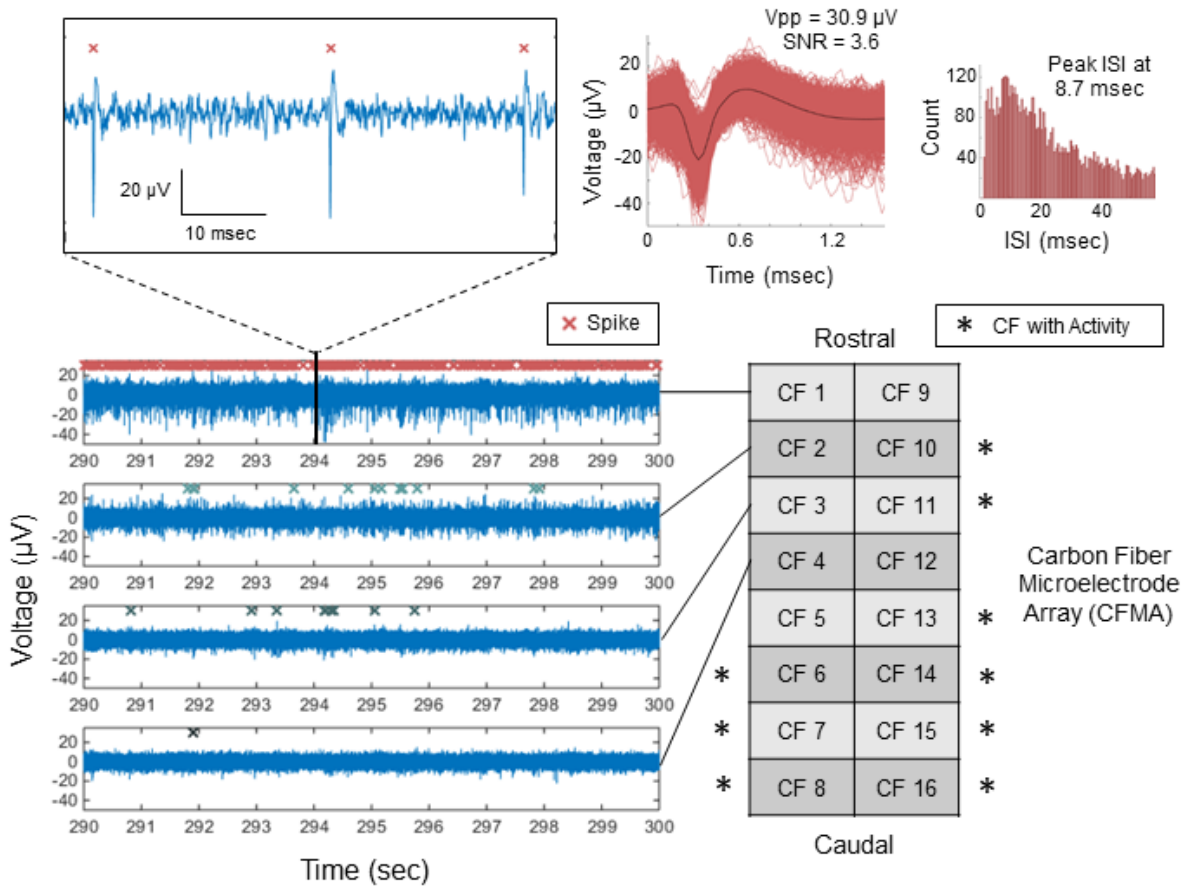
Figure 5.3 Representative recordings of physiological vagal nerve activity using 16-channel CFMA.
Recordings on 4 adjacent carbon fibers (CF) in experiment 15 showing distinctive signals. The markers (x) indicate the occurrence of a sorted spike on each CF, which are unique across CFs. The spike waveforms and inter-spike intervals (ISIs) are shown for CF 1. Other CFMA CFs that also recorded neural activity are marked (*).

5.4.2 Signal Propagation and Conduction Velocity

Propagation of vagal signals were detected along adjacent recording carbon fibers in some experiments. We observed neural signals in 10 experiments propagating in the afferent direction with conduction velocities of 0.7-1.0 m/sec over the span of 2-7 carbon fibers (132-792 µm). Furthermore, we monitored efferent signals conducting at 0.7-8.8 m/sec along 2-4 carbon fibers (132-396 µm) in 5 experiments. Examples of propagating afferent signals are shown in Figure 5.4.
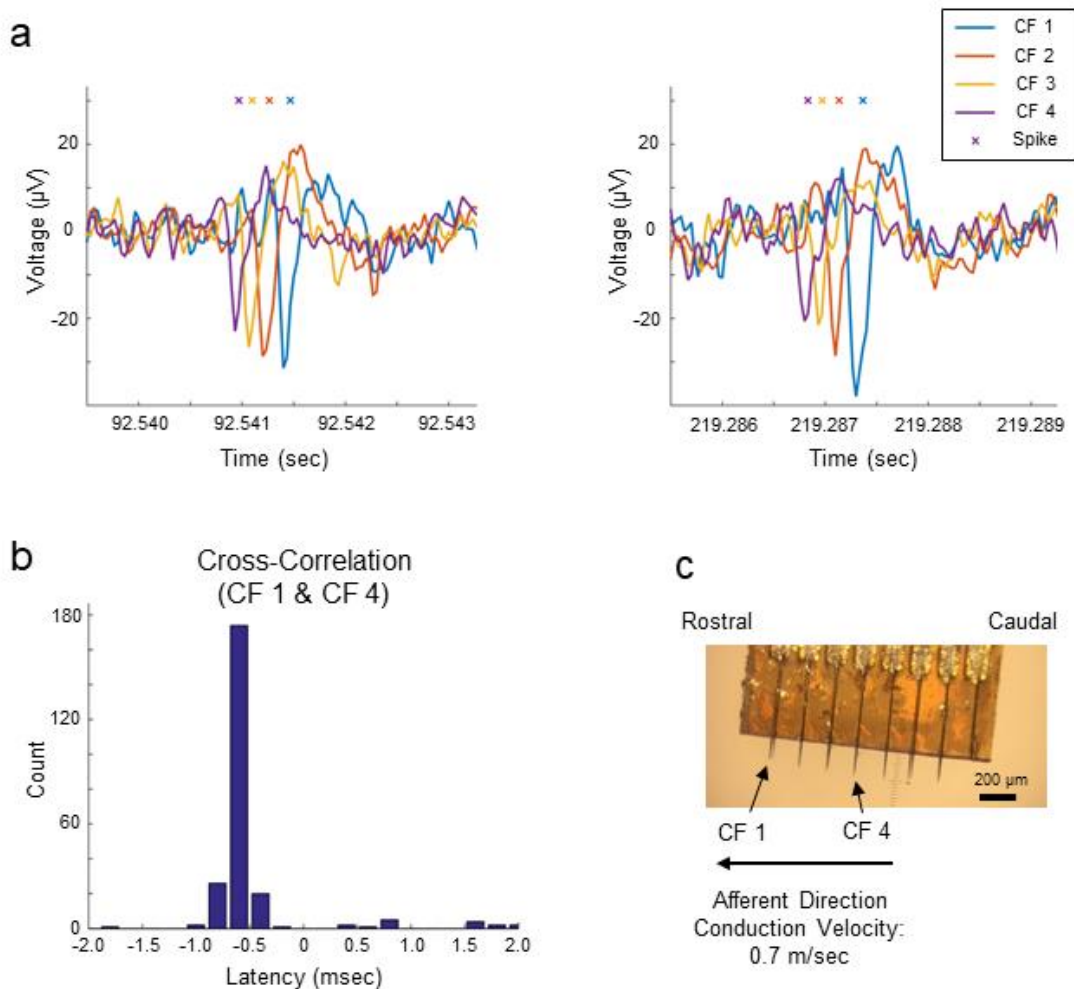
Figure 5.4 Signal propagation along CFMA carbon fibers (CF). (a) Instances of signal propagation along CF 1 – CF 4 (experiment 15). (b) Cross correlation of spikes on CF 1 and CF 4. The prevalent latency occurred at -0.6 msec with a count of 174 spikes (55.8% of spikes on CF 4). (c) At latency of -0.6 msec, the spikes occurred on CF 4 before CF 1, suggesting that the signal is propagating in the afferent direction at a conduction velocity of 0.7 m/sec.

5.4.3   Breathing-Related Neural Activity

We observed vagal signals with periodic bursting firing behavior (n=6 experiments) at repetition rates of 39.4 ± 10.8 cycles/min, which were similar to the animals' breathing rates of 39.3 ± 9.9 breaths/min (Figure 5.5). In a subset of experiments (n=3), we reduced the breathing rate to 20.0 ± 8.0 breaths/min by increasing the depth of anesthesia, and the firing-burst repetition rates reduced to a similar level at 19.1 ± 10.3 cycles/min, with maintained peak-to-peak amplitudes

84

(31.7 ± 11.6 µV to 29.3 ±10.1 µV) and inter-spike interval (ISI) values (9.2 ±1.6 msec to 10.5 ±

1.6 msec), as shown in the example in Figure 5.5a. The periodic bursting behaviors were usually

firing at one ISI peak of 9.5 ± 1.3 msec. However, in two experiments, two distinct ISI peaks were

observed at 9.8 ± 1.8 msec and 24.2 ± 6.0 msec (e.g. Figure 5.5b).
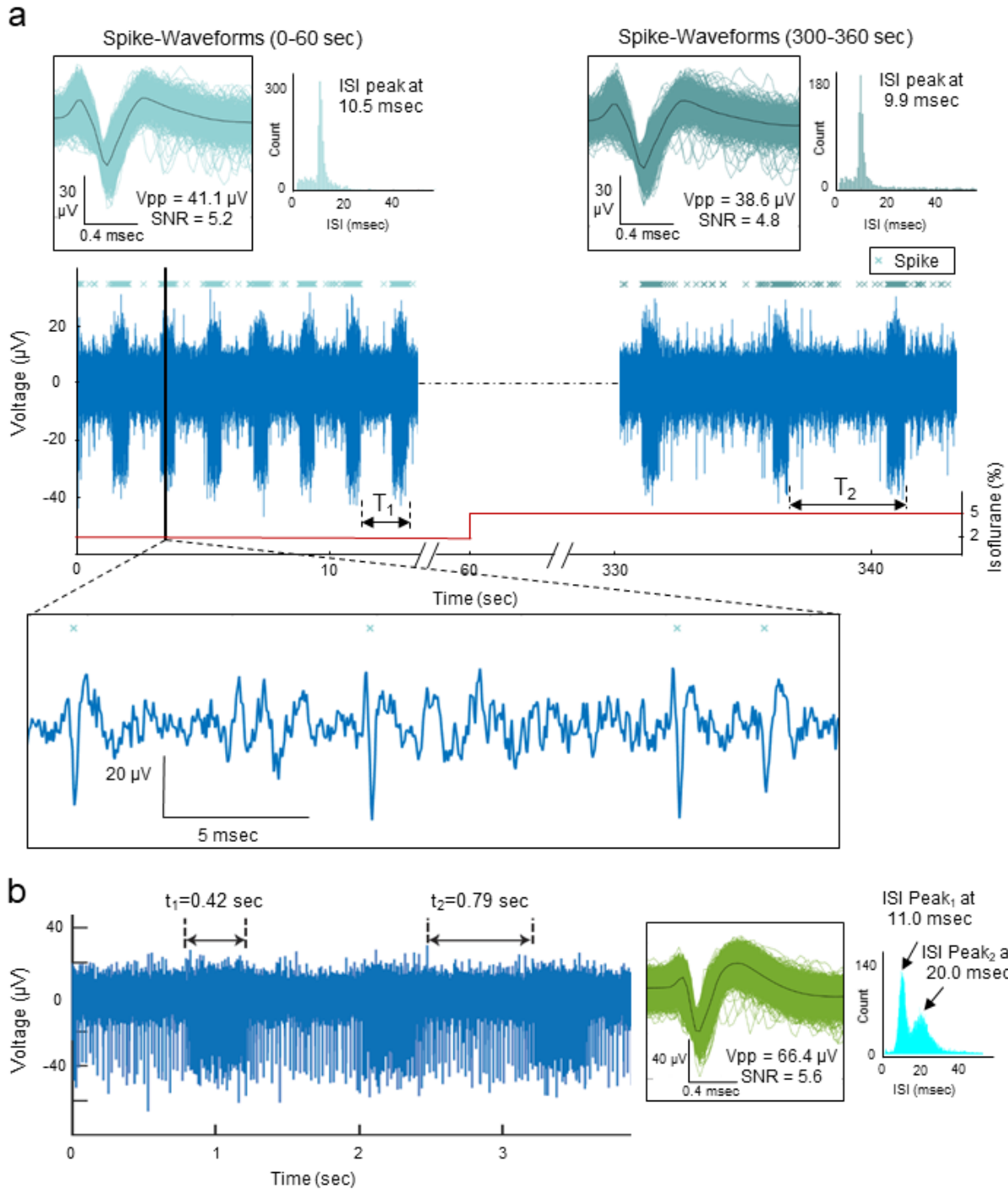
Figure 5.5 Breathing-related neural activity. (a) Recordings of vagus nerve activity at 2% and 5% isoflurane (experiment 16). The bursting firing behavior had a repetition rate of 32.2 cycles/min (1/T_1) during animal's breathing rate of 32 breaths/min at 2% isoflurane. The firing-behavior repetition rate reduced to 14.2 cycles/min (1/T_2) as the breathing rate reduced to ~12 breaths/min at 5% isoflurane. The waveform amplitude and inter-spike interval (ISI) peaks were similar at 2% and 5% isoflurane. (b) Bursting firing behavior at two distinct ISIs indicated at t_1 and t_2. The animal's breathing rate was ~44 breaths/min and the repetition rate for the bursting firing behavior was 47.3 cycles/min (experiment 4).

5.4.4 Neural Firing Rate Behavior with Physiological Parameters in Blood Glucose Modulation Conditions

In each experiment, we recorded vagal nerve activity for 60 minutes after administration of a blood glucose modulation dose (glucose, insulin, 2-DG, or saline), while monitoring physiological parameters (blood glucose concentration, breathing rate, and heart rate). The recorded neural activity were sorted into 174 clusters. The firing rate of these clusters showed moderate or high correlation coefficients ($|\rho| \geq 0.3$) with one (n=16), two (n=35), or all three (n=95) of the tracked physiological parameters. Across experiments, correlation coefficients did not show clear associations between any glucose modulation dosing and any of the physiological parameters. An experiment with a carbon fiber that recorded the activity of 2 sorted clusters, along with the physiological measurements (blood glucose concentration, breathing rate and heart rate) and correlation coefficients, is shown in Figure 5.6.

Although correlation coefficients did not show a clear relationship between any of the glucose modulation doses and physiological parameters, we observed clusters with interesting firing rate behaviors after injection of a modulation dose, as shown in Figure 5.7. In some glucose injection experiments (n=4), we observed neural clusters (n=11) with an average peak-to-peak amplitude of 24.7 ± 6.4 µV with an initial firing rate of 6.8 ± 8.9 spikes/sec that decreased after administration of glucose to 1.8 ± 2.4 spikes/sec (e.g. Figure 5.7a). In some experiments with an insulin injection (n=4), neural clusters (n=4) with amplitudes of 53.3 ± 28.0 µV peak-to-peak increased their firing rates from 1.2 ± 1.8 spikes/sec to 7.6 ± 10.4 spikes/sec at 1-13 minutes after insulin administration (e.g. Figure 5.7b). Injection of 2-DG induced a similar neural response to insulin in some experiments (n=2). Starting at 5.6 ± 3.7 minutes after 2-DG administration, clusters (n=6) with an average amplitude of 29.2 ± 8.1 µV peak-to-peak increased their firing rates from

3.8 ± 4.6 spikes/sec to 9.8 ± 10.1 spikes/sec (e.g. Figure 5.7c). A summary of all the performed

experiments is shown in Table 5.1.
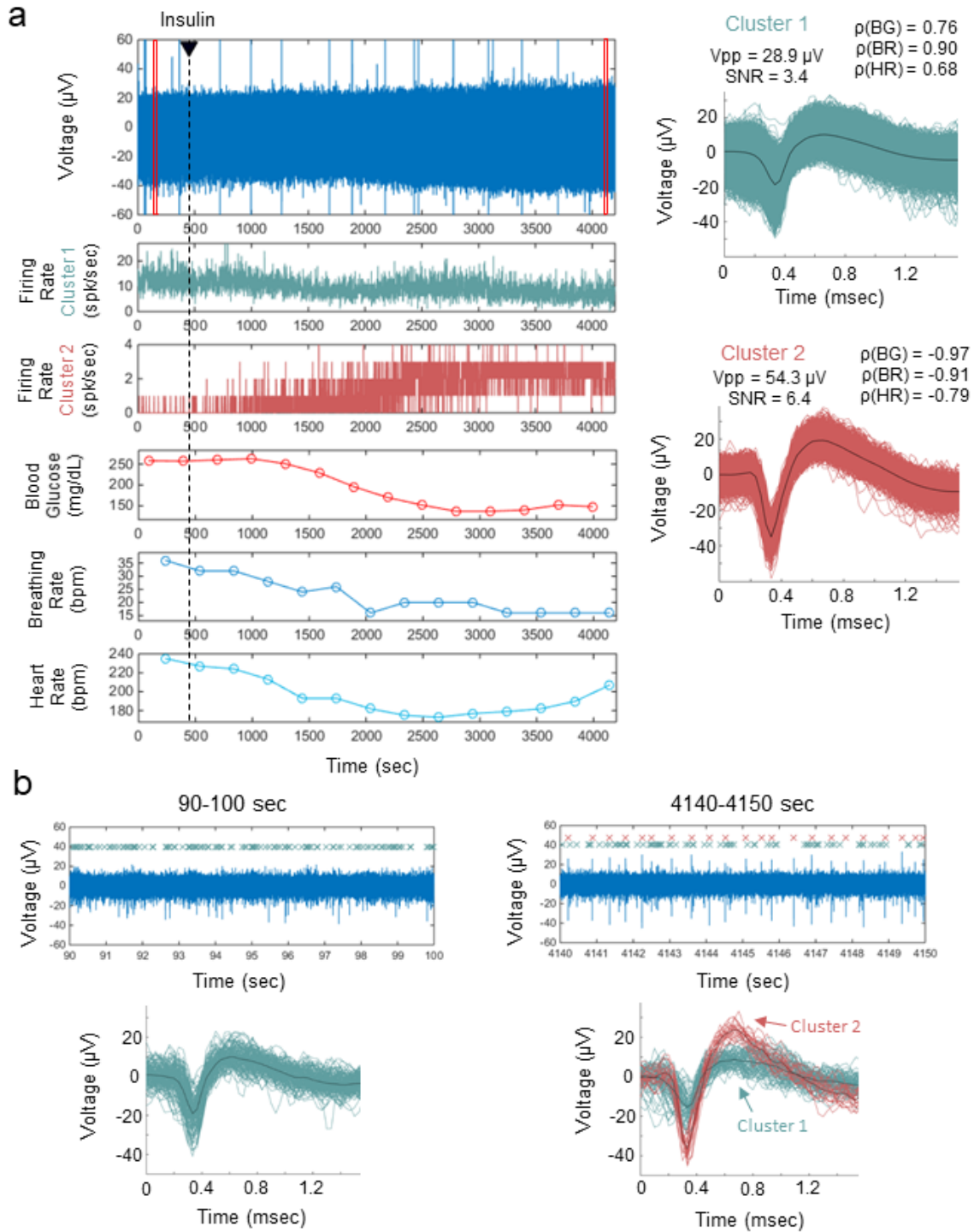
Figure 5.6 Vagus nerve recordings with sorted clusters in an insulin-injected experiment (15). (a) Filtered signal, firing rate of two sorted clusters, blood glucose (BG) concentration, breathing rate (BR) and heart rate (HR) measurements. The waveforms of the sorted clusters are shown with the average peak-to-peak amplitude (Vpp), signal-to-noise ratio (SNR), and correlation coefficients (ρ) between cluster firing rate and blood glucose (BG), breathing rate (BR) and heart rate (HR). The red boxes in the voltage plot indicate the time-window for the plots in b. (b) Filtered signals before and after insulin injection, and the spike waveforms of the two sorted clusters within each 10-sec window.
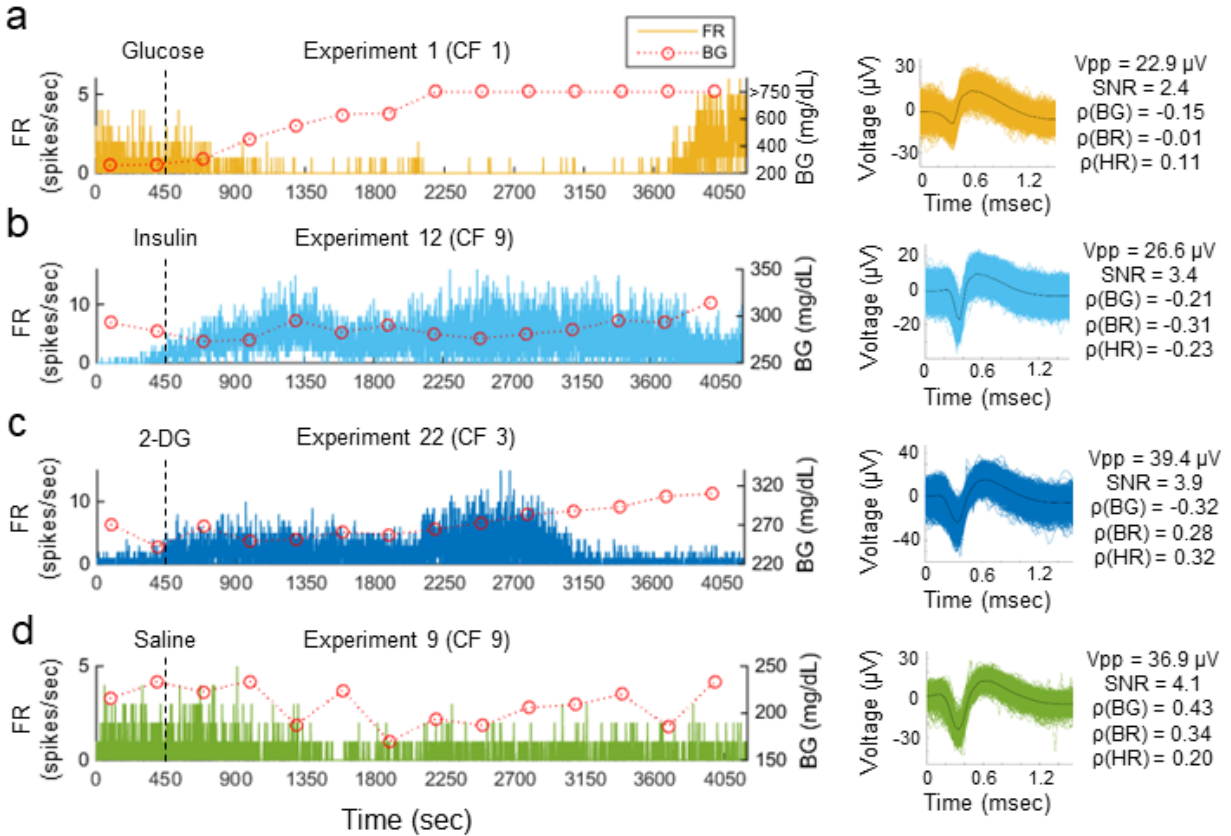
Figure 5.7 Examples of sorted clusters with interesting firing rate behavior in blood glucose modulated conditions. The clusters were observed in glucose modulation experiments with an injection of (a) glucose, (b) insulin, (c) 2-deoxy-D-glucose (2-DG), or (d) saline. The waveforms of the sorted clusters are shown with the average peak-to-peak amplitude (Vpp), signal-to-noise ratio (SNR), correlation coefficients (ρ) between cluster firing rate (FR) and blood glucose (BG), breathing rate (BR) and heart rate (HR). BG measurements above 750 mg/dL were not available due to the limitations of the glucometer.

Table 5.1 Summary for all the experiments with inserted CFMA in the vagus nerve.

ID	IP Dose	Array	Functional CF	CF with Activity	Clusters	Vpp (µV)	SNR	Clusters with |ρ| ≥ 0.3			Signal Propagation (m/sec)		
								BG	BR	HR	Afferent	Efferent	Max Span (µm)
1	Glucose	A	16	16	16	21.7 - 27.5	2.0 - 2.9	0	0	0	-	-	-
2	2-DG	A	16	6	6	18.4 - 34.9	2.3 - 3.4	6	6	3	-	-	-
3	Glucose	A	15	5	5	17.8 - 30.3	2.0 - 2.8	3	2	1	-	-	-
4	Insulin	A	15	14	15	23.2 - 91.7	2.2 - 6.9	14	15	15	0.7	0.7 - 1.0	396
5	Saline	A	15	7	8	22.0 - 43.9	2.8 - 3.6	7	7	6	0.7	0.7	264
6	Insulin	A	14	0	0	-	-	-	-	-	-	-	-
7	Glucose	B	16	0	0	-	-	-	-	-	-	-	-
8	Insulin	C	16	7	8	20.4 - 40.4	2.7 - 4.6	8	8	8	-	-	-
9	Saline	C	16	6	7	20.7 - 59.1	3.1 - 6.5	2	2	5	-	0.7	132
10	2-DG	C	16	16	16	21.0 - 58.7	2.7 - 5.4	13	11	14	0.7	0.7 - 8.8	264
11	Glucose	D	16	6	6	15.1 - 38.3	2.6 - 3.6	6	6	4	0.7	-	132
12	Insulin	E	14	5	6	17.7 - 78.2	2.6 - 7.0	2	6	5	-	-	-
13	2-DG	C	14	2	2	27.4 - 44.0	2.9 - 4.3	2	2	2	-	-	-
14	Saline	A	14	14	14	27.4 - 62.5	2.5 - 4.9	13	14	14	0.7-0.9	-	792
15	Insulin	D	16	14	16	18.8 - 54.3	2.4 - 6.4	11	11	12	0.7	-	660
16	2-DG	D	16	13	13	17.3 - 35.6	2.4 - 4.1	10	9	4	0.7	-	792
17	Insulin	D	16	14	14	20.0 - 26.6	2.8 - 3.5	11	12	11	0.7-1.0	-	528
18	Glucose	D	15	2	2	18.8 - 26.0	2.8 - 3.2	2	0	2	0.7	-	132
19	2-DG	D	15	4	4	19.3 - 36.5	2.9 - 4.7	4	4	4	-	-	-
20	Saline	F	8	0	0	-	-	-	-	-	-	-	-
21	Glucose	A	12	1	1	26.8	2.8	1	1	1	-	-	-
22	2-DG	D	15	15	15	27.5 - 54.0	3.0 - 5.5	8	10	11	0.7 - 0.9	0.7	528
Total			326	167	174	15.0 - 91.7	2.0 - 7.0	123	126	122	0.7-1.0	0.7 - 8.8	132 - 792

Correlation coefficients (ρ) were calculated between cluster firing rates and blood glucose (BG) concentrations, breathing rate (BR) and heart rate (HR).

5.5 Discussion

We developed a multi-channel, intraneural carbon fiber microelectrode array (CFMA) for recording neural signals in autonomic nerves (Figure 5.1). Using the CFMA, we obtained axonal recordings in rat cervical vagus nerves with signal-to-noise ratio (SNR) of 2.0-7.0. We recorded physiological vagal nerve activity on multiple channels per experiment (Figure 5.3), determined the propagation direction and conduction velocity of some vagal signals (Figure 5.4), and monitored changes in neural activity in physiologically modulated conditions (Figures 5.5-7). These findings suggest that CFMA is a viable electrode for obtaining intraneural recordings in small autonomic nerves. Monitoring physiological signaling in autonomic nerves will help researchers better understand the neural control and feedback processes, which may assist in the development of innovative treatment modalities to restore vital body functions regulated by these nerves.

Our experimental recordings demonstrated CFMA as a multi-channel, intraneural array for small-diameter ($\leq$ 0.5 mm) autonomic nerves. In prior work, intraneural carbon nanotube (CNT) electrodes obtained high SNR (>10 dB) physiological recordings in small diameter (100-300 µm) rat glossopharyngeal and vagus nerves (McCallum et al. 2017). Two single-channel CNT electrodes were inserted in a nerve target to obtain only a single differential recording. In our study, 16-channel CFMAs were inserted in rat vagus nerves (diameter of 300-500 µm) and recorded physiological neural activity (SNR of 2.0-7.0) on multiple channels (up to 16), which also provided information on the propagation direction and conduction velocity of some signals (Figure 5.4). The recording exposure site on a carbon fiber spanned 135-160 µm in length from the tip, which provided better spatial selectivity recordings than CNT electrodes that had an exposed recording segment of ~500 µm. Another research group developed an intraneural 4-channel carbon fiber

array that recorded from tracheosyringeal nerves (diameter of 125 µm) of zebra finch birds (Gillis et al. 2018). They demonstrated an innovative blowtorching technique for sharpening carbon fibers to directly insert carbon fibers in a nerve, which we adopted. Although an example of spontaneous activity was shown using the 4-channel array, the majority of the demonstrated signals were evoked responses from electrical stimulation, and no information was reported on physiologically-modulated activity or signal propagation along the array.

The observed spike waveforms in CFMA recordings from the vagus nerve (e.g. Figures 5.3-7) closely resemble action potentials generated by an individual neuron (Moffitt and McIntyre 2005; Henze et al. 2000), based on the waveform shape and time scale (~1-2 msec). Furthermore, we observed propagation of signals in the afferent and efferent direction within the conduction velocity range for myelinated (Aδ and B) and unmyelinated (C) fibers (Figure 5.4), which are present in the vagus nerve (Qing et al. 2018; Kajekar et al. 1999). However, due to the similarity in the waveform shape and the normal variations in waveform amplitudes, we were not able to sort the action potentials into clear single units, with only a few channels yielding more than one sortable cluster. The active recording site for a CFMA carbon fiber spans 135-160 µm in length from the tip (Figure 5.1), which exposes the recording site to an estimation of over 200 axons within a distance of 5 µm from the recording site (Figure 5.8). This estimation is based on the approximate axon density in the rat vagus nerve, which has around 11,000 axons (Gabella and Pease 1973; Prechtl and Powley 1990) and a nerve diameter of about 300 µm. Further work on reducing the exposed recording site area may assist in monitoring more localized axon activity with a lower background noise level (P. R. Patel et al. 2015; Welle et al. 2020; D. Yan et al. 2019). Moreover, current spike-sorting algorithms are mostly designed for central nervous system recordings (Rey, Pedreira, and Quian Quiroga 2015), which assume the waveforms are from

neuron cell bodies that generate higher amplitude waveforms and have more diverse shapes than axons. Future work is needed to study the recording nature in autonomic nerves and develop spike-sorting algorithms for axonal recordings.
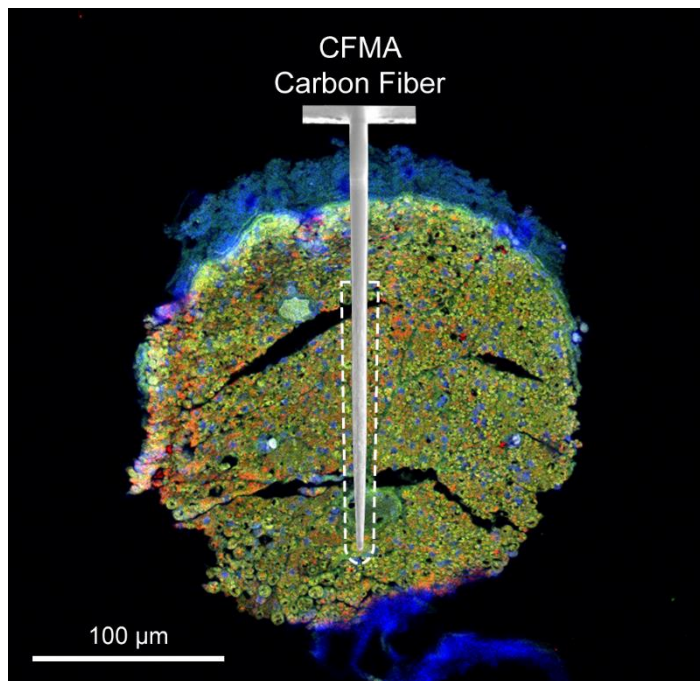
Figure 5.8 Immunohistochemistry (IHC) image of a rat cervical vagus nerve with a diagram of an inserted CFMA carbon fiber. The dashed lines show a region with a distance of 5 µm from the exposed recording site of a CFMA carbon fiber. The region is estimated to be occupied by over 200 axons based on the typical axon density of a rat vagus nerve (~11,000 axons in 300 µm diameter nerve) (Gabella and Pease 1973; Prechtl and Powley 1990). The nerve sample in this image was stained with 4', 6-diamino-2-phenylindole (DAPI), myelin basic protein (MBP), and anti-beta III tubuline (TUJ1) to show nucleotides (blue), myelin (green) and axons (red), respectively.

Sorted clusters from our recorded vagal nerve activity showed interesting firing rate behavior that may be related to the measured physiological parameters of breathing rate, heart rate and blood glucose concentrations. We observed neural clusters with periodic firing-burst behavior at repetition rates similar to the measured breathing rates (Figure 5.5). Vagus nerve fibers innervate the lungs, with critical relevance for breathing control (Chang et al. 2015; Berthoud and Neuhuber 2000; McAllen et al. 2018). Our observed vagal signals may be related to the neural control over

breathing or an afferent response to chest and/or lung expansion (Chang et al. 2015). We also observed interesting changes in vagal firing rate behavior after injection of blood glucose modulation doses (Figure 5.7). These experiments were performed on fasted rats, and neural signals before the dose injection may represent vagal afferent signals to drive an increase in glucose intake. The firing rate of clusters decreased after administration of glucose (e.g. Figure 5.7a), which may suggest that the signaling for glucose intake was met. This observation aligns with previous studies that showed neural recordings in the afferent hepatic branch of the vagus nerve (Niijima 1983) and overall cervical vagus activity (Masi et al. 2019) which changed in a similar manner following glucose injection. The increase in firing rate observed after insulin or 2-deoxy-D-glucose (2-DG) injection, which induces insulin-like symptoms, may represent a surge of afferent activity to enhance the request for glucose intake (e.g. Figure 5.7b,c), which aligns with previous studies that showed increased afferent activity in the hepatic branch or cervical vagus nerve within 10 minutes after administration of insulin or 2-DG (Niijima 1983; Masi et al. 2019). However, these observed responses were inconsistent across our experiments with identical injection doses, which may be due to the variation in CMFA sampling of neural activity within the nerve. Moreover, there were similarities in the blood glucose concentration trends during an experiment to other measured physiological parameters (i.e. breathing rate and heart rate) in most experiments (e.g. Figure 5.6-7). The anesthetic agent we used in our experiments was isoflurane, which maintained consistent and stable depth of anesthesia for recording vagal nerve activity with ultra-small carbon fibers. In preliminary experiments using other agents (e.g. ketamine), occasional muscle twitches would lead to CFMA movement or carbon fiber breakage, which were not observed under isoflurane. However, isoflurane anesthesia suppresses neural activity in the central and autonomic nervous systems and impacts multiple physiological parameters, including

blood glucose concentrations, respiration, and arterial pressure (Skovsted and Sapthavichaikul 1977; Carli et al. 1993). Experiments with minimal or no anesthesia would allow more physiological activities to occur and may be necessary to clearly link vagal nerve activity to physiological changes.

This work had numerous limitations. The exact insertion location for the CFMA arrays in the vagus nerve varied between our experiments. The rat cervical vagus nerve is estimated to contain around 11,000 axons (Gabella and Pease 1973; Prechtl and Powley 1990) that regulate many autonomic functions (Berthoud and Neuhuber 2000). To illustrate this variation, potential breathing-related signals (e.g. Figure 5.5) were only observed in 6 out of the 22 experiments, although all the rats were breathing normally during the experiments. Additional work on redesigning the electrode configuration may be needed to cover a wider range of axonal activity while providing high selectivity for individual recording sites, such as with staggered rows of carbon fibers with variable lengths. Another limitation is the requirement to lift the nerve for CFMA insertion, which applies tension on the nerve, during the implantation procedure due to the nerve-holder design. Although the nerve-holder added the risk of nerve injury, the nerve-holder was necessary to position a camera to visualize the accurate alignment of CFMA carbon fibers with the vagus nerve for insertion (Figure 5.2). Redesigning the nerve-holder and possibly restructuring the implantation procedure may be needed to eliminate the applied tension and avoid the risk of injuring the nerve.

Overall, our experiments demonstrated CFMA as a viable multi-channel intraneural electrode for recording neural activity in autonomic nerves. Further work is needed to refine the selectivity of CFMA and develop a chronic form to monitor long-term recordings in autonomic nerves without the presence of anesthesia. This work provided insights in intraneural axonal

recordings and is a milestone towards the comprehensive understanding of physiological signaling in autonomic nerves, which may lead to the development of innovative treatment modalities for restoring regulatory functions.

5.6 Conclusion

The aim of this study was to demonstrate intraneural recordings in a small autonomic nerve using the carbon fiber microelectrode array (CFMA). Our results showed axonal recordings in the rat cervical vagus nerve. We recorded physiological vagal nerve activity on multiple channels, determined the propagation direction and conduction velocity of vagal signals, and observed changes in firing rate behavior in modulated conditions. Future work is needed to enhance the selectivity of CFMA and validate CFMA recordings in various autonomic nerves. This work suggests that CFMA may be used to better understand neural regulation signaling in various physiological and pathophysiological conditions, which may assist in the development of new treatments.

5.7 Acknowledgements

Chapter 6: Conclusions

6.1 Summary of Results

Diabetes is a global disease that has altered the lives of millions of people around the world. Although diabetic medications are critical for the treatment of current patients with diabetes (American Diabetes Association 2020), many of these medications are associated with undesirable side effects and lose their glycemic control effectiveness over time (Blak et al. 2012; Khunti et al. 2013; American Diabetes Association 2020). Furthermore, sustained patient adherence to these medications in a lifelong therapy is a major challenge (García-Pérez et al. 2013). There is an opportunity for developing an implantable and automated treatment for diabetic patients by accurately detecting and altering neural activity in autonomic nerves for effective glycemic control. This will help patients overcome therapeutic limitations with current medications and is the core motivation for the research presented in this dissertation.

The dissertation investigated alteration of renal nerve activity for glucose regulation in normal (Aim 1) and diabetic animals (Aim 2), assembled a new chronic implantation procedure for neural interface arrays designed for small autonomic nerves (Aim 3), and detected physiological action potential signals in an autonomic nerve (Aim 4). The results of this work support the potential development of an alternative implantable treatment modality for diabetic patients by altering and detecting neural activity in autonomic nerves.

6.1.1 Specific Aim 1 - Determine Effective Stimulation Parameters for the Modulation of Urine Glucose by Stimulation of Renal Nerves in Normal Rats

The accomplishment of specific aim 1 is detailed in Chapter 2. To our knowledge, this was the first study to investigate electrical stimulation of renal nerves to modulate urine glucose excretion. We hypothesized that stimulation of renal nerves in rats at kilohertz frequencies (1–50 kHz) would increase urine glucose excretion (UGE), while low frequency stimulation (2–5 Hz) would decrease UGE. Although stimulation at kilohertz frequencies did not always lead to an increase in UGE, 33 kHz showed a notable average increase in UGE (+ 24.5%). In contrast, low frequency stimulation typically showed a decrease in UGE, with the strongest effect observed at 5 Hz stimulation (− 40.4%). The average differences in UGE were similar to the average differences observed in urine flow rate (UFR), suggesting an associated response. Although this may indicate that either UGE or UFR was the primary effect of stimulation, UFR and UGE are normally associated, as increased urination is a common adverse event in diabetic patients treated with sodium-glucose co-transporter 2 (SGLT2) inhibitors that primarily increase urine glucose excretion (Seufert 2015; Wilding 2014). Overall, the experiments in this aim showed that stimulation of renal nerves may modulate urine glucose excretion. Future work is needed to distinguish the glucose excretion and urine flow effects for stimulation of renal nerves and examine the underlying mechanisms. Stimulation of renal nerves may provide an alternative treatment approach for glycemic control that avoids patient compliance issues typically seen with current medications (Polonsky and Henry 2016).

6.1.2 Specific Aim 2 - Evaluate Impact of Kilohertz Frequency Stimulation of Renal Nerves on Blood Glucose Concentration in Diabetic Rats

The work in Chapter 3 described the accomplishment of this aim. The study of the previous aim showed that electrical stimulation of renal nerves may modulate urinary glucose excretion in glucose-bolus infusion experiments. In this aim, we hypothesized that bilateral kilohertz frequency stimulation of renal nerves would reduce blood glucose concentration levels in diabetic rats by increasing urinary glucose excretion. Kilohertz frequency stimulation of renal nerves showed a significant average decrease (-168.4%) in blood glucose concentration rate, and an increase (+18.9%) in the overall average area under the curve for urine glucose concentration, with respect to values before stimulation. The experimental results of this study suggest that kilohertz frequency stimulation of renal nerves is a potential approach for glycemic control in diabetic conditions. Although further studies are necessary to inspect the safety of kilohertz frequency stimulation of renal nerves, the work in this aim and the previous aim introduce a novel approach for glycemic control in diabetic patients through glucose regulation at the kidneys, which occupy a vital role in glucose homeostasis.

6.1.3 Specific Aim 3 - Develop Surgical Procedure for the Chronic Implantation of Microneedle Nerve Arrays in Rat Vagus Nerves

The accomplishment of this specific aim is detailed in Chapter 4. In this aim, we assembled an innovative chronic implantation procedure for novel intraneural MIcroneedle Nerve Arrays (MINAs) in rat vagus nerves. We investigated two array attachment approaches (fibrin sealant and rose-bengal bonding) to secure non-wired MINAs in rat vagus nerves. The fibrin sealant approach was unsuccessful in securing the MINA-nerve interface for 4- and 8-week implant durations. The rose-bengal coated MINAs were in close proximity to axons (≤ 50 μm) in 75% of 1-week and 14%

of 6-week implants. The MINA-implanted nerves showed stimulation-evoked neural responses, with no statistical significant differences between body weight, blood glucose concentration, or stimulation threshold values between MINA-implanted and sham-implant animals, suggesting that the MINA implants did not cause significant harm to the overall health of the rats. This work, to the best of our knowledge, was the first to demonstrate the chronic implantation of an intraneural electrode array in a fine autonomic nerve (diameter $\leq$ 0.5 mm). Further work is needed to demonstrate the neural recording capabilities of functional MINA. The chronic implantation of fully-functional intraneural arrays in autonomic nerves may provide novel insights in physiological neural signaling and allow selective microstimulation of function-specific axons to restore vital functions regulated by autonomic nerves.

6.1.4 Specific Aim 4 - Demonstrate Intraneural Recordings in Rat Vagus Nerves Using Carbon Fiber Microelectrode Arrays

The accomplishment of this aim is detailed in Chapter 5. In this aim, we hypothesized that Carbon Fiber Microelectrode Arrays (CFMAs) can obtain physiological recordings with high signal-to-noise ratio (SNR) in a small autonomic nerve. Using the CFMA, we obtained axonal recordings in rat cervical vagus nerves. We observed physiological neural activity on 51% of inserted functional carbon fibers, and sorted 1-2 neural clusters on each carbon fiber with activity. The mean peak-to-peak amplitudes of the sorted clusters were 15.1-91.7 µV with SNR of 2.0-7.0. We detected propagation of vagal signals in the afferent direction at conduction velocities of 0.7-1.0 m/sec, and efferent signals at 0.7-8.8 m/sec, which are within the conduction velocity range of myelinated and unmyelinated vagus fibers. Furthermore, we monitored changes in vagal activity in breathing and blood glucose modulated conditions. The observed spike waveforms in CFMA recordings closely resemble action potentials generated by an individual neuron, based on the

waveform shape and time scale (Moffitt and McIntyre 2005; Henze et al. 2000), supporting our hypothesis that they are from individual axons. However, due to the similarity in the waveform shapes and the normal variations in waveform amplitudes, we were not able to differentiate the action potentials into clear single units from putative individual axons. Further work is needed to refine the selectivity of CFMA and validate CFMA recordings in various autonomic nerves. Overall, our experiments demonstrated CFMA as a viable multi-channel intraneural electrode for recording neural activity in autonomic nerves. This work provided insights in intraneural axonal recordings and is a milestone towards the comprehensive understanding of physiological signaling in autonomic nerves for glycemic control.

6.2 Impact on the Field

6.2.1 Kilohertz Frequency Stimulation of Renal Nerves

To our knowledge, our work in Chapter 2 and Chapter 3 was the first to investigate kilohertz frequency stimulation of renal nerves. Our experimental results showed that kilohertz frequency stimulation of renal nerves may reduce blood glucose concentration levels in diabetic conditions. Prior studies have shown the influence of renal nerves on glucose regulation by renal denervation (Mahfoud et al. 2011; Rafiq et al. 2015), which is considered an irreversible procedure. The finding of this work is impactful by demonstrating a reversible and controllable glycemic control approach that alters renal nerve activity in desired conditions (i.e. hyperglycemia) without removing the renal nerves, which provide neural control of complex functions performed by the kidneys (DiBona 2000). Although further work is needed to improve the electrode interface and evaluate the safety of this approach, this work initiated a potential alternative treatment modality for diabetic patients by kilohertz frequency stimulation of renal nerves.

6.2.2 Chronic Implantation Procedure for Intraneural Arrays

The work in Chapter 4 demonstrated a new chronic implantation procedure for an intraneural array in a fine autonomic nerve (diameter ≤ 0.5 mm). Multiple intraneural electrodes have been implanted in somatic or large autonomic nerves (diameter ≥ 1 mm) (Wark et al. 2014; Mathews et al. 2014; Byun et al. 2017), but only a few have been developed for fine autonomic nerves. Carbon nanotube (CNT) electrodes (McCallum et al. 2017) were chronically implanted in fine autonomic nerves (diameter of 100-300 µm), but a relatively-large tungsten needle (diameter ≥ 75 µm) was used to insert each of the two single-channel CNT electrodes in a nerve target, which may have caused permanent nerve damage. A carbon fiber array (Gillis et al. 2018) was directly inserted in a fine autonomic nerve (diameter of 125 µm), but was only demonstrated in an acute setup. Securing a multi-channel array in a small-diameter autonomic nerve is extremely challenging due to the fine structure of autonomic nerves. We developed a new implantation procedure that involved the design of a vacuum suction adaptor to handle the array, a nerve-holder to facilitate the array insertion process, and a nerve-release tool to accurately and safely relocate the implanted nerve. The MINA array was inserted directly into a rat vagus nerve (diameter of 300-500 µm) with a manual micromanipulator, without a shuttle or high-pressure insertion tool (e.g. tungsten needle for CNT electrode, pneumatic inserter for Utah array). The procedure also incorporated an innovative attachment approach to secure an array interface on a nerve by applying a coating of rose-bengal on the array. Once the rose-bengal is activated with a laser, crosslink bonding between collagen fibers in the array coating and the nerve are formed. These implantation components are easily adjustable and may be useful for implanting other electrodes in or on various nerves across the peripheral nervous system.

6.2.3   Intraneural Recordings in an Autonomic Nerve

The work detailed in Chapter 5 demonstrated CFMA as a multi-channel, intraneural array for small-diameter ($\leq$ 0.5 mm) autonomic nerves. Recording physiological neural signals from autonomic nerves is very challenging due to the small nature of these nerves, and the low-amplitude signals from their micron-diameter axons (Gabella and Pease 1973; Prechtl and Powley 1990). As mentioned earlier, intraneural carbon nanotube (CNT) electrodes obtained high SNR (>10 dB) physiological recordings in small diameter (100-300 µm) rat glossopharyngeal and vagus nerves (McCallum et al. 2017). Two single-channel CNT electrodes were inserted in a nerve target to obtain only a single differential recording. In the work of this aim, 16-channel CFMAs were inserted in rat vagus nerves (diameter of 300-500 µm) and recorded physiological neural activity (SNR of 2.0-7.0) on multiple channels, which also provided information on the propagation direction and conduction velocity of some signals. Another research group developed an intraneural 4-channel carbon fiber array that recorded from tracheosyringeal nerves (diameter of 125 µm) of zebra finch birds (Gillis et al. 2018). Although an example of spontaneous activity was shown using the 4-channel array, the majority of their demonstrated signals were evoked responses from electrical stimulation, and no information was reported on physiologically-modulated activity or signal propagation along the array. Moreover, our intraneural axonal recordings provide a source of reference for designing future intraneural electrodes for autonomic nerves, which are currently sparse in the field despite the immense benefit that could be gained from monitoring and controlling signals in these nerves. A class of therapies that has gained considerable interest in recent years is bioelectronic medicine, which targets autonomic nerves to detect and alter neural activity for restoring autonomic functions (Tracey 2014; Birmingham et al. 2014; Pavlov and Tracey 2019). The variety of bioelectronic medicine applications that target the vagus nerve have

led to clinical trials on vagus nerve stimulation (VNS) for patients with rheumatoid arthritis (Koopman et al. 2016), obesity (Apovian et al. 2017), and type-2 diabetes (Shikora et al. 2015), among others. Despite the therapeutic benefits of VNS and bioelectronic medicine, stimulation patterns are generally selected by experimenting with different parameters without monitoring the physiological signaling in the nerve. A key element that is needed to achieve the full potential of bioelectronic medicine is a better understanding of neural signaling in physiological and pathophysiological conditions. Our obtained intraneural CFMA recordings from the vagus nerve, which conveys important glucose regulation signals (Berthoud 2008; Waise, Dranse, and Lam 2018), is an advancement towards a better understanding of neural signaling and may assist in the development of an effective bioelectronic medicine for diabetic patients.

6.3 Future Studies

6.3.1 Additional Studies on Stimulation of Renal Nerves for Glycemic Control

Although glucose regulation changes were observed in response to kilohertz frequency stimulation of renal nerves (Chapter 2 and Chapter 3), further studies are needed to examine the underlying mechanisms. It is unknown if the observed glucose regulation responses to stimulation of renal nerves were consequences of changes in urine flow rate, or directly related to the glucose transport pathways in the proximal tubules, which are innervated by renal nerves (Mather and Pollock 2011; Muller and Barajas 1972; Luff et al. 1992). Additionally, exploring longer and more complex stimulation patterns may be needed to enhance the glucose regulation response. Kilohertz frequency stimulation at 50 kHz, which is the same frequency used in our experiments, was applied continuously for 9 weeks on the carotid sinus nerve in diabetic rats (Sacramento et al. 2018). Improvements in insulin sensitivity and glucose tolerance were observed at the end of the 9-week stimulation period. The study reported no behavioral alterations for the rats, and carotid sinus nerve

responses to hypoxia returned to baseline after continuous 1-week stimulation of carotid sinus nerve. Although the nerve targets are different, these findings are encouraging for kilohertz frequency stimulation of renal nerves at long continuous durations. Above all, safety studies on stimulation of renal nerve is an absolute necessity for the advancement of this approach. Continuous measurements to assess renal function, such as glomerular filtration rate, renal plasma flow and sodium excretion measurements (Toto 1995; Phillips and Hamilton 1948), are necessary to evaluate the safety of kilohertz frequency stimulation of renal nerves and to proceed with confidence towards clinical trials on this potential treatment modality for diabetic patients.

6.3.2   Long-Term Recordings of Autonomic Nerves for Glucose Regulation Signaling

The work in Chapter 4 demonstrated a chronic procedure for implanting non-wired intraneural arrays in small-diameter autonomic nerves, while Chapter 5 showed intraneural recordings from a small autonomic nerve in an acute setting. Although previously mentioned carbon nanotube electrodes were chronically implanted in small-diameter autonomic nerves (McCallum et al. 2017), a need remains for the chronic implantation of highly-selective intraneural arrays that can record physiological single-neuron activity in fine autonomic nerves. Monitoring physiological signaling in autonomic nerves will help researchers better understand the neural control process, which may assist in the development of innovative treatment modalities to restore vital body functions regulated by these nerves. Furthermore, future studies on physiological neural activity recordings from various autonomic nerves that contribute in the glucose regulation process, such as renal nerves, splanchnic nerves, and hepatic and pancreas branches of the vagus nerve (Chhabra et al. 2017; Yi et al. 2010; Verberne, Sabetghadam, and Korim 2014), may provide novel perspectives on neural glycemic control. Recording neural activity may also be useful in monitoring physiological changes by decoding neural signals and providing sensory feedback for

closed-loop stimulation applications (Ouyang et al. 2019; Vu et al. 2018; Horbach et al. 2016). Additionally, monitoring changes in neural activity during the progression of diabetes in diabetic animal models (Has-Georg Joost and Al-Hasani 2012; King 2012) may provide new information that will assist in the development of new diabetic treatments.

6.3.3 Closed-Loop Bioelectronic Medicine for Glycemic Control

Our ultimate goal is to provide a reversible, automated and effective treatment that will assist diabetic patients in the commitment of a lifelong therapy. Our envisioned diabetic therapy is an implantable bioelectronic medicine that targets autonomic nerves to accurately detect elevations in blood glucose levels and trigger effective stimulation patterns to regulate blood glucose concentration levels. As detailed in Chapters 2 and 3, the renal nerve is a potential target for this therapy. Reduced renal nerve activity in mutant (hypothalamic POMC-deficient) mice (Chhabra et al. 2016; 2017) and renal denervation animal models (Rafiq et al. 2015; Iyer et al. 2016) showed improvements in glucose regulation. A potential bioelectronic medicine approach for glycemic control is the detection of neural patterns in renal nerve activity in hyperglycemia conditions to trigger selective stimulation of renal nerve fibers to regulate the glucose homeostasis functions of the kidney (DeFronzo, Davidson, and Del Prato 2012; Mather and Pollock 2011). Alternatively, the vagus nerve conveys important afferent and efferent neural signals for glucose regulation (Waise, Dranse, and Lam 2018; Matsuhisa et al. 2000). Fibers of the vagus nerve supply the liver, pancreas, gastrointestinal tract (Powley et al. 1983; Berthoud and Neuhuber 2000), and also conduct glucose sensing signals from the oral cavity and portal vein (Berthoud 2008; Watts and Donovan 2010). Consequently, the vagus nerve is an attractive nerve target for glycemic control in bioelectronic medicine. Patients enrolled in clinical trials on vagal nerve block (vBloc) therapy and transcutaneous auricular vagus nerve stimulation (taVNS) showed improvements in glycemic

control (Shikora et al. 2015; Huang et al. 2016). However, stimulation in vBloc therapy is applied by placing cuff electrodes on abdominal vagus nerves, while taVNS uses non-invasive stimulator electrodes that are placed on the auricular concha area of the ear to target vagus nerve branches in that area. The electrodes used in both therapies lack selectivity, which is critical for an effective bioelectronic medicine treatment that targets function-specific fibers in the vagus nerve. The development of an efficient bioelectronic medicine that targets the vagus nerve requires incorporating the chronic implantation of selective electrodes in the vagus nerve, which was demonstrated with MINA in Chapter 4, and can detect physiological action potential signals, as shown using CFMA in Chapter 5, along with highly-selective stimulation techniques, which may be achieved with MINA or CFMA, to precisely target axons in the vagus nerve that control specific regulation functions. The complete development of this bioelectronic medicine application may provide a reversible, automated and effective treatment that will assist diabetic patients in the commitment of a lifelong therapy and overcome the therapeutic limitations and compliance issues associated with current medications for diabetes.

6.4 Conclusions

This dissertation investigated modulation of neural activity for glucose regulation, assembled a new chronic implantation procedure for intraneural arrays, and monitored physiological signaling in an autonomic nerve. Future work is needed to evaluate the long-term efficacy and safety of these approaches. Overall, this work supports the potential development of an alternative implantable treatment modality for diabetic patients by modulating and monitoring neural activity in autonomic nerves.

Over 450 million people around the world are diabetic, and an estimate of 1.5 million deaths in a year are caused by diabetes (Cho et al. 2018; World Health Organization 2016). My

dissertation is devoted to these patients. My ultimate hope is to see this research, and future work built on this research, contributing, even in the slightest way, to limit the suffering and deaths caused by diabetes, and to improve the lives of the millions who are currently struggling with this disease.

Appendices

Appendix A: Stimulation of Renal Nerves on Renal Artery Blood Flow and Kidney Perfusion

In the experiments of Chapter 2 and Chapter 3, stimulation of renal nerves was applied through a bipolar nerve cuff electrode (1.00 mm inner-diameter, 100 µm platinum contacts, Microprobes for Life Science, Gaithersburg, MD, USA), which was placed around the renal artery, encircling renal nerves that run along the artery. A main concern with this stimulation approach is the occlusion or disruption of blood flow during stimulation. To evaluate this concern, renal artery blood flow during stimulation was measured using a perivascular flow meter system (TS420, Transonic Systems Inc., Ithaca, NY, USA) in one experiment. A nerve cuff electrode was placed on the renal artery, encircling the renal nerves. Proximal to the nerve cuff electrode, a flow sensor probe (1.5 mm inner-diameter, 1.5PS) was placed on the renal artery. Measurements of renal artery blood flow were obtained during stimulation of renal nerves at kilohertz frequencies (1-100 kHz) and low frequencies (2-10 Hz) at different amplitudes (10-50 V). The mean renal blood flow (mRBF) ratio was calculated for each stimulation trial [mRBF ratio = $mRBF_{stim}/mRBF_{pre-stim}$]. The mRBF values were computed at manually-identified steady-state conditions, with a minimum time interval of 7 sec for $mRBF_{pre-stim}$, and 19 sec for $mRBF_{stim}$.

Similarly, we monitored kidney perfusion in another experiment using a laser speckle contrast imager (moorFLPI-2, Moor Instruments Ltd, Devon, UK). The kidney was exposed, and a nerve cuff electrode was placed on the renal artery as in other experiments. The imager was

positioned directly above the exposed kidney. The kidney superficial blood perfusion (flux) was measured at a specified region of interest (kidney perimeter manually traced) during stimulation at kilohertz frequencies (1-100 kHz, 15 V) and low frequencies (2-10 Hz, 10 V). The mean flux (mFlux) ratio was calculated in the same manner as mRBF ratio, with a minimum time interval of 30 sec for mFlux$_{pre-stim}$, and 14 sec for mFlux$_{stim}$.

The mean renal blood flow (mRBF) ratio for all stimulation parameters are shown in Figure A.1a. Stimulation at kilohertz frequencies (1-100 kHz, 15-30 V) had minimal effect on renal blood flow (mRBF ratio ≥ 0.95) except at 1 kHz, 30 V (mRBF ratio = 0.57) and 5 kHz, 30 V (mRBF ratio = 0.91). Similarly, low frequency, low-amplitude stimulation (2-10 Hz, 10-20 V) had minimal effect on renal blood flow (mRBF ratio ≥ 0.98). However, 10 Hz stimulation at 40 V and 50 V showed a major reduction in renal blood flow (mRBF ratio of 0.69 and 0.47, respectively).
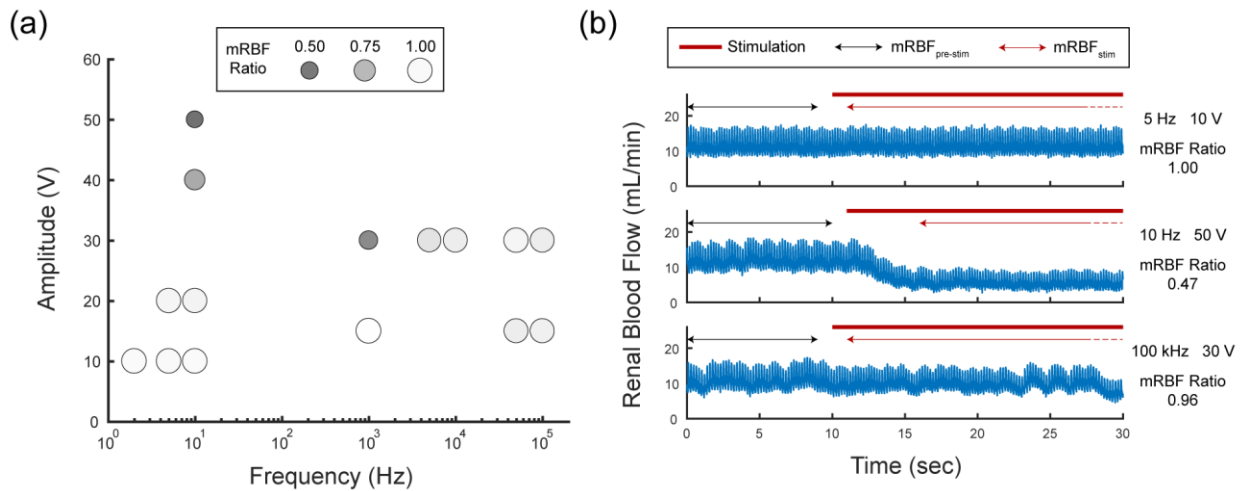

Figure A.1 Renal artery blood flow at applied stimulation. (a) Mean renal blood flow (mRBF) ratio for performed stimulation trials. (b) Renal blood flow measurements in three example trials. The double arrows indicate the manually-identified steady-state intervals for mRBF$_{pre-stim}$ and mRBF$_{stim}$.

The mean flux (mFlux) ratio for all stimulation parameters are shown in Figure A.2a. A minimal effect on kidney perfusion was observed for kilohertz frequency stimulation at 10 kHz and above with an amplitude of 15 V (mFlux ratio $\geq$ 0.97). However, at 1 and 5 kHz stimulation, mFlux ratio was 0.59 and 0.42, respectively. In low frequency stimulation trials with an amplitude of 10 V, mFlux ratio was 0.94, 0.79 and 0.39 at 2, 5 and 10 Hz, respectively.
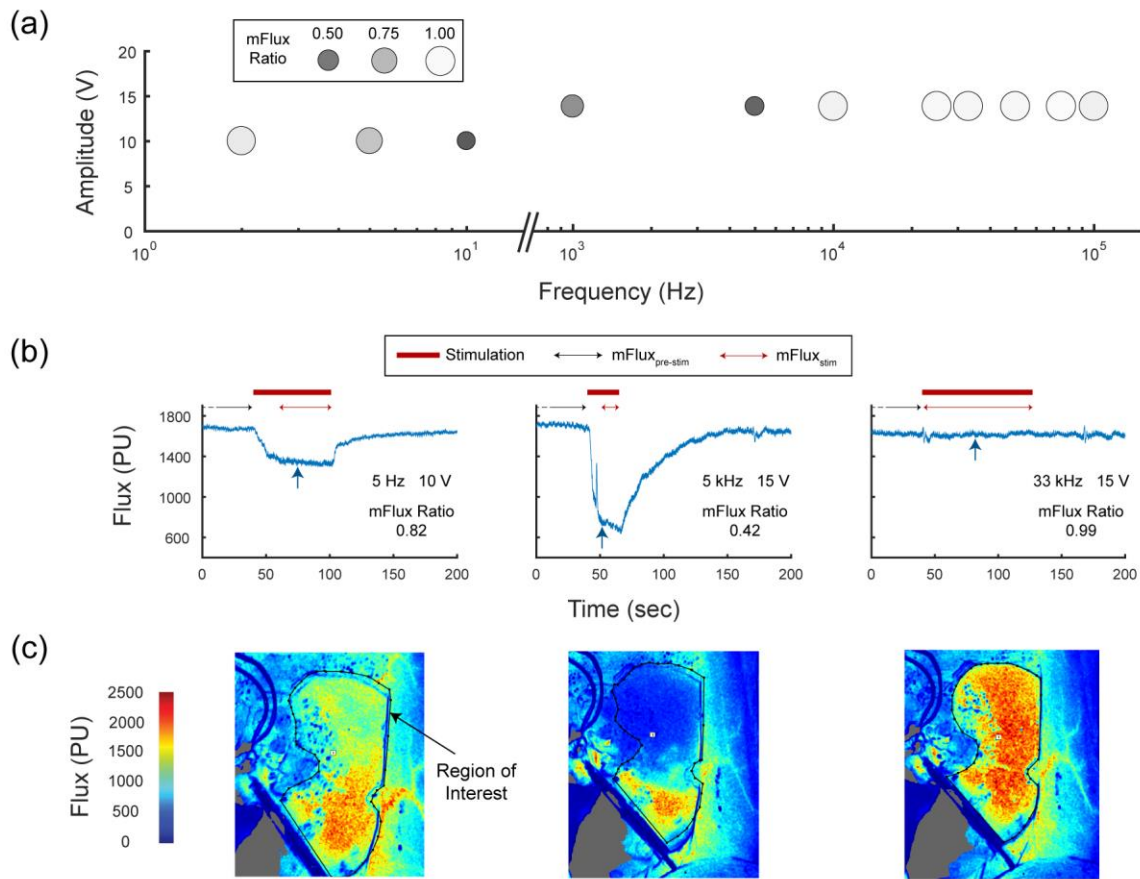
Figure A.2 Kidney perfusion at applied stimulation. (a) Mean kidney perfusion (mFlux) ratio for performed stimulation trials. (b) Perfusion (flux) measurements in arbitrary perfusion units (PU) for three example trials. Single arrows indicate the timing of the perfusion images shown in c. Double arrows indicate the manually-identified steady-state intervals for mFlux$_{pre-stim}$ and mFlux$_{stim}$. (c) Corresponding perfusion images at time points indicated in b. The kidney perimeter was specified manually as the region of interest for analysis.

Renal blood flow (Figure A.1) and kidney perfusion (Figure A.2) were monitored in separate one-off pilot experiments, and minimal-to-moderate changes were observed at the specified stimulation parameters in this study. We cannot specifically determine if these changes were a consequence of neural control of renal nerves or vasoconstriction of renal arteries. However, it was promising that 5 Hz stimulation at our typical stimulus amplitude did not affect blood flow and 33 and 50 kHz did not affect blood flow or renal perfusion, suggesting that blood flow to the kidneys themselves was not significantly limited in the experimental trials of Chapters 2 and 3. Additional imaging experiments involving Doppler ultrasound or angiography techniques on renal vessels at stimulation locations may provide further insight (Greene et al. 1981).

Appendix B: Microneedle Penetrating Array with Axon-Sized Dimensions for Cuff-less Peripheral Nerve Interfacing

D. Yan, **A. Jiman**, D. Ratze, S. Huang, S. Parizi, E. Welle, Z. Ouyang, P. Patel, M. J. Kushner, C. Chestek, T. M. Bruns, E. Yoon, and J. Seymour, "Microneedle Penetrating Array with Axon-Sized Dimensions for Cuff-less Peripheral Nerve Interfacing," *Proc. 9th Int. IEEE EMBS Conf. Neural Eng.*, pp. 827–830, 2019.

Abstract

Autonomic nerves are typically only hundreds of microns in diameter near their organ targets and these carry all of the sympathetic and parasympathetic control signals. We present a cuff-less microneedle array specifically designed to potentially map small autonomic nerves. The focus of this paper is the design and fabrication of an ultra-miniaturized silicon needle array on a silicone substrate. We demonstrate arrays having 25 to 100 microneedles. Each needle has a 1-micron tip and dual-taper shaft. We demonstrate an ability to control the tip shape, angle, and shaft

angle which is important for balancing sharpness and stiffness. These high-density arrays also include a special backside anchor embedded in silicone for stability in the elastic substrate, yet the array freely wraps over a 300-µm nerve. Another critical method presented here is a surgical technique for inserting and securing an array without a cuff (as small as 0.3 mm wide and 1.2 mm long) by photochemical bonding of collagen/Rose Bengal adhesive agents to epineurium. Future work will focus on device functionalization and histological characterization in a rat vagus model.

Introduction

Implantable peripheral nerve interfaces can be categorized as cuff (surrounding the epineurial surface), intrafascicular (through the perineurium), and regenerative (bridging two nerve ends). Cuff devices do not have the ability to detect individual or local axon activity through the highly resistive epineurium and thus lack spatial resolution. Intrafascicular arrays, by contrast, implant electrodes transversely or longitudinally to the nerve and may have significant tissue damage. Even thin polymer arrays, which for the last decade represent the state-of-the-art in this field, result in tissue encapsulation around the microelectrodes on the order of 50-100 µm (Wurth et al. 2017). While an improvement over past technologies such as the high-density Utah electrode array (HD-UEA) (Wark et al. 2014) which showed excellent longevity for stimulation in larger nerves, flexible polymer arrays are greatly oversized for most autonomic nerves, which are often below 1 mm in diameter.

The goal of MIcroneedle Nerve Array (MINA) is to offer a minimally invasive intrafascicular penetrating technology that ideally extends just beyond the epineurium and perineurium of a fascicular bundle and with recording needles similar in size to large axons (~20 µm). We hypothesize that the size of each individual penetrating structure is a critical factor

117

influencing the tissue response. Additionally, the way in which the array is secured to the nerve is also a critical factor.

Methods

Each individual penetrating microneedle of MINA has a total height of 180 µm. As they are anchored onto the neutral plane of an 80-µm thick PDMS layer, the exposed needle bodies have an average length of 140 µm. The average diameter of the needle tip and whole needle body is 6.3 µm and 17.6 µm. Table B.1 shows a comparison of the individual needle diameter of MINA with the current state-of-the-art silicon needle array, HD-UEA. As shown in Figure B.1, the ultra-fine silicon microneedles were placed in a honeycomb pattern with 150 µm spacing.
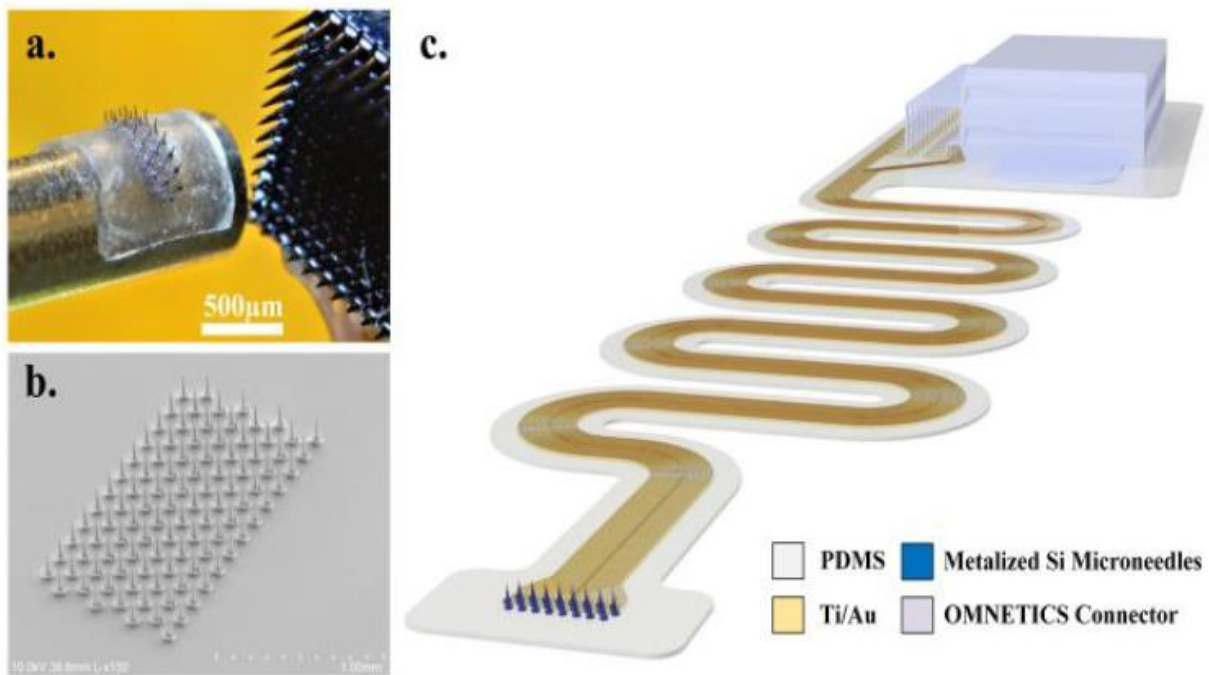

Figure B.1 Microneedle Nerve Array (MINA). (a) Size comparison between MINA and high-density Utah slant array. MINA wrapped around a metal rod (0.56-mm diameter). (b) SEM image of 100-site silicon microneedle array in a 0.9mm×1.8mm rectangular area. (c) Conceptual image of a future functional version of MINA.

Axon-Dimension Microneedle Design, Simulation and Microfabrication

The process of scaling down the cross-section of the penetrating structures requires careful design to ensure mechanical robustness. A ~10μm diameter high-aspect-ratio silicon structure can be extremely fragile during penetration or while implanted. To optimize the structural mechanics of the ultra-fine silicon microneedle, we used finite element methods (FEM) in COMSOL to evaluate tip angles and shaft angles while trying to keep the upper portion in particular smaller than a large axon diameter ($< 20\,\mu m$). A dual-taper-profile (i.e. a full tip angle of 30° degrees and a shaft side-wall angle of 3°) with a cylindrical backside anchor provided us with the greatest stability inside the soft bulk material of the array body.

The yield stress of silicon is around 7 GPa. Simulation using COMSOL predicted a maximum stress of only 13.4 MPa under 1 gram force applied both lateral and longitudinal on a nerve phantom laying over the top of the needle with non-slip boundary condition. (Figure B.2) The Young's module of the nerve was set at 300 kPa.

Table B.1 Needle comparison of MINA vs HD-UEA

Device	Average Diameter at % Distance to the Tip (µm)			
	5%	*20%*	*50%*	*90%*
MINA	4.3	13.3	16.9	24.2
HD-UEA	-	41.2	73.3	107.3

Deep reactive ion etching (DRIE) of silicon creates a negative sidewall angle unsuitable for microneedles if a modification is not introduced. In our case we used a thin, protective ring to create a micro-loading effect in the etch around our needles (Figure B.3), which is a modified approach from Hanein 2003 (Hanein et al. 2003). A computational study of DRIE of silicon

microneedles was conducted to improve our understanding of the etching and resulting sidewall profiles. We modeled the fabrication process in two steps: reactor scale modeling of the inductively coupled plasma (ICP) providing reactive fluxes to the substrate and single microneedle scale etching process simulation. The reactor scale modeling was performed using the Hybrid Plasma Equipment Model (HPEM), from which the neutral and ion fluxes and ion energy and angular distributions (IEADs) to the wafer surface were obtained (Kushner 2009). The resulting microneedle profiles were predicted using the Monte Carlo Feature Profile Model (MCFPM) (Huard et al. 2018).

MINA was fabricated starting with a Silicon on Insulator (SOI) wafer where the buried oxide layer depth defines the desired needle length. A silicon dioxide hard mask was deposited and patterned through lithography and oxide etching. Next the silicon was etched in a series of isotropic-anisotropic-isotropic conditions. The buried oxide layer was used as an etch-stop layer. High-quality insulation of the silicon was grown using thermal oxidation. Future versions of the microneedle electrode will require tip etching, metallization, and interconnection. Next, silicone was formed over the needles. Specifically, 1:1 diluted 20:1 PDMS (Sylgard 184) was spun over the microneedle arrays. Next, a PDMS stamp was pressed over the arrays to improve planarity of the uncured silicone. The wafer was then temporarily bonded onto a glass wafer to protect the topside. Finally, the handling layer of the SOI wafer was dissolved in 20% KOH solution and the arrays were released.

Photochemical Device-Epineurium Bonding Agent

Collagen (C9791 Sigma) and Rose Bengal (330000 Aldrich) were dissolved in 30% ethanol separately at 0.1 wt.%. Then the collagen ethanol solution was ultrasonicated for 10 min at room temperature. Next, the collagen and RB ethanol solution were mixed at a 10:1 ratio. Next,

the device was treated by oxygen plasma for surface activation. Oxygen plasma generated Si-O-groups on the silicone surface to bond with collagen matrices. The obtained collagen/RB ethanol solution was drop-cast onto the MINA surface shortly after plasma exposure. Finally, the devices were air-dried at 50°C and sterilized using low-temperature (37.7°C) ethylene oxide (EtO).

Surgical Method to Access Cervical Vagus Nerve

All experimental procedures were approved by the University of Michigan Institutional Animal Care and Use Committee. Experiments were performed on female 220-270 g Sprague-Dawley rats (Charles Rivers Laboratories). One day prior to surgery, animals were injected subcutaneously with dexamethasone (0.2 mg/kg). For the implant procedure, animals were anesthetized with isoflurane (1-5%) and injected subcutaneously with carprofen (5 mg/kg), lidocaine (0.4%), and dexamethasone (0.20 mg/kg). A midline cervical incision was made to access the right cervical vagus nerve. Under a dissection microscope (Lynx EVO, Vision Engineering Inc.), the vagus nerve was isolated (5-7 mm) from the carotid artery and surrounding tissue and placed on a custom 3D-printed nerve holder (Figure 4). MINA was held on a custom vacuum adapter connected to a micromanipulator for accurate placement. A small pencil-shaped camera (MS100, Teslong) was positioned in the surgical opening to allow for visualization of device implantation.

Cuff-less Technique for MINA implantation

The key to achieving cuff-free implantation was the novel photochemical bonding of the nerve epineurium to the surface of the MINA. This approach was inspired by previous work demonstrating a Rose Bengal-chitosan patch as a means to adhere two halves of tissue (Lauto et al. 2012). Previously, Rose Bengal was demonstrated as a suture-less wound closure technique (Chan, Kochevar, and Redmond 2002) and more recently for nerve grafting (Fairbairn et al. 2015).

121

The mechanism of action is covalent cross-linking of collagen molecules facilitated by light activation of Rose Bengal (a fluorescein-like molecule). Light activation at the MINA/nerve interface was by a laser beam (532 nm, 85 mW) for 2-3 minutes. A 0.8-mm diameter beam was positioned along MINA on 3-4 spots, moving to new position every two seconds. Saline was periodically rinsed over the nerve to dissipate heat after laser exposure. After adhesion, the vagus nerve was removed from the nerve holder and surgical clips were used to close the skin incision. A subcutaneous injection of carprofen (5 mg/kg) and dexamethasone (0.2-0.05 mg/kg) were administered daily after surgery for 2-3 days. Animal's health was checked daily.

Terminal Electrophysiology Assessment

A terminal procedure under isoflurane anesthesia (1-5%) was performed to assess nerve function prior to sample removal for imaging. A bipolar cuff electrode (0.75 mm inner-diameter, Microprobes for Life Science,) was placed on the vagus nerve distal to the implant region to record neural activity (PowerLab, ADInstruments). A stimulation probe was placed on the vagus nerve proximal to the implant region and connected to an isolated pulse generator (Model 2100, A-M Systems). Electrical stimulation (1-8 mA, 2 Hz) was applied to evoke neural activity. After testing animals were euthanized with an overdose of sodium pentobarbital (400 mg/kg). The implanted nerves were extracted and kept in 3% glutaraldehyde.

Micro-CT Imaging

Microscopic X-Ray Computed Tomography (micro-CT, Zeiss Versa 520), where X-rays are emitted from an X-ray generator, travel through a rotating nerve sample, and are recorded by a detector on the other side to produce a radiograph series, was used to visualize chronic MINA nerve implants. By varying the focus depth, the 3D tomography was constructed from 2.0~3.5 μm

cubic pixels. Osmium-tetroxide staining of samples after soaking in glutaraldehyde provided greatly improved contrast (Figure B.4c, d).

Results and Discussion

Axon-dimension Microneedle in Ultra-flexible Array

We successfully fabricated silicon microneedles having the three stress-reducing features predicted by COMSOL simulations: a large angle on the tip, modest tapering on the sidewall, and a wide base (Figure B.2) to minimize lateral and angular movement of the stand-alone needles embedded in a soft, thin elastomer. These low-stress features still allowed us to maintain an average diameter of 7 µm over the tip segment, which we hypothesize will mitigate axon damage, demyelination, and collagenous encapsulation. Results from COMSOL simulation illustrated the stress distribution along one individual silicon microneedle under longitudinal and lateral forces. The maximum local stress, which reflect the most fragile point of the structure, along the needle body was compared between different needle shapes. For a cylindrical profile microneedle, high stress is localized around the "foot" (Figure B.2, top). For a simple cone profile microneedle, high stress is localized around the "neck". By introducing a dual-taper (tip and shaft separated), the stress is distributed more evenly across the whole microneedle. The simulation results suggest that more than an order of magnitude maximum stress can be reduced by introducing a couple of micro-engineered features (Fig. B.2). The size of each dot represents a different shaft diameter and angles. Each needle has a total length of 160 µm and a backside anchor base of 20 µm thickness. Three sub-groups for the dual-taper shape (Figure 2, lower right) represent three different shaft angles, 2.5°, 3.5° and 5°. With approximately equal average cross-section diameter at 17.6 µm, a dual-taper shape design (3.5° shaft angle and 15° tip angle) has 20.8 times less maximum stress than

cylindrical shape and 7 times less than the simple conical shape. Moreover, the backside anchor structure significantly prevents rotational movement.
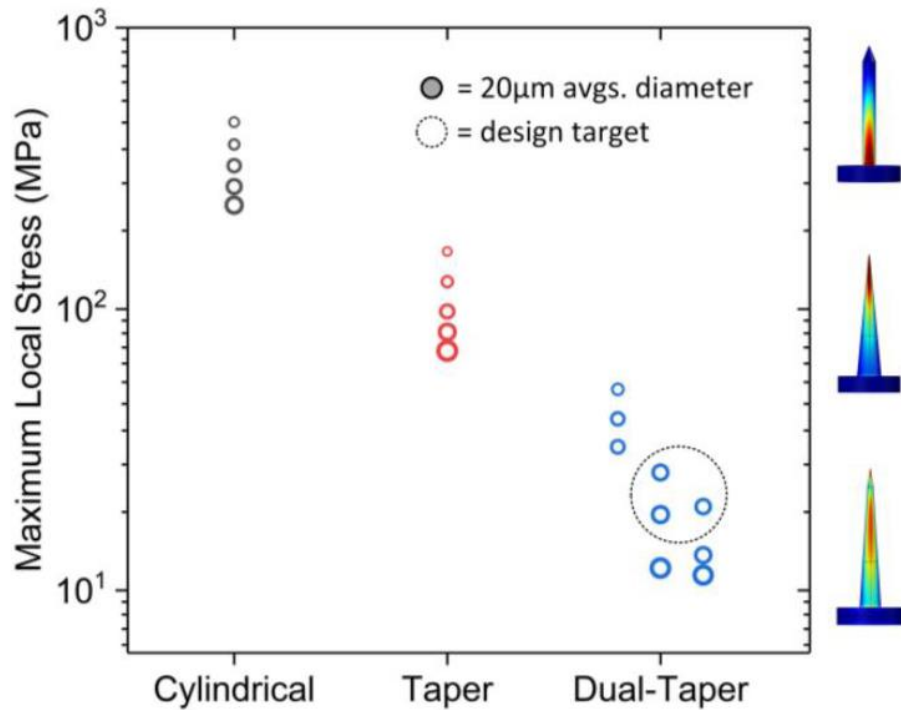

Figure B.2 Summary of maximum local stress comparison among different needle shapes. Dot sizes represent the average cross-section diameter. The gray-filled circle in the legend gives a scale bar of 20 µm diameter. Heat maps on needle shapes show where the stress.

Integrated plasma reactor and microneedle scale modeling helped us improve our fabrication process. The model predicted time evolution of profiles defining the needles are shown in Figure 3 (lower right). The first pseudo-isotropic etch step creates a straight angle taper on the cylinder beneath the SiO_2 mask (Figure B.3a). As the etching proceeds, the surrounding ring becomes thinner (Figure B.3b & c) and is eventually removed (Figure B.3d). The gap between the needle and the ring forms a trench with an aspect ratio of 8, which limits the transport of F atoms to the bottom and results in a micro-loading effect. The decreasing height of the surrounding ring

during the etching increases access to the central needle by F atoms, eventually trimming the needle shaft from a cylinder into a cone (Figure B.3d, f). Experimentally, the first two steps of the plasma etching created the vertical structure shown in in Figure 3a. The last-step isotropic silicon plasma etching process resulted in a profile close to the prediction. The microneedle tip was shaped into an average 13.8° taper while the microneedle body had a 3.3° shaft angle.
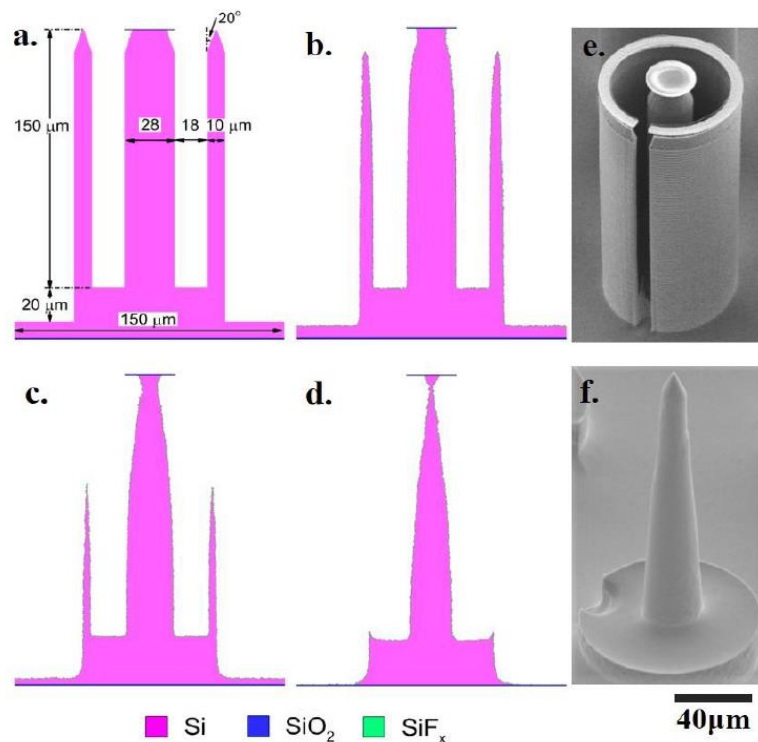

Figure B.3 Reactive ion etching model and results. (a)-(d) Time evolution of etching profile during the removal of surrounding rings using ICP sustained in SF6 at relative time points approximately: t=0, 30s, 60s and 90s. (e) & (f) SEM of image of one single structure corresponding to model steps (b) and (d).

Implantation and Device-Nerve Adhesion Using Photochemical Bonding

We demonstrate MINA can also be reliably inserted at a higher needle density 61/mm^2, compared with the high-density Utah array (Wark et al. 2013) at 25/mm^2, and a flexible penetrating microelectrode array (FPMA) (Byun et al. 2017) at 3.3/mm^2. We have implanted MINA into the

rat vagus nerve (300-500 µm) 4 out of 4 times with no observed needle damage or fracture. This robustness of such a fine silicon structure was expected from the short length and tapered shaft (Euler's buckling equation and COMSOL model). While higher density MINA arrays have been fabricated (100 µm pitch) we hypothesize the current pitch of 150 µm has a higher likelihood of minimizing tissue reactivity—but this important question should be tested in future work.

During terminal electrophysiology tests (not recorded from MINA) evoked compound action potentials (CAPs) were observed in all implanted nerves, demonstrating that nerves remained functional. Stimulation thresholds for eliciting CAP responses were 1-4 mA. Primary CAP features had conduction velocities of 2.1-6.8 m/s, which aligns with prior recordings from the vagus nerve.
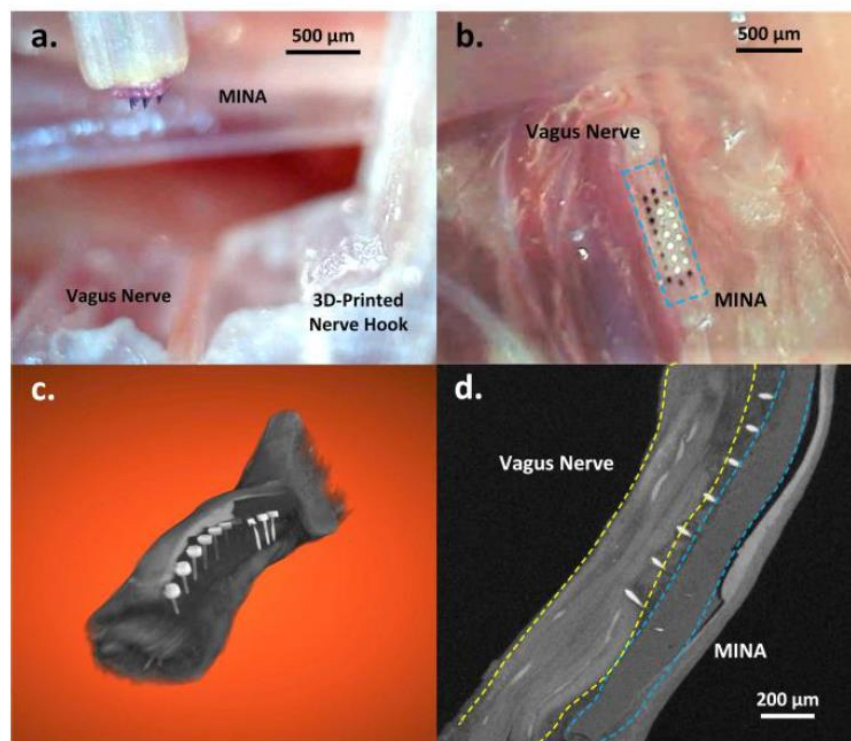

Figure B.4 MINA implantation and nerve sample at 1-week time point. (a) Top view of MINA and vagus nerve after implantation. (b) Side view photo during implantation. (c) A reconstructed 3D image from micro-CT showing unbroken needles implanted into the nerve. (d) Micro-CT scanned longitudinal nerve section with MINA implanted.

MINA implantation results were investigated through micro-CT imaging. Figure B.4b shows the cross-section views of a one-week implanted nerve sample. While some needles are in the nerve, we currently observe epineurium reactivity of connective tissue growth pushes some of the needles out. This may be due to damage from the needles, damage from the laser photochemical activation, or a foreign body reaction. We are currently testing improvements to the insertion process and laser application.

Ex vivo Evaluation of Device-Epineurium Adhesion

Similar to our in vivo implantation protocol, four freshly explanted rat nerves were implanted with a MINA and placed in a vial of held at either or 50°C for at least 5 weeks. No detachment of MINA was observed during soaking for any samples, providing further evidence this form of photochemical bonding creates a strong nerve-device bonding interface that remains flexible.

Conclusion

We demonstrate that axon-dimension needles can be precisely machined and implanted into fine autonomic nerves. We also demonstrate these small, flexible arrays remain on the nerve at a 1-week time point without the use of a cuff. The novel use of Rose Bengal to putatively form thin covalent bonding between a nerve and a sensor array has the advantage of being flexible, unlike cyanoacrylate and other glues. Our future work will demonstrate fully functional arrays and improved surgical techniques.

Acknowledgment

Appendix C: Computer-Aided Designs for 3D-Printed Components Used in Surgical Procedures

The computer-aided designs (CAD) for the 3D-printed components in Chapter 4 and Chapter 5 are shown in this appendix. For the microneedle nerve array (MINA) implantation procedure, we used a vacuum suction adaptor (Figure C.1), a nerve-holder for the fibrin sealant approach (Figure C.2), a nerve-holder and lens flap for the rose-bengal coating approach (Figure C.3 and 4), and a nerve-release tool (Figure C.5). For inserting a carbon fiber microelectrode array (CFMA) in the vagus nerve, we used a CFMA nerve-holder (Figure C.6).
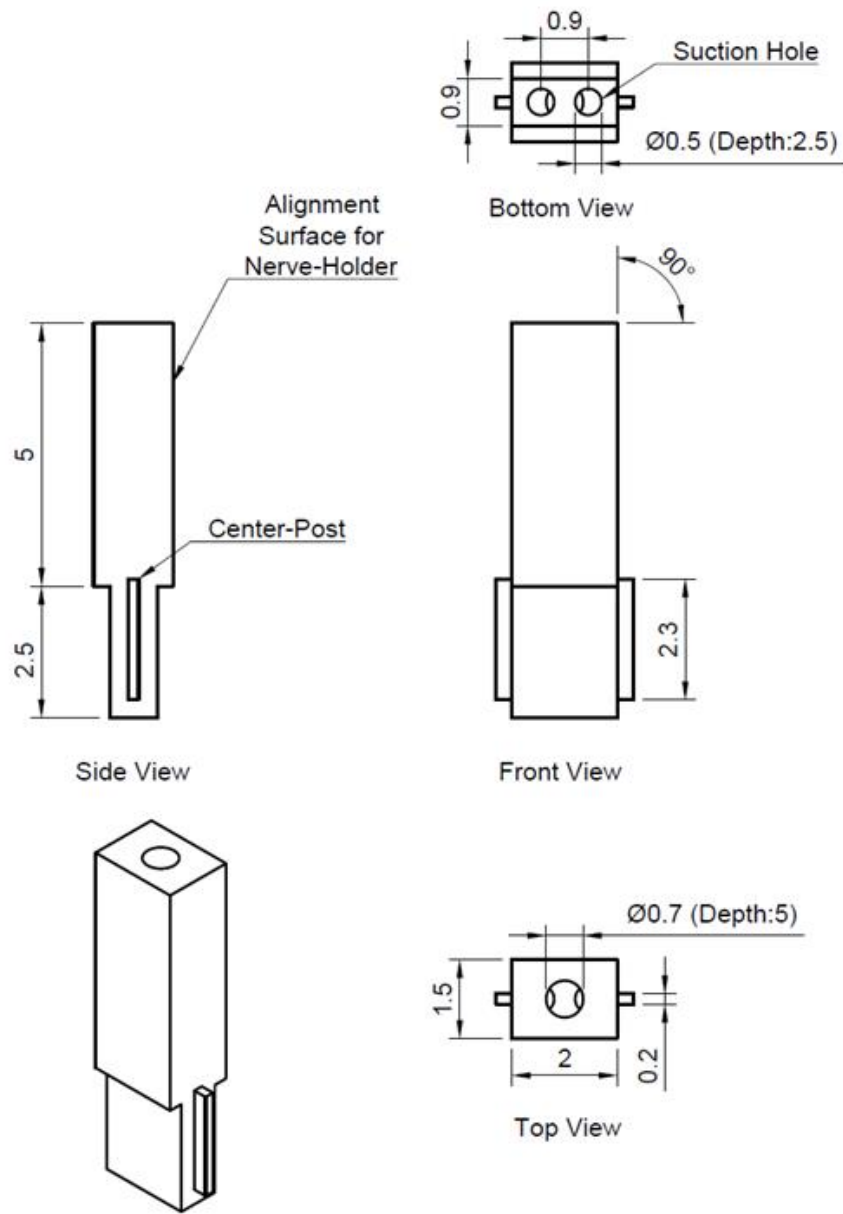
Figure C.1 Design of the vacuum suction adaptor. All dimensions are in millimeters (mm).
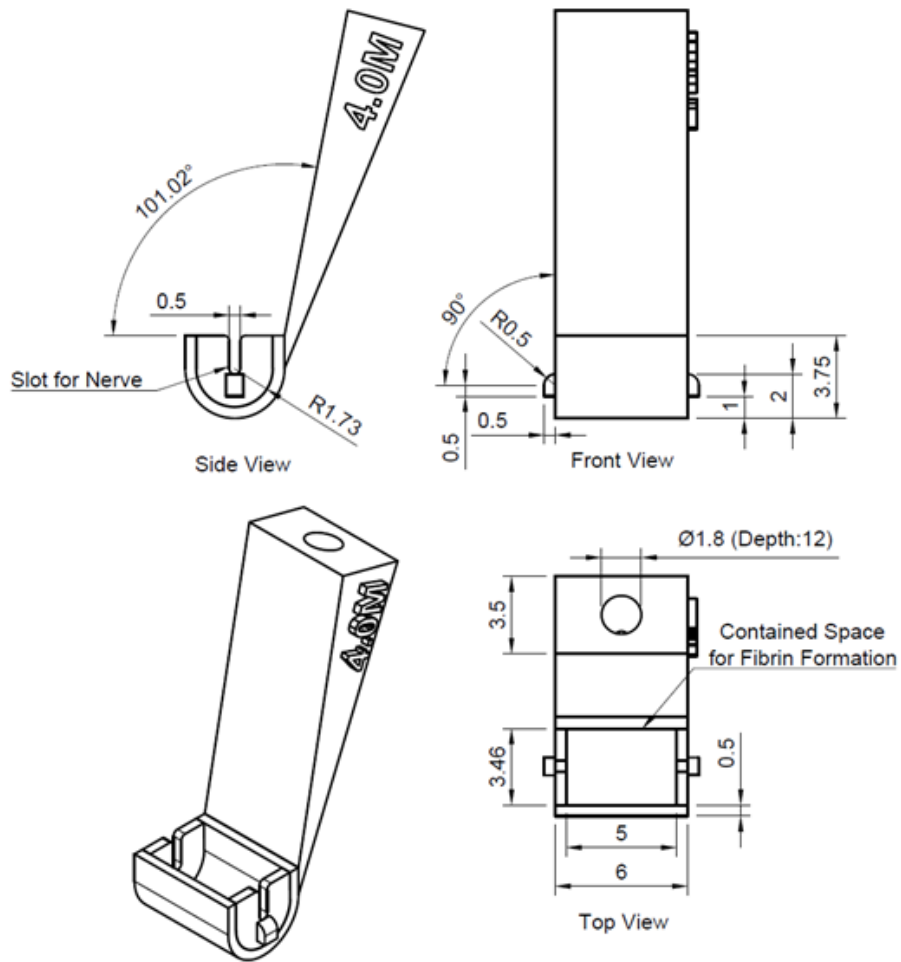
Figure C.2 Design of the nerve-holder for the fibrin sealant approach. All dimensions are in millimeters (mm).

Figure C.3 Design of the nerve-holder for rose-bengal coated MINA. All dimensions are in millimeters (mm).

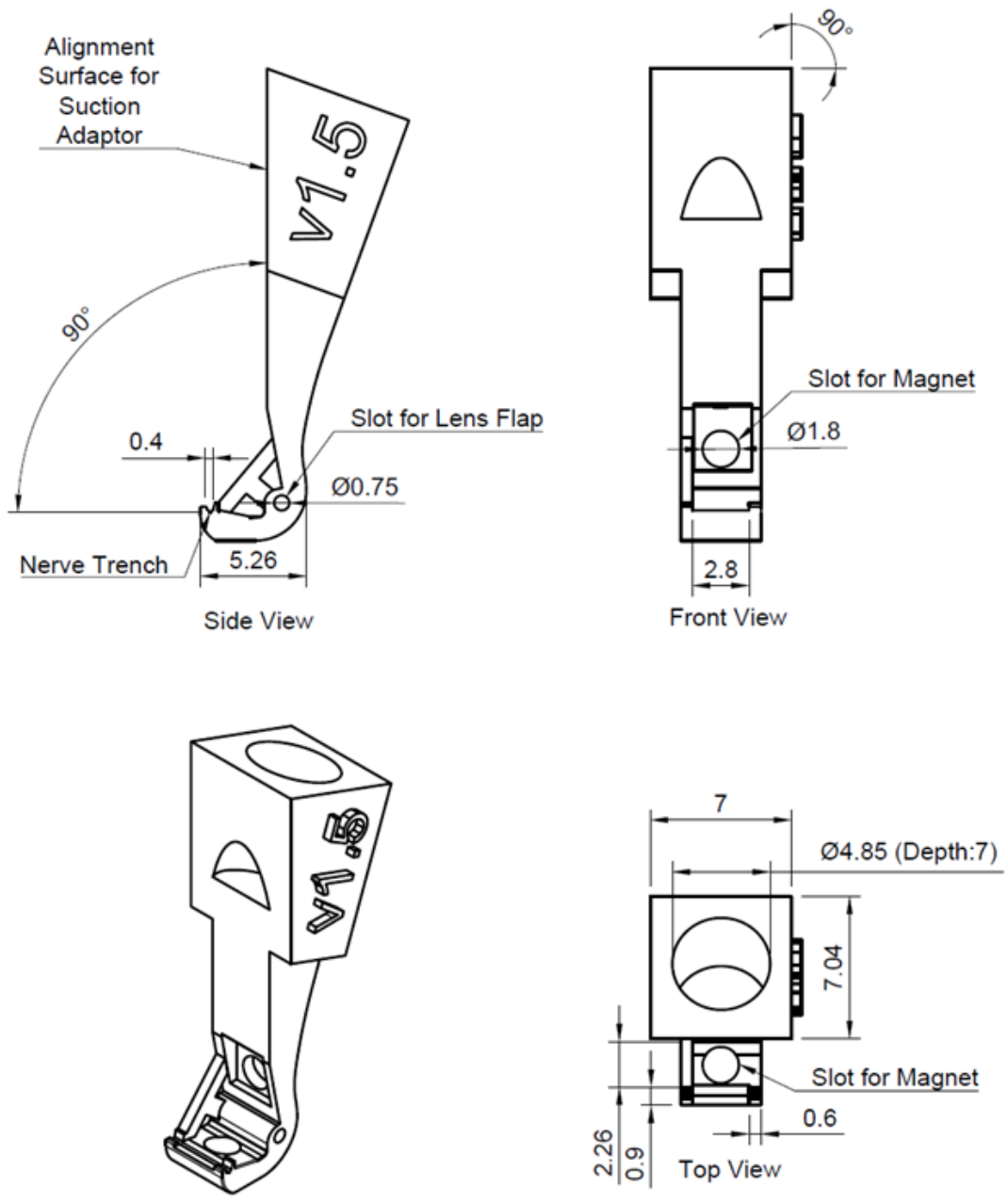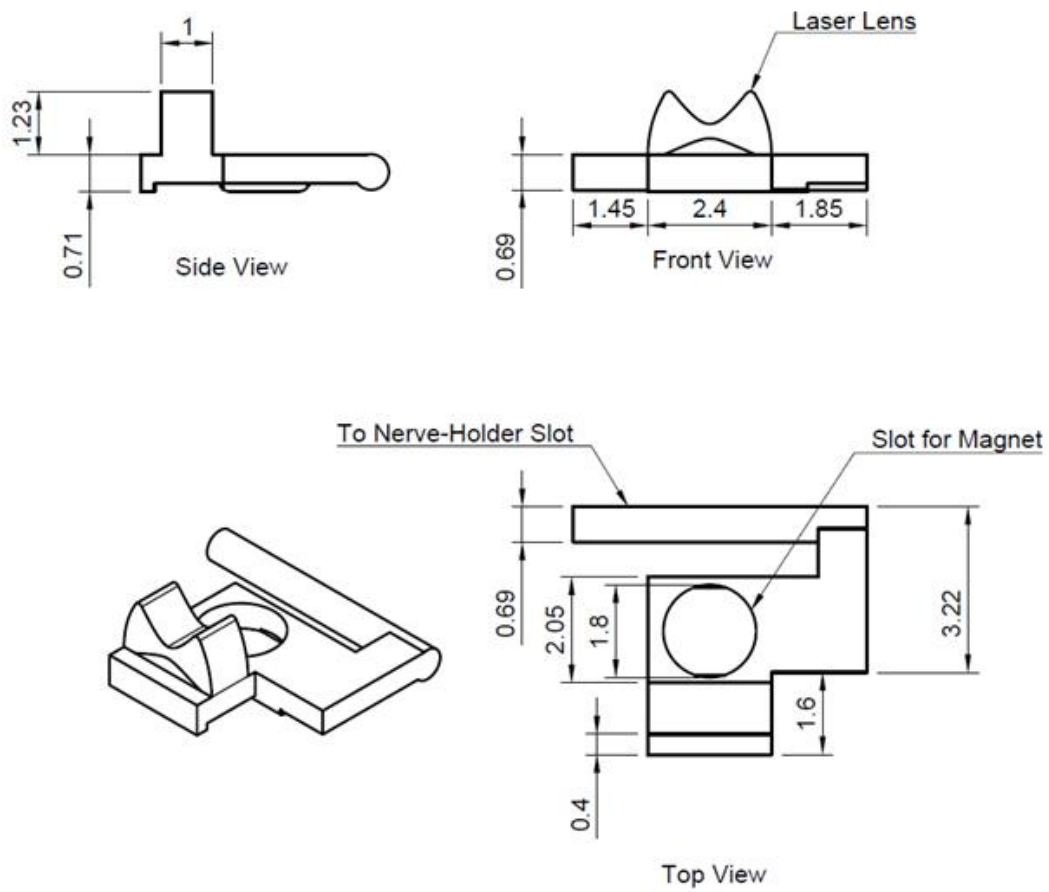**Figure C.4 Design of the laser lens flap.** All dimensions are in millimeters (mm).
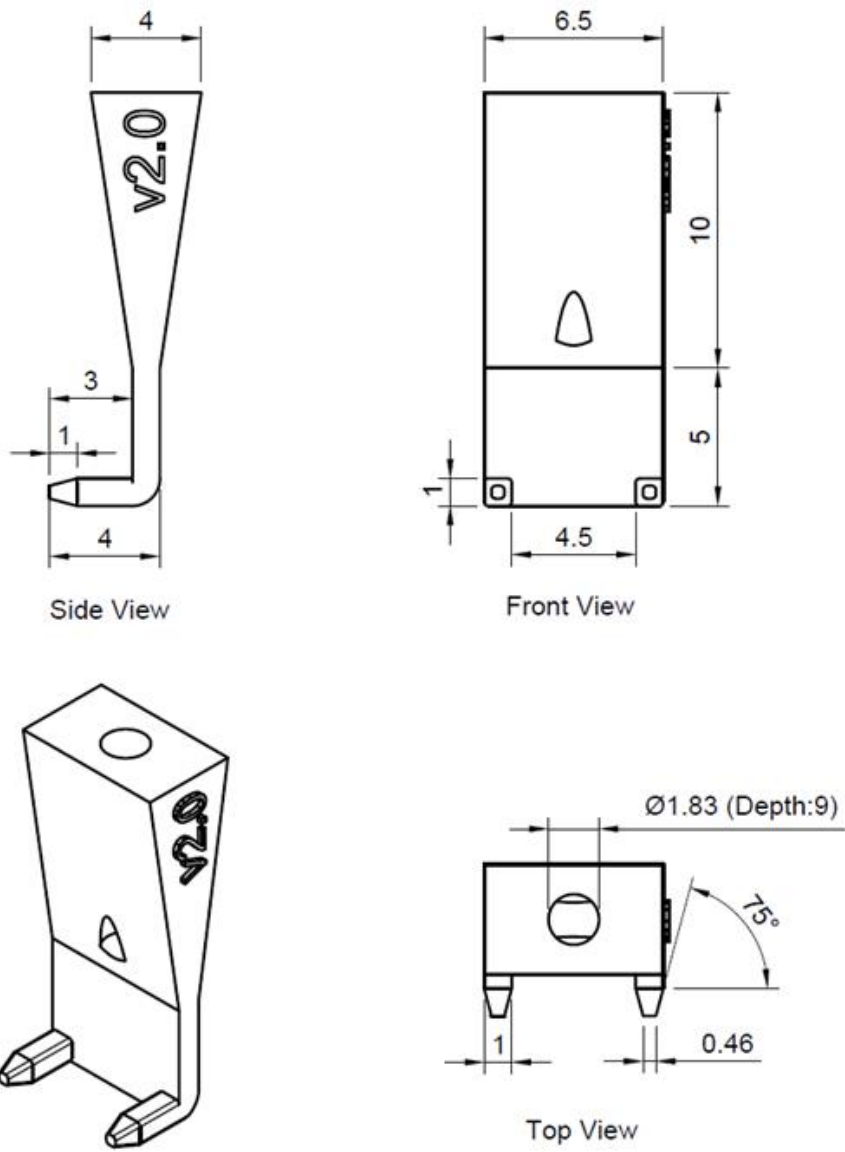
Figure C.5 Design of the nerve-release tool. All dimensions are in millimeters (mm).
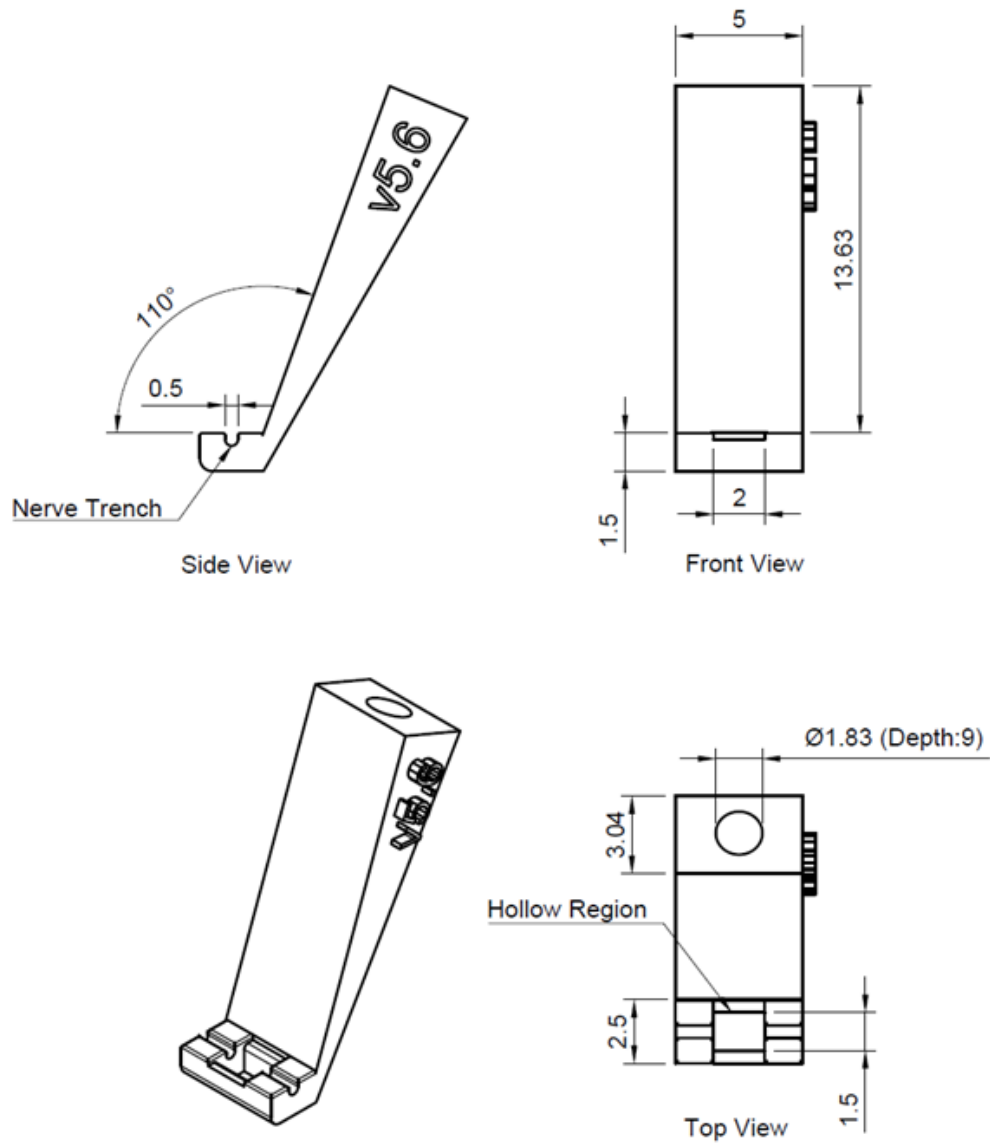
Figure C.6 Nerve-holder design for the carbon fiber microelectrode array (CFMA). The dimensions are in millimeters (mm).

Bibliography

Abell, Thomas, Richard McCallum, Michael Hocking, Kenneth Koch, Hasse Abrahamsson, Isabelle Leblanc, Greger Lindberg, et al. 2003. "Gastric Electrical Stimulation for Medically Refractory Gastroparesis." *Gastroenterology* 125: 421–28. https://doi.org/10.1016/S0016-5085(03)00878-3.

Agostoni, E, J E Chinnock, M De Burgh Daly, and J G Murray. 1957. "Functional and Histological Studies of the Vagus Nerve and Its Branches to the Heart, Lungs and Abdominal Viscera in the Cat." *J. Physiol.*

Ali, Mohammed K, Kai McKeever Bullard, Jinan B Saaddine, Catherine C Cowie, Giuseppina Imperatore, and Edward W Gregg. 2013. "Achievement of Goals in U.S. Diabetes Care, 1999-2010." *N Engl J Med* 368 (17): 1613–24. https://doi.org/10.1056/NEJMsa1213829.

American Diabetes Association. 2020. "Standards of Medical Care in Diabetes - 2020." *Diabetes Care* 43: S205–6. https://doi.org/10.2337/dc20-Sdis.

American Diabetes Association (ADA). 2018. "Standards of Medical Care in Diabetes - 2018." *Diabetes Care* 41 Suppl 1: S1–159.

Amsterdam, Wouter A. C. van, Peter J. Blankestijn, Roel Goldschmeding, and Ronald L.A.W. Bleys. 2016. "The Morphological Substrate for Renal Denervation: Nerve Distribution Patterns and Parasympathetic Nerves. A Post-Mortem Histological Study." *Annals of Anatomy* 204: 71–79. https://doi.org/10.1016/j.aanat.2015.11.004.

Andrews, P L R. 1986. "Vagal Afferent Innervation of the Gastrointestinal Tract." *Progress in Brain Research* 67: 65–86.

Apovian, Caroline M., Sajani N. Shah, Bruce M. Wolfe, Sayeed Ikramuddin, Christopher J. Miller, Katherine S. Tweden, Charles J. Billington, and Scott A. Shikora. 2017. "Two-Year Outcomes of Vagal Nerve Blocking (VBloc) for the Treatment of Obesity in the ReCharge Trial." *Obesity Surgery* 27: 169–76. https://doi.org/10.1007/s11695-016-2325-7.

Bacha, Tatiana El, Mauricio R.M.P. Luz, and Andrea T. Da Poian. 2010. "Dynamic Adaptation of Nutrient Utilization in Humans." *Nature Education* 3.

Badia, Jordi, Tim Boretius, Arán Pascual-Font, Esther Udina, Thomas Stieglitz, and Xavier Navarro. 2011. "Biocompatibility of Chronically Implanted Transverse Intrafascicular Multichannel Electrode (TIME) in the Rat Sciatic Nerve." *IEEE Transactions on Biomedical Engineering* 58 (8): 2324–32. https://doi.org/10.1109/TBME.2011.2153850.

Barton, Mathew, John W. Morley, Marcus A. Stoodley, Kheng Seong Ng, Sabine C. Piller, Hong Duong, Damia Mawad, David A. Mahns, and Antonio Lauto. 2013. "Laser-Activated Adhesive Films for Sutureless Median Nerve Anastomosis." *Journal of Biophotonics* 6 (11–12): 938–49. https://doi.org/10.1002/jbio.201300054.

Bello-Reuss, Elisa, Daniel L Trevino, and Carl W Gottschalk. 1976. "Effect of Renal Sympathetic Nerve Stimulation on Proximal Water and Sodium Reabsorption." *Journal of Clinical Investigation* 57: 1104–7.

Ben-Menachem, Elinor. 2002. "Vagus-Nerve Stimulation for the Treatment of Epilepsy." *The Lancet Neurology* 1 (8): 477–82. https://doi.org/10.1016/j.nec.2018.12.005.

Berthoud, Hans Rudolf. 2008. "The Vagus Nerve, Food Intake and Obesity." *Regulatory Peptides* 149 (1–3): 15–25. https://doi.org/10.1016/j.regpep.2007.08.024.

Berthoud, Hans Rudolf, and Winfried L. Neuhuber. 2000. "Functional and Chemical Anatomy of the Afferent Vagal System." *Autonomic Neuroscience: Basic and Clinical* 85 (1–3): 1–17. https://doi.org/10.1016/S1566-0702(00)00215-0.

Bhadra, Niloy, and Kevin L. Kilgore. 2005. "High-Frequency Electrical Conduction Block of Mammalian Peripheral Motor Nerve." *Muscle Nerve* 32: 782–90. https://doi.org/10.1002/mus.20428.

Bhatt, D L, D E Kandzari, W W O'Neill, R D'Agostino, J M Flack, B T Katzen, M B Leon, et al. 2014. "A Controlled Trial of Renal Denervation for Resistant Hypertension." *N Engl J Med* 370 (15): 1393–1401. https://doi.org/10.1056/NEJMoa1402670.

Birmingham, Karen, Viviana Gradinaru, Polina Anikeeva, Warren M. Grill, Victor Pikov, Bryan McLaughlin, Pankaj Pasricha, Douglas Weber, Kip Ludwig, and Kristoffer Famm. 2014. "Bioelectronic Medicines: A Research Roadmap." *Nature Reviews Drug Discovery* 13 (6): 399–400. https://doi.org/10.1038/nrd4351.

Blak, B. T., H. T. Smith, M. Hards, A. Maguire, and V. Gimeno. 2012. "A Retrospective Database Study of Insulin Initiation in Patients with Type 2 Diabetes in UK Primary Care." *Diabetic Medicine* 29: e191–98. https://doi.org/10.1111/j.1464-5491.2012.03694.x.

Borovikova, L V, S Ivanova, M Zhang, H Yang, G I Botchkina, L R Watkins, H Wang, N Abumrad, J W Eaton, and K J Tracey. 2000. "Vagus Nerve Stimulation Attenuates the Systemic Inflammatory Response to Endotoxin." *Nature* 405 (6785): 458–62. https://doi.org/10.1038/35013070.

Browning, Kirsteen N., Simon Verheijden, and Guy E. Boeckxstaens. 2017. "The Vagus Nerve in Appetite Regulation, Mood, and Intestinal Inflammation." *Gastroenterology* 152 (4): 730–44. https://doi.org/10.1053/j.gastro.2016.10.046.

Byun, Donghak, Sung Joon Cho, Byeong Han Lee, Joongkee Min, Jong Hyun Lee, and Sohee Kim. 2017. "Recording Nerve Signals in Canine Sciatic Nerves with a Flexible Penetrating Microelectrode Array." *Journal of Neural Engineering* 14 (4). https://doi.org/10.1088/1741-

2552/aa7493.

Carli, F., G. Ronzoni, J. Webster, K. Khan, and M. Elia. 1993. "The Independent Metabolic Effects of Halo Thane and Isoflurane Anaesthesia." *Acta Anaesthesiologica Scandinavica* 37: 672–78. https://doi.org/10.1111/j.1399-6576.1993.tb03787.x.

Centers for Disease Control and Prevention. 2020. "National Diabetes Statistics Report 2020." *Centers for Disease Control and Prevention (CDC).*

Chambers, Adam P., Lene Jessen, Karen K. Ryan, Stephanie Sisley, Hilary E. Wilsonp??rez, Margaret a. Stefater, Shrawan G. Gaitonde, et al. 2011. "Weight-Independent Changes in Blood Glucose Homeostasis after Gastric Bypass or Vertical Sleeve Gastrectomy in Rats." *Gastroenterology* 141 (3): 950–58. https://doi.org/10.1053/j.gastro.2011.05.050.

Chan, Barbara P., Irene E. Kochevar, and Robert W. Redmond. 2002. "Enhancement of Porcine Skin Graft Adherence Using a Light-Activated Process." *Journal of Surgical Research* 108 (1): 77–84. https://doi.org/10.1006/jsre.2002.6516.

Chang, Rui B., David E. Strochlic, Erika K. Williams, Benjamin D. Umans, and Stephen D. Liberles. 2015. "Vagal Sensory Neuron Subtypes That Differentially Control Breathing." *Cell* 161 (3): 622–33. https://doi.org/10.1016/j.cell.2015.03.022.

Chatterjee, Sudesna, and Melanie J Davies. 2015. "Current Management of Diabetes Mellitus and Future Directions in Care." *Postgraduate Medical Journal* 91: 612–21. https://doi.org/10.1136/postgradmedj-2014-133200.

Chaure, Fernando J., Hernan G. Rey, and Rodrigo Quian Quiroga. 2018. "A Novel and Fully Automatic Spike-Sorting Implementation with Variable Number of Features." *Journal of Neurophysiology* 120 (4): 1859–71. https://doi.org/10.1152/jn.00339.2018.

Chhabra, Kavaljit H., Jessica M. Adams, Brian Fagel, Daniel D. Lam, Nathan Qi, Marcelo Rubinstein, and Malcolm J. Low. 2016. "Hypothalamic POMC Deficiency Improves Glucose Tolerance despite Insulin Resistance by Increasing Glycosuria." *Diabetes* 65: 660–72. https://doi.org/10.2337/db15-0804.

Chhabra, Kavaljit H., Donald A. Morgan, Benjamin P. Tooke, Jessica M. Adams, Kamal Rahmouni, and Malcolm J. Low. 2017. "Reduced Renal Sympathetic Nerve Activity Contributes to Elevated Glycosuria and Improved Glucose Tolerance in Hypothalamus-Specific Pomc Knockout Mice." *Molecular Metabolism*, 1–12. https://doi.org/10.1016/j.molmet.2017.07.005.

Chinushi, M., D. Izumi, K. Iijima, K. Suzuki, H. Furushima, O. Saitoh, Y. Furuta, Y. Aizawa, and M. Iwafuchi. 2013. "Blood Pressure and Autonomic Responses to Electrical Stimulation of the Renal Arterial Nerves Before and After Ablation of the Renal Artery." *Hypertension* 61: 450–56. https://doi.org/10.1161/HYPERTENSIONAHA.111.00095.

Cho, N. H., J. E. Shaw, S. Karuranga, Y. Huang, J. D. da Rocha Fernandes, A. W. Ohlrogge, and B. Malanda. 2018. "IDF Diabetes Atlas: Global Estimates of Diabetes Prevalence for 2017

and Projections for 2045." *Diabetes Research and Clinical Practice* 138: 271–81. https://doi.org/10.1016/j.diabres.2018.02.023.

Dawson, Jesse, David Pierce, Anand Dixit, Teresa J. Kimberley, Michele Robertson, Brent Tarver, Omar Hilmi, et al. 2016. "Safety, Feasibility, and Efficacy of Vagus Nerve Stimulation Paired with Upper-Limb Rehabilitation after Ischemic Stroke." *Stroke* 47 (1): 143–50. https://doi.org/10.1161/STROKEAHA.115.010477.

DeFronzo, R. A., J. A. Davidson, and S. Del Prato. 2012. "The Role of the Kidneys in Glucose Homeostasis: A New Path towards Normalizing Glycaemia." *Diabetes, Obesity and Metabolism* 14: 5–14. https://doi.org/10.1111/j.1463-1326.2011.01511.x.

DiBona, G F. 2000. "Neural Control of the Kidney: Functionally Specific Renal Sympathetic Nerve Fibers." *Am J Physiol Regulatory Integrative Comp Physiol* 279: R1517–24.

DiBona, G F, and U C Kopp. 1997. "Neural Control of Renal Function." *Physiological Reviews* 77 (1): 75–197.

DiBona, G F, and L L Sawin. 1982. "Effect of Renal Nerve Stimulation on NaCl and H_2O Transport in Henle's Loop of the Rat." *American Journal of Physiology* 243: F576–80.

DiBona, G F, L L Sawin, and S Y Jones. 1996. "Differentiated Sympathetic Neural Control of the Kidney." *American Journal of Physiology* 271: R84–90.

Donovan, Casey M., and Alan G. Watts. 2014. "Peripheral and Central Glucose Sensing In Hypoglycemic Detection." *Physiology* 29 (5): 314–24. https://doi.org/10.1152/physiol.00069.2013.

Elliott, Lisa, Carrie Fidler, Andrea Ditchfield, and Trine Stissing. 2016. "Hypoglycemia Event Rates: A Comparison Between Real-World Data and Randomized Controlled Trial Populations in Insulin-Treated Diabetes." *Diabetes Therapy* 7 (1): 45–60. https://doi.org/10.1007/s13300-016-0157-z.

Esler, Murray D., Henry Krum, Markus Schlaich, Roland E. Schmieder, Michael Böhm, and Paul A. Sobotka. 2012. "Renal Sympathetic Denervation for Treatment of Drug-Resistant Hypertension: One-Year Results from the Symplicity Htn-2 Randomized, Controlled Trial." *Circulation* 126 (25): 2976–82. https://doi.org/10.1161/CIRCULATIONAHA.112.130880.

Esler, Murray D., Henry Krum, Paul A. Sobotka, Markus P. Schlaich, Roland E. Schmieder, Michael Böhm, Felix Mahfoud, et al. 2010. "Renal Sympathetic Denervation in Patients with Treatment-Resistant Hypertension (The Symplicity HTN-2 Trial): A Randomised Controlled Trial." *The Lancet* 376: 1903–9. https://doi.org/10.1016/S0140-6736(10)62039-9.

Evans, D. H. L., and J. G. Murray. 1954. "Histological and Functional Studies on the Fibre Composition of the Vagus Nerve of the Rabbit." *Journal of Anatomy* 88: 320–37. http://www.ncbi.nlm.nih.gov/pubmed/13192020%0Ahttp://www.pubmedcentral.nih.gov/articlerender.fcgi?artid=PMC1244678.

Fairbairn, Neil G., Joanna Ng-Glazier, Amanda M. Meppelink, Mark A. Randolph, Ian L. Valerio, Mark E. Fleming, Jonathan M. Winograd, and Robert W. Redmond. 2015. "Light-Activated Sealing of Nerve Graft Coaptation Sites Improves Outcome Following Large Gap Peripheral Nerve Injury." *Plastic and Reconstructive Surgery* 136 (4): 739–50. https://doi.org/10.1097/PRS.0000000000001617.

Famm, Kristoffer, Brian Litt, Kevin J. Tracey, Edward S. Boyden, and Moncef Slaoui. 2013. "A Jump-Start for Electroceuticals." *Nature* 496: 159–61.

Foley, J. O., and F. S. DuBois. 1937. "Quantitative Studies of the Vagus Nerve in the Cat. I. The Ratio of Sensory to Motor Fibers." *Journal of Comparative Neurology* 67 (1). https://doi.org/10.1097/00005053-193711000-00019.

Forbes, Josephine M, and Mark E Cooper. 2013. "Mechanisms of Diabetic Complications." *Physiological Reviews* 93 (1): 137–88. https://doi.org/10.1152/physrev.00045.2011.

Gabella, Giorgio, and Hilary L. Pease. 1973. "Number of Axons in the Abdominal Vagus of the Rat." *Brain Research* 58 (2): 465–69. https://doi.org/10.1016/0006-8993(73)90015-2.

Gal, P, M R de Jong, J J J Smit, A Adiyaman, J a Staessen, and A Elvan. 2015. "Blood Pressure Response to Renal Nerve Stimulation in Patients Undergoing Renal Denervation: A Feasibility Study." *Journal of Human Hypertension* 29: 292–95. https://doi.org/10.1038/jhh.2014.91.

Garai, Purbasha, Ryan G.L. Koh, Martin Schuettler, Thomas Stieglitz, and Jose Zariffa. 2017. "Influence of Anatomical Detail and Tissue Conductivity Variations in Simulations of Multi-Contact Nerve Cuff Recordings." *IEEE Transactions on Neural Systems and Rehabilitation Engineering* 25 (9): 1653–62. https://doi.org/10.1109/TNSRE.2016.2633005.

García-Pérez, Luis-Emilio, María Alvarez, Tatiana Dilla, Vicente Gil-Guillén, and Domingo Orozco-Beltrán. 2013. "Adherence to Therapies in Patients with Type 2 Diabetes." *Diabetes Therapy* 4: 175–94. https://doi.org/10.1007/s13300-013-0034-y.

Gattone, V H, C F Marfurt, and S Dallie. 1986. "Extrinsic Innervation of the Rat Kidney: A Retrograde Tracing Study." *The American Journal of Physiology* 250 (2 Pt 2): F189-96. http://www.ncbi.nlm.nih.gov/pubmed/3753828.

Gaunt, Robert A., and Arthur Prochazka. 2006. *Control of Urinary Bladder Function with Devices: Successes and Failures*. *Progress in Brain Research*. Vol. 152. https://doi.org/10.1016/S0079-6123(05)52011-9.

Gillis, Winthrop F., Charles A. Lissandrello, Jun Shen, Ben W. Pearre, Alket Mertiri, Felix Deku, Stuart Cogan, et al. 2018. "Carbon Fiber on Polyimide Ultra-Microelectrodes." *Journal of Neural Engineering* 15 (1). https://doi.org/10.1088/1741-2552/aa8c88.

Goldstein, David S., David Robertson, Murray Esler, Stephen E. Straus, and Graeme Eisenhofer. 2002. "Dysautonomias: Clinical Disorders of the Autonomic Nervous System." *Annals of Internal Medicine* 137 (9): 753–63. https://doi.org/10.7326/0003-4819-137-9-200211050-

00011.

González-González, María A., Aswini Kanneganti, Alexandra Joshi-Imre, Ana G. Hernandez-Reynoso, Geetanjali Bendale, Romil Modi, Melanie Ecker, et al. 2018. "Thin Film Multi-Electrode Softening Cuffs for Selective Neuromodulation." *Scientific Reports* 8 (1): 1–15. https://doi.org/10.1038/s41598-018-34566-6.

Greene, E. R., M. D. Venters, P. S. Avasthi, R. L. Conn, and R. W. Jahnke. 1981. "Noninvasive Characterization of Renal Artery Blood Flow." *Kidney International* 20: 523–29.

Grempler, R., L. Thomas, M. Eckhardt, F. Himmelsbach, A. Sauer, D. E. Sharp, R. A. Bakker, M. Mark, T. Klein, and P. Eickelmann. 2012. "Empagliflozin, a Novel Selective Sodium Glucose Cotransporter-2 (SGLT-2) Inhibitor: Characterisation and Comparison with Other SGLT-2 Inhibitors." *Diabetes, Obesity and Metabolism* 14 (1): 83–90. https://doi.org/10.1111/j.1463-1326.2011.01517.x.

Groat, William C de, Derek Griffiths, and Naoki Yoshimura. 2015. "Neural Control of the Lower Urinary Tract." Edited by Ronald Terjung. *Comprehensive Physiology* 5 (January): 327–96. https://doi.org/10.1002/cphy.c130056.

Hanein, Y., C. G.J. Schabmueller, G. Holman, P. Lücke, D. D. Denton, and K. F. Böhringer. 2003. "High-Aspect Ratio Submicrometer Needles for Intracellular Applications." *Journal of Micromechanics and Microengineering* 13 (4). https://doi.org/10.1088/0960-1317/13/4/315.

Hao, Zheng, R. Leigh Townsend, Michael B. Mumphrey, Laurel M. Patterson, Jianping Ye, and Hans Rudolf Berthoud. 2014. "Vagal Innervation of Intestine Contributes to Weight Loss After Roux-En-Y Gastric Bypass Surgery in Rats." *Obesity Surgery* 24 (12): 2145–51. https://doi.org/10.1007/s11695-014-1338-3.

Harjutsalo, Valma, Lena Sjöberg, and Jaakko Tuomilehto. 2008. "Time Trends in the Incidence of Type 1 Diabetes in Finnish Children: A Cohort Study." *The Lancet* 371 (9626): 1777–82. https://doi.org/10.1016/S0140-6736(08)60765-5.

Henry, Robert R., Robert Chilton, and W. Timothy Garvey. 2013. "New Options for the Treatment of Obesity and Type 2 Diabetes Mellitus (Narrative Review)." *Journal of Diabetes and Its Complications* 27 (5): 508–18. https://doi.org/10.1016/j.jdiacomp.2013.04.011.

Henze, Darrell A., Zsolt Borhegyi, Jozsef Csicsvari, Akira Mamiya, Kenneth D. Harris, and György Buzsáki. 2000. "Intracellular Features Predicted by Extracellular Recordings in the Hippocampus in Vivo." *Journal of Neurophysiology* 84 (1): 390–400. https://doi.org/10.1152/jn.2000.84.1.390.

Hermansson, K, M Larson, O Källskog, and M Wolgast. 1981. "Influence of Renal Nerve Activity on Arteriolar Resistance, Ultrafiltration Dynamics and Fluid Reabsorption." *Pflugers Archiv* 389: 85–90.

Herrera, Miguel F, James Toouli, Bård Kulseng, Roy Brancatisano, Lilian Kow, Juan P Pantoja, Gjermund Johnsen, et al. 2017. "Vagal Nerve Block for Improvements in Glycemic Control in Obese Patients with Type 2 Diabetes Mellitus: Three-Year Results of the VBLOC DM2 Study." *Journal of Diabetes and Obesity* 4 (1): 1–6.

Hoerger, TJ, JE Segel, and EW Gregg. 2008. "Is Glycemic Control Improving in U.S.?" *Diabetes Care* 31 (1). https://doi.org/10.2337/dc07-1572.The.

Hoffman, Henry Harland, and Harold Norman Schnitzlein. 1961. "The Numbers of Nerve Fibers in the Vagus Nerve of Man." *The Anatomical Record* 139 (3): 429–35. https://doi.org/10.1002/ar.1091390312.

Horbach, T., G. Meyer, S. Morales-Conde, I. Alarcón, F. Favretti, M. Anselmino, G. M. Rovera, et al. 2016. "Closed-Loop Gastric Electrical Stimulation versus Laparoscopic Adjustable Gastric Band for the Treatment of Obesity: A Randomized 12-Month Multicenter Study." *International Journal of Obesity* 40 (12): 1891–98. https://doi.org/10.1038/ijo.2016.159.

Huang, Feng, Jianxun Dong, Jian Kong, Hongcai Wang, Hong Meng, Rosa B. Spaeth, Stephanie Camhi, et al. 2016. "Effect of Transcutaneous Auricular Vagus Nerve Stimulation on Impaired Glucose Tolerance: A Pilot Randomized Study." *BMC Complementary and Alternative Medicine* 16 (1): 1–8. https://doi.org/10.1186/s12906-016-1190-1.

Huard, Chad M., Saravanapriyan Sriraman, Alex Paterson, and Mark J. Kushner. 2018. "Transient Behavior in Quasi-Atomic Layer Etching of Silicon Dioxide and Silicon Nitride in Fluorocarbon Plasmas." *Journal of Vacuum Science & Technology A* 36 (6): 06B101. https://doi.org/10.1116/1.5049225.

Ikramuddin, Sayeed, Robin P. Blackstone, Anthony Brancatisano, James Toouli, Sajani N. Shah, Bruce M. Wolfe, Ken Fujioka, et al. 2014. "Effect of Reversible Intermittent Intra-Abdominal Vagal Nerve Blockade on Morbid Obesity: The ReCharge Randomized Clinical Trial." *Jama* 312: 915–22. https://doi.org/10.1001/jama.2014.10540.

Inzucchi, Silvio E., Richard M. Bergenstal, John B. Buse, Michaela Diamant, Ele Ferrannini, Michael Nauck, Anne L. Peters, et al. 2012. "Management of Hyperglycemia in Type 2 Diabetes: A Patient-Centered Approach: Position Statement of the American Diabetes Association (ADA) and the European Association for the Study of Diabetes (EASD)." *Diabetes Care* 35 (6): 1364–79. https://doi.org/10.2337/dc12-0413.

Ionescu, E., F. Rohner-Jeanrenaud, H. R. Berthoud, and B. Jeanrenaud. 1983. "Increases in Plasma Insulin Levels in Response to Electrical Stimulation of the Dorsal Motor Nucleus of the Vagus Nerve." *Endocrinology* 112 (3): 904–10. https://doi.org/10.1210/endo-112-3-904.

Iyer, Malini S., Richard N. Bergman, Jeremy E. Korman, Orison O. Woolcott, Morvarid Kabir, Ronald G. Victor, Deborah J. Clegg, and Cathryn Kolka. 2016. "Renal Denervation Reverses Hepatic Insulin Resistance Induced by High-Fat Diet." *Diabetes* 65: 3453–63. https://doi.org/10.2337/db16-0698.

Jackson, Mark R. 2001. "Fibrin Sealants in Surgical Practice: An Overview." *American Journal*

of Surgery 182 (2 SUPPL. 1). https://doi.org/10.1016/S0002-9610(01)00770-X.

Jansen, A. S.P., J. L. Hoffman, and A. D. Loewy. 1997. "CNS Sites Involved in Sympathetic and Parasympathetic Control of the Pancreas: A Viral Tracing Study." *Brain Research* 766 (1–2): 29–38. https://doi.org/10.1016/S0006-8993(97)00532-5.

Jiman, Ahmad A., Kavaljit H. Chhabra, Alfor G. Lewis, Paul S. Cederna, Randy J. Seeley, Malcolm J. Low, and Tim M. Bruns. 2018. "Electrical Stimulation of Renal Nerves for Modulating Urine Glucose Excretion in Rats." *Bioelectronic Medicine* 4 (7). https://doi.org/10.1186/s42234-018-0008-5.

Jiman, Ahmad A, Kavaljit H Chhabra, David C Ratze, Alfor G Lewis, Paul S Cederna, Randy J Seeley, Malcolm J Low, and Tim M Bruns. 2019. "Kilohertz Frequency Stimulation of Renal Nerves for Modulating Blood Glucose Concentration in Diabetic Rats." *Proceedings of the 9th International IEEE EMBS Conference on Neural Engineering*, 746–49. https://ieeexplore.ieee.org/document/8717153.

Johnson, Mark. 2014. "Transcutaneous Electrical Nerve Stimulation: Review of Effectiveness." *Nursing Standard* 28 (40): 44-53 10p. https://doi.org/10.7748/ns.28.40.44.e8565.

Jones, Russell L. 1937. "Cell Fiber Ratios in the Vagus Nerve." *Journal of Comparative Neurology* 67 (3): 469–82.

Joost, Has-Georg, and Hadi Al-Hasani. 2012. *Animal Models in Diabetes Research*. Edited by Hans-Georg Joost, Hadi Al-Hasani, and Annette Schurmann. *Humana Press*. Humana Press. https://doi.org/10.1007/978-1-62703-068-7_10.

Joseph, Laveeta, and Robert J. Butera. 2009. "Unmyelinated Aplysia Nerves Exhibit a Nonmonotonic Blocking Response to High-Frequency Stimulation." *IEEE Transactions on Neural Systems and Rehabilitation Engineering* 17 (6): 537–44. https://doi.org/10.1109/TNSRE.2009.2029490.

———. 2011. "High-Frequency Stimulation Selectively Blocks Different Types of Fibers in Frog Sciatic Nerve." *IEEE Transactions on Neural Systems and Rehabilitation Engineering* 19 (5): 550–57. https://doi.org/10.1109/TNSRE.2011.2163082.

Kahn, Steven E, Ronald L Prigeon, David K Mcculloch, Edward J Boyko, Richard N Bergman, Michael W Schwartz, James L Neifing, et al. 1993. "Quantification of the Relationship Between Insulin Sensitiyity and P-Cell Function in Human Subjects Evidence for a Hyperbolic Function with a Regulated Feedback Loop Control System Such That for Any Difference in S, a Proportionate Reciprocal Difference." *Diabetes* 42 (11): 1663–72.

Kajekar, Radhika, David Proud, Allen C. Myers, Sonya N. Meeker, and Bradley J. Undem. 1999. "Characterization of Vagal Afferent Subtypes Stimulated by Bradykinin in Guinea Pig Trachea." *Journal of Pharmacology and Experimental Therapeutics* 289 (2): 682–87.

Khunti, Kamlesh, Michael Wolden, Brian Larsen Thorsted, Marc Andersen, and Melanie J. Davies. 2013. "Clinical Inertia in People with Type 2 Diabetes." *Diabetes Care* 36: 3411–

17.

Kilgore, Kevin L., and Niloy Bhadra. 2014. "Reversible Nerve Conduction Block Using Kilohertz Frequency Alternating Current." *Neuromodulation* 17: 242–55. https://doi.org/10.1111/ner.12100.

King, Aileen J F. 2012. "The Use of Animal Models in Diabetes Research." *British Journal of Pharmacology* 166 (3): 877–94. https://doi.org/10.1111/j.1476-5381.2012.01911.x.

Koopman, Frieda A., Sangeeta S. Chavan, Sanda Miljko, Simeon Grazio, Sekib Sokolovic, P. Richard Schuurman, Ashesh D. Mehta, et al. 2016. "Vagus Nerve Stimulation Inhibits Cytokine Production and Attenuates Disease Severity in Rheumatoid Arthritis." *Proceedings of the National Academy of Sciences of the United States of America* 113 (29): 8284–89. https://doi.org/10.1073/pnas.1605635113.

Kozai, TDY, NB Langhals, PR Patel, Xiaopei Deng, Huanan Zhang, Karen L Smith, Joerg Lahann, Nicholas A Kotov, and Daryl R Kipke. 2012. "Ultrasmall Implantable Composite Microelectrodes with Bioactive Surfaces for Chronic Neural Interfaces." *Nature Materials* 11 (12): 1065–73. https://doi.org/10.1038/nmat3468.

Krames, Elliot, P. Hunter Peckham, and Ali Rezai. 2009. *Neuromodulation*. 1st ed. Academic Press.

Krum, Henry, Markus Schlaich, Rob Whitbourn, Paul A. Sobotka, Jerzy Sadowski, Krzysztof Bartus, Boguslaw Kapelak, et al. 2009. "Catheter-Based Renal Sympathetic Denervation for Resistant Hypertension: A Multicentre Safety and Proof-of-Principle Cohort Study." *The Lancet* 373: 1275–81. https://doi.org/10.1016/S0140-6736(09)60566-3.

Kumar, Krishna, Rod S. Taylor, Line Jacques, Sam Eldabe, Mario Meglio, Joan Molet, Simon Thomson, et al. 2007. "Spinal Cord Stimulation versus Conventional Medical Management for Neuropathic Pain: A Multicentre Randomised Controlled Trial in Patients with Failed Back Surgery Syndrome." *Pain* 132 (1–2): 179–88. https://doi.org/10.1016/j.pain.2007.07.028.

Kushner, Mark J. 2009. "Hybrid Modelling of Low Temperature Plasmas for Fundamental Investigations and Equipment Design." *Journal of Physics D: Applied Physics* 42 (19). https://doi.org/10.1088/0022-3727/42/19/194013.

la Oliva, Natàlia de, Xavier Navarro, and Jaume del Valle. 2018. "Time Course Study of Long-Term Biocompatibility and Foreign Body Reaction to Intraneural Polyimide-Based Implants." *Journal of Biomedical Materials Research - Part A* 106 (3): 746–57. https://doi.org/10.1002/jbm.a.36274.

Larson, Christopher E., and Ellis Meng. 2019. "A Review for the Peripheral Nerve Interface Designer." *Journal of Neuroscience Methods* 332 (June 2019): 108523. https://doi.org/10.1016/j.jneumeth.2019.108523.

Lauto, Antonio, Damia Mawad, Matthew Barton, Sabine C. Piller, and Leonardo Longo. 2011.

"Chitosan Adhesive Films for Photochemical Tissue Bonding." *AIP Conference Proceedings* 1364: 87–93. https://doi.org/10.1063/1.3626916.

Lauto, Antonio, Marcus Stoodley, Matthew Barton, John W. Morley, David A. Mahns, Leonardo Longo, and Damia Mawad. 2012. "Fabrication and Application of Rose Bengal-Chitosan Films in Laser Tissue Repair." *Journal of Visualized Experiments*, no. 68: 1–5. https://doi.org/10.3791/4158.

Lebovitz, H., B. Ludvik, I. Yaniv, T. Schwartz, M. Zelewski, and D. Gutterman. 2015. "Treatment of Patients with Obese Type 2 Diabetes with Tantalus-DIAMOND® Gastric Electrical Stimulation: Normal Triglycerides Predict Durable Effects for at Least 3 Years." *Hormone and Metabolic Research* 47: 456–62. https://doi.org/10.1055/s-0035-1548944.

Lee, Sanghoon, Wendy Yen Xian Peh, Jiahui Wang, Fengyuan Yang, John S. Ho, Nitish V. Thakor, Shih-Cheng Yen, and Chengkuo Lee. 2017. "Toward Bioelectronic Medicine-Neuromodulation of Small Peripheral Nerves Using Flexible Neural Clip." *Advanced Science* 1700149: 1700149. https://doi.org/10.1002/advs.201700149.

Lew, Kelley Newlin, and Allison Wick. 2015. "Pharmacotherapy of Type 2 Diabetes Mellitus: Navigating Current and New Therapies." *MEDSURG Nursing* 24 (6).

Liang, Yin, Kenji Arakawa, Kiichiro Ueta, Yasuaki Matsushita, Chiaki Kuriyama, Tonya Martin, Fuyong Du, et al. 2012. "Effect of Canagliflozin on Renal Threshold for Glucose, Glycemia, and Body Weight in Normal and Diabetic Animal Models." *PLoS ONE* 7 (2): e30555. https://doi.org/10.1371/journal.pone.0030555.

López-Soldado, Iliana, Rebeca Fuentes-Romero, Jordi Duran, and Joan J. Guinovart. 2017. "Effects of Hepatic Glycogen on Food Intake and Glucose Homeostasis Are Mediated by the Vagus Nerve in Mice." *Diabetologia* 60 (6): 1076–83. https://doi.org/10.1007/s00125-017-4240-4.

Luff, Susan E., Sandra G. Hengstberger, Elspeth M. McLachlan, and W. P. Anderson. 1992. "Distribution of Sympathetic Neuroeffector Junctions in the Juxtaglomerular Region of the Rabbit Kidney." *Journal of the Autonomic Nervous System* 40: 239–54.

Madhavan, Malini, Christopher V. Desimone, Elisa Ebrille, Siva K. Mulpuru, Susan B. Mikell, Susan B. Johnson, Scott H. Suddendorf, et al. 2014. "Transvenous Stimulation of the Renal Sympathetic Nerves Increases Systemic Blood Pressure: A Potential New Treatment Option for Neurocardiogenic Syncope." *Journal of Cardiovascular Electrophysiology* 25: 1115–18. https://doi.org/10.1111/jce.12466.

Maeda, Seishi, Sachi Kuwahara-Otani, Koichi Tanaka, Tetsu Hayakawa, and Makoto Seki. 2014. "Origin of Efferent Fibers of the Renal Plexus in the Rat Autonomic Nervous System." *Journal of Veterinary Medical Science* 76 (5): 763–65. https://doi.org/10.1292/jvms.13-0617.

Mahfoud, Felix, Elazer R. Edelman, and Michael Böhm. 2014. "Catheter-Based Renal Denervation Is No Simple Matter: Lessons to Be Learned From Our Anatomy?" *Journal of*

the American College of Cardiology 64 (7): 644–46.
https://doi.org/10.1016/j.jacc.2014.05.037.

Mahfoud, Felix, M. Schlaich, I. Kindermann, C. Ukena, B. Cremers, M. C. Brandt, U. C. Hoppe, et al. 2011. "Effect of Renal Sympathetic Denervation on Glucose Metabolism in Patients With Resistant Hypertension: A Pilot Study." *Circulation* 123: 1940–46. https://doi.org/10.1161/CIRCULATIONAHA.110.991869.

Masi, Emily Battinelli, Todd Levy, Tea Tsaava, Chad E. Bouton, Kevin J. Tracey, Sangeeta S. Chavan, and Theodoros P. Zanos. 2019. "Identification of Hypoglycemia-Specific Neural Signals by Decoding Murine Vagus Nerve Activity." *Bioelectronic Medicine* 5 (9). https://doi.org/10.1073/pnas.1719083115.

Masi, Emily Battinelli, Sergio Iván Valdés-Ferrer, and Benjamin Ethan Steinberg. 2018. "The Vagus Neurometabolic Interface and Clinical Disease." *International Journal of Obesity* 42 (6): 1101–11. https://doi.org/10.1038/s41366-018-0086-1.

Mather, Amanda, and Carol Pollock. 2011. "Glucose Handling by the Kidney." *Kidney International* 79 ((Suppl 120)): S1–6. https://doi.org/10.1038/ki.2010.509.

Mathews, Kiran S., Heather A C Wark, David J. Warren, Michael B. Christensen, Nicholas F. Nolta, Patrick C. Cartwright, and Richard A. Normann. 2014. "Acute Monitoring of Genitourinary Function Using Intrafascicular Electrodes: Selective Pudendal Nerve Activity Corresponding to Bladder Filling, Bladder Fullness, and Genital Stimulation." *Urology* 84 (3): 722–29. https://doi.org/10.1016/j.urology.2014.05.021.

Mathias, Christopher J., and Roger Bannister. 2013. *Autonomic Failure: A Textbook of Clinical Disorders of the Autonomic Nervous System. Oxford University Press*. 5th ed.

Matous, Daniel, Otakar Jiravsky, Igor Nykl, and Marian Branny. 2015. "Effect of Renal Denervation on Glucose Metabolism after a 12 Month Follow-Up." *Biomedical Papers of the Medical Faculty of the University Palacky, Olomouc, Czechoslovakia* 159 (2): 246–50. https://doi.org/10.5507/bp.2015.030.

Matsuhisa, M, Y Yamasaki, Y Shiba, I Nakahara, a Kuroda, T Tomita, M Iida, et al. 2000. "Important Role of the Hepatic Vagus Nerve in Glucose Uptake and Production by the Liver." *Metabolism: Clinical and Experimental* 49 (1): 11–16. https://doi.org/10.1016/S0026-0495(00)90538-9.

Matthaei, Stephan, R. Bierwirth, a. Fritsche, B. Gallwitz, H. U. Häring, H. G. Joost, M. Kellerer, et al. 2009. "Medical Antihyperglycaemic Treatment of Type 2 Diabetes Mellitus : Update of the Evidence-Based Guideline of the German Diabetes Association." *Experimental and Clinical Endocrinology and Diabetes* 117 (9): 522–57. https://doi.org/10.1055/s-0029-1239559.

McAllen, Robin M, Anthony D Shafton, Bradford O Bratton, David Trevaks, and John B Furness. 2018. " Calibration of Thresholds for Functional Engagement of Vagal A, B and C Fiber Groups in Vivo ." *Bioelectronics in Medicine* 1 (1): 21–27.

https://doi.org/10.2217/bem-2017-0001.

McCallum, Grant A., Xiaohong Sui, Chen Qiu, Joseph Marmerstein, Yang Zheng, Thomas E. Eggers, Chuangang Hu, Liming Dai, and Dominique M. Durand. 2017. "Chronic Interfacing with the Autonomic Nervous System Using Carbon Nanotube (CNT) Yarn Electrodes." *Scientific Reports* 7 (1): 1–14. https://doi.org/10.1038/s41598-017-10639-w.

McCorry, Laurie Kelly. 2007. "Physiology of the Autonomic Nervous System." *American Journal of Pharmaceutical Education* 71 (4). https://doi.org/10.1111/j.1399-6576.1964.tb00252.x.

Micera, Silvestro, and Xavier Navarro. 2009. "Bidirectional Interfaces with the Peripheral Nervous System." *International Review of Neurobiology* 86 (09): 23–38. https://doi.org/10.1016/S0074-7742(09)86002-9.

Miki, Kenju, Atuko Kosho, and Yoshiaki Hayashida. 2002. "Method for Continuous Measurements of Renal Sympathetic Nerve Activity and Cardiovascular Function during Exercise in Rats." *Experimental Physiology* 87 (1): 33–39.

Mizuno, Kei, and Yoshiyuki Ueno. 2017. "Autonomic Nervous System and the Liver." *Hepatology Research* 47 (2): 160–65. https://doi.org/10.1111/hepr.12760.

Moffitt, Michael a, and Cameron C McIntyre. 2005. "Model-Based Analysis of Cortical Recording with Silicon Microelectrodes." *Clinical Neurophysiology : Official Journal of the International Federation of Clinical Neurophysiology* 116 (9): 2240–50. https://doi.org/10.1016/j.clinph.2005.05.018.

Mosala Nezhad, Zahra, Alain Poncelet, Laurent De Kerchove, Pierre Gianello, Caroline Fervaille, and Gebrine El Khoury. 2016. "Small Intestinal Submucosa Extracellular Matrix (CorMatrix®) in Cardiovascular Surgery: A Systematic Review." *Interactive Cardiovascular and Thoracic Surgery* 22 (6): 839–50. https://doi.org/10.1093/icvts/ivw020.

Muller, Jacqueline, and Luciano Barajas. 1972. "Electron Microscopic and Histochemical Evidence for a Tubular Innervation in the Renal Cortex of the Monkey." *J Ultrastructure Research* 41: 533–49.

Nathan, David M. 1993. "Long-Term Complications of Diabetes Mellitus." *The New England Journal of Medicine* 328 (23).

Niijima, Akira. 1983. "Glucose-Sensitive Afferent Nerve Fibers in the Liver and Their Role in Food Intake and Blood Glucose Regulation." *Journal of the Autonomic Nervous System* 9 (1): 207–20. https://doi.org/10.1016/0165-1838(83)90142-X.

———. 1989. "Neural Mechanisms in the Control of Blood Glucose Concentration." *American Institute of Nutrition*, no. January: 833–40.

Ouyang, Zhonghua, Zachariah J. Sperry, Nikolas D. Barrera, and Tim M. Bruns. 2019. "Real-Time Bladder Pressure Estimation for Closed-Loop Control in a Detrusor Overactivity

Model." *IEEE Transactions on Neural Systems and Rehabilitation Engineering* 27 (6): 1209–16. https://doi.org/10.1109/TNSRE.2019.2912374.

Paintal, A. S. 1965. "Effects of Temperature on Conduction in Single Vagal and Saphenous Myelinated Nerve Fibres of the Cat." *The Journal of Physiology* 180 (1): 20–49. https://doi.org/10.1113/jphysiol.1965.sp007687.

Pan, Tao, Jin-he Guo, and Gao-jun Teng. 2015. "Renal Denervation, A Potential Novel Treatment for Type 2 Diabetes Mellitus?" *Medicine* 94 (44). https://doi.org/10.1097/MD.0000000000001932.

Papatheodorou, Loukia K., Benjamin G. Williams, and Dean G. Sotereanos. 2015. "Preliminary Results of Recurrent Cubital Tunnel Syndrome Treated with Neurolysis and Porcine Extracellular Matrix Nerve Wrap." *Journal of Hand Surgery* 40 (5): 987–92. https://doi.org/10.1016/j.jhsa.2015.02.031.

Park, Gayoung, Hyun Joong Chung, Kwanghee Kim, Seon Ah Lim, Jiyoung Kim, Yun Soung Kim, Yuhao Liu, et al. 2014. "Immunologic and Tissue Biocompatibility of Flexible/Stretchable Electronics and Optoelectronics." *Advanced Healthcare Materials* 3 (4): 515–25. https://doi.org/10.1002/adhm.201300220.

Patel, Paras R, Kyounghwan Na, Huanan Zhang, Takashi D Y Kozai, Nicholas a Kotov, Euisik Yoon, and Cynthia a Chestek. 2015. "Insertion of Linear 8.4 μ m Diameter 16 Channel Carbon Fiber Electrode Arrays for Single Unit Recordings." *Journal of Neural Engineering* 12 (4): 046009. https://doi.org/10.1088/1741-2560/12/4/046009.

Patel, Paras R, Huanan Zhang, Matthew T Robbins, Justin B Nofar, Shaun P Marshall, Michael J Kobylarek, Takashi D Y Kozai, Nicholas A Kotov, and Cynthia A Chestek. 2016. "Chronic in Vivo Stability Assessment of Carbon Fiber Microelectrode Arrays." *Journal of Neural Engineering* 13 (6): 066002. https://doi.org/10.1088/1741-2560/13/6/066002.

Patel, Yogi A., and Robert J. Butera. 2015. "Differential Fiber-Specific Block of Nerve Conduction in Mammalian Peripheral Nerves Using Kilohertz Electrical Stimulation." *Journal of Neurophysiology* 113: 3923–29. https://doi.org/10.1152/jn.00529.2014.

Pavlov, Valentin A., and Kevin J. Tracey. 2019. "Bioelectronic Medicine: Updates, Challenges and Paths Forward." *Bioelectronic Medicine* 5 (1): 1–4. https://doi.org/10.1186/s42234-019-0018-y.

Phillips, R A, and P B Hamilton. 1948. "Effect of 20, 60 and 120 Minutes of Renal Iscemia on Glomerular and Tubular Function." *American Journal of Physiology* 152: 523–30.

Polonsky, William, and Robert Henry. 2016. "Poor Medication Adherence in Type 2 Diabetes: Recognizing the Scope of the Problem and Its Key Contributors." *Patient Preference and Adherence* 10 (July): 1299–1307. https://doi.org/10.2147/PPA.S106821.

Pontes, R B, R O Crajoinas, E E Nishi, E B Oliveira-Sales, A C Girardi, R R Campos, and C T Bergamaschi. 2015. "Renal Nerve Stimulation Leads to the Activation of the Na$^+$/H$^+$

Exchanger Isoform 3 via Angiotensin II Type I Receptor." *Am J Physiol Renal Physiol* 308: F848–56. https://doi.org/10.1152/ajprenal.00515.2014.

Powley, Terry L., James C. Prechtl, Edward A. Fox, and Hans Rudolf Berthoud. 1983. "Anatomical Considerations for Surgery of the Rat Abdominal Vagus: Distribution, Paraganglia and Regeneration." *Journal of the Autonomic Nervous System* 9 (1): 79–97. https://doi.org/10.1016/0165-1838(83)90133-9.

Prechtl, James C., and Terry L. Powley. 1990. "The Fiber Composition of the Abdominal Vagus of the Rat." *Anatomy and Embryology* 181 (2): 101–15. https://doi.org/10.1007/BF00198950.

Qing, Kurt Y., Kelsey M. Wasilczuk, Matthew P. Ward, Evan H. Phillips, Pavlos P. Vlachos, Craig J. Goergen, and Pedro P. Irazoqui. 2018. "B Fibers Are the Best Predictors of Cardiac Activity during Vagus Nerve Stimulation." *Bioelectronic Medicine* 4 (1): 5. https://doi.org/10.1186/s42234-018-0005-8.

Rafiq, Kazi, Yoshihide Fujisawa, Shamshad J. Sherajee, Asadur Rahman, Abu Sufiun, Hiroyuki Kobori, Hermann Koepsell, Masaki Mogi, Masatsugu Horiuchi, and Akira Nishiyama. 2015. "Role of the Renal Sympathetic Nerve in Renal Glucose Metabolism during the Development of Type 2 Diabetes in Rats." *Diabetologia* 58 (12): 2885–98. https://doi.org/10.1007/s00125-015-3771-9.

Ramachandran, Anup, Martin Schuettler, Natalia Lago, Thomas Doerge, Klaus Peter Koch, Xavier Navarro, Klaus Peter Hoffmann, and Thomas Stieglitz. 2006. "Design, in Vitro and in Vivo Assessment of a Multi-Channel Sieve Electrode with Integrated Multiplexer." *Journal of Neural Engineering* 3 (2): 114–24. https://doi.org/10.1088/1741-2560/3/2/005.

Rasminsky, Michael. 1973. "The Effects of Temperature on Conduction in Demyelinated Single Nerve Fibers." *Archives of Neurology* 28 (5): 287–92. https://doi.org/10.1001/archneur.1973.00490230023001.

Rey, Hernan Gonzalo, Carlos Pedreira, and Rodrigo Quian Quiroga. 2015. "Past, Present and Future of Spike Sorting Techniques." *Brain Research Bulletin* 119: 106–17. https://doi.org/10.1016/j.brainresbull.2015.04.007.

Sabaté, Eduardo. 2003. *Adherence to Long-Term Therapies: Evidence for Action*. *World Health Organization*. World Health Organization. https://doi.org/10.1016/S1474-5151(03)00091-4.

Sacramento, J.F., D.J. Chew, B.F. Melo, M. Donegá, W. Dopson, M.P. Guarino, A. Robinson, et al. 2018. "Bioelectronic Modulation of Carotid Sinus Nerve Activity in the Rat: A Potential Therapeutic Approach for Type 2 Diabetes." *Diabetologia* 61 (3): 700–710. https://doi.org/10.1007/s00125-017-4533-7.

Sakakura, Kenichi, Elena Ladich, Qi Cheng, Fumiyuki Otsuka, Kazuyuki Yahagi, David R. Fowler, Frank D. Kolodgie, Renu Virmani, and Michael Joner. 2014. "Anatomic Assessment of Sympathetic Peri-Arterial Renal Nerves in Man." *Journal of the American College of Cardiology* 64 (7): 635–43. https://doi.org/10.1016/j.jacc.2014.03.059.

Schindelin, Johannes, Ignacio Arganda-Carreras, Erwin Frise, Verena Kaynig, Mark Longair, Tobias Pietzsch, Stephan Preibisch, et al. 2012. "Fiji: An Open-Source Platform for Biological-Image Analysis." *Nature Methods* 9 (7): 676–82. https://doi.org/10.1038/nmeth.2019.

Seufert, Jochen. 2015. "SGLT2 Inhibitors - an Insulin-Independent Therapeutic Approach for Treatment of Type 2 Diabetes: Focus on Canagliflozin." *Diabetes, Metabolic Syndrome and Obesity: Targets and Therapy* 8: 543–54. https://doi.org/10.2147/DMSO.S90662.

Seymour, John P., and Daryl R. Kipke. 2007. "Neural Probe Design for Reduced Tissue Encapsulation in CNS." *Biomaterials* 28 (25): 3594–3607. https://doi.org/10.1016/j.biomaterials.2007.03.024.

Shikano, Yu, Yuya Nishimura, Toya Okonogi, Yuji Ikegaya, and Takuya Sasaki. 2019. "Vagus Nerve Spiking Activity Associated with Locomotion and Cortical Arousal States in a Freely Moving Rat." *European Journal of Neuroscience* 49 (10): 1298–1312. https://doi.org/10.1111/ejn.14275.

Shikora, S., J. Toouli, M. F. Herrera, B. Kulseng, H. Zulewski, R. Brancatisano, L. Kow, et al. 2013. "Vagal Blocking Improves Glycemic Control and Elevated Blood Pressure in Obese Subjects with Type 2 Diabetes Mellitus." *Journal of Obesity* 2013. https://doi.org/10.1155/2013/245683.

Shikora, S a, J Toouli, M F Herrera, B Kulseng, R Brancatisano, L Kow, J P Pantoja, et al. 2015. "Intermittent Vagal Nerve Block for Improvements in Obesity, Cardiovascular Risk Factors, and Glycemic Control in Patients with Type 2 Diabetes Mellitus: 2-Year Results of the VBLOC DM2 Study." *Obes Surg*. https://doi.org/10.1007/s11695-015-1914-1.

Shimazu, Takashi. 1967. "Glycogen Synthetase Activity in Liver : Regulation by the Autonomic Nerves." *American Association for the Advancement of Science* 156 (3779): 1256–57.

Shimazu, Takashi, and Aoi Fukuda. 1965. "Increased Activities of Glycogenolytic Enzymes in Liver after Splanchnic-Nerve Stimulation." *American Association for the Advancement of Science* 150 (3703): 1607–8.

Shrayyef, Muhammad Z., and John E. Gerich. 2010. "Normal Glucose Homeostasis." In *Principles of Diabetes Mellitus*, edited by L. Poretsky, 1–887. Springer. https://doi.org/10.1007/978-0-387-09841-8.

Silverman, Harold A, Andrew Stiegler, Téa Tsaava, Justin Newman, Benjamin E Steinberg, Emily Battinelli Masi, Sergio Robbiati, et al. 2018. "Standardization of Methods to Record Vagus Nerve Activity in Mice." *Bioelectronic Medicine* 4 (3): 1–13. https://doi.org/10.1186/s42234-018-0002-y.

Singhal, Pooja, Jennifer N. Rodriguez, Ward Small, Scott Eagleston, Judy Van De Water, Duncan J. Maitland, and Thomas S. Wilson. 2012. "Ultra Low Density and Highly Crosslinked Biocompatible Shape Memory Polyurethane Foams." *Journal of Polymer Science, Part B: Polymer Physics* 50 (10): 724–37. https://doi.org/10.1002/polb.23056.

Skovsted, Per, and Sanguan Sapthavichaikul. 1977. "The Effects of Isoflurane on Arterial Pressure, Pulse Rate, Autonomic Nervous Activity, and Barostatic Reflexes." *Canad. Anaesth. Soc. J.* 24 (3).

Sliow, Ashour, Zhi Ma, Gaetano Gargiulo, David Mahns, Damia Mawad, Paul Breen, Marcus Stoodley, et al. 2019. "Stimulation and Repair of Peripheral Nerves Using Bioadhesive Graft-Antenna." *Advanced Science* 6 (11). https://doi.org/10.1002/advs.201801212.

Sohtell, Morgan, Bertil Karlmark, and Hans Ulfendahl. 1983. "FITC-Inulin as a Kidney Tubule Marker in the Rat." *Acta Physiol Scand* 119: 313–16.

Soty, Maud, Amandine Gautier-Stein, Fabienne Rajas, and Gilles Mithieux. 2017. "Gut-Brain Glucose Signaling in Energy Homeostasis." *Cell Metabolism* 25 (6): 1231–42. https://doi.org/10.1016/j.cmet.2017.04.032.

Spearman, Benjamin S., Vidhi H. Desai, Sahba Mobini, Matthew D. McDermott, James B. Graham, Kevin J. Otto, Jack W. Judy, and Christine E. Schmidt. 2018. "Tissue-Engineered Peripheral Nerve Interfaces." *Advanced Functional Materials* 28: 1–18. https://doi.org/10.1002/adfm.201701713.

Spindler, Philipp, Katja Bohlmann, Hans Beatus Straub, Peter Vajkoczy, and Ulf Christoph Schneider. 2019. "Effects of Vagus Nerve Stimulation on Symptoms of Depression in Patients with Difficult-to-Treat Epilepsy." *Seizure* 69 (April): 77–79. https://doi.org/10.1016/j.seizure.2019.04.001.

Srinivasan, Akhil, John Tipton, Mayank Tahilramani, Adel Kharbouch, Eric Gaupp, Chao Song, Poornima Venkataraman, et al. 2016. "A Regenerative Microchannel Device for Recording Multiple Single-Unit Action Potentials in Awake, Ambulatory Animals." *European Journal of Neuroscience* 43 (3): 474–85. https://doi.org/10.1111/ejn.13080.

Stocker, Sean D, and Martin S Muntzel. 2013. "Recording Sympathetic Nerve Activity Chronically in Rats: Surgery Techniques, Assessment of Nerve Activity, and Quantification." *Am J Physiol Heart Circ Physiol* 305: H1407–16. https://doi.org/10.1152/ajpheart.00173.2013.

Taplin, Craig E., Maria E. Craig, Margaret Lloyd, Claire Taylor, Patricia Crock, Martin Silink, and Neville J. Howard. 2005. "The Rising Incidence of Childhood Type 1 Diabetes in New South Wales, 1990-2002." *Medical Journal of Australia* 183 (5): 243–46. https://doi.org/10.5694/j.1326-5377.2005.tb07028.x.

Thorens, B. 2011. "Brain Glucose Sensing and Neural Regulation of Insulin and Glucagon Secretion." *Diabetes, Obesity and Metabolism* 13 (SUPPL. 1): 82–88. https://doi.org/10.1111/j.1463-1326.2011.01453.x.

Tirone, Thomas A., and F. Charles Brunicardi. 2001. "Overview of Glucose Regulation." *World Journal of Surgery* 25 (4): 461–67. https://doi.org/10.1007/s002680020338.

Toto, Robert D. 1995. "Conventional Measurement of Renal Function Utilizing Serum

Creatinine, Creatinine Clearence, Inulin and Para-Aminohippuric Acid Clearance." *Current Opinion in Nephrology and Hypertension* 4: 505–9.

Tracey, Kevin J. 2014. "The Revolutionary Future of Bioelectronic Medicine." *Bioelectronic Medicine* 1 (1). https://doi.org/10.15424/bioelectronmed.2014.00001.

Tse, Raymond, and Jason H. Ko. 2012. "Nerve Glue for Upper Extremity Reconstruction." *Hand Clinics* 28 (4): 529–40. https://doi.org/10.1016/j.hcl.2012.08.006.

Verberne, Anthony J M, Azadeh Sabetghadam, and Willian S. Korim. 2014. "Neural Pathways That Control the Glucose Counterregulatory Response." *Frontiers in Neuroscience* 8 (8 FEB): 1–12. https://doi.org/10.3389/fnins.2014.00038.

Verloop, Willemien L., Wilko Spiering, Eva E. Vink, Martine M A Beeftink, Peter J. Blankestijn, Pieter A. Doevendans, and Michiel Voskuil. 2015. "Denervation of the Renal Arteries in Metabolic Syndrome: The DREAMS-Study." *Hypertension* 65 (4): 751–57. https://doi.org/10.1161/HYPERTENSIONAHA.114.04798.

Vliet, B N Van, M J Smith, and a C Guyton. 1991. "Time Course of Renal Responses to Greater Splanchnic Nerve Stimulation." *Am J Physiol* 260 ((Regulatory Integrative Comp. Physiol. 29)): R894–905.

Vu, Philip P., Zachary T. Irwin, Autumn J. Bullard, Shoshana W. Ambani, Ian C. Sando, Melanie G. Urbanchek, Paul S. Cederna, and Cynthia A. Chestek. 2018. "Closed-Loop Continuous Hand Control via Chronic Recording of Regenerative Peripheral Nerve Interfaces." *IEEE Transactions on Neural Systems and Rehabilitation Engineering* 26 (2): 515–26. https://doi.org/10.1109/TNSRE.2017.2772961.

Waataja, Jonathan J, Katherine S Tweden, and Christopher N Honda. 2011. "Effects of High-Frequency Alternating Current on Axonal Conduction through the Vagus Nerve." *Journal of Neural Engineering* 8 (5): 056013. https://doi.org/10.1088/1741-2560/8/5/056013.

Waise, T. M.Zaved, Helen J. Dranse, and Tony K.T. Lam. 2018. "The Metabolic Role of Vagal Afferent Innervation." *Nature Reviews Gastroenterology and Hepatology* 15 (10): 625–36. https://doi.org/10.1038/s41575-018-0062-1.

Wall, E. J., J. B. Massie, M. K. Kwan, B. L. Rydevik, R. R. Myers, and S. R. Garfin. 1992. "Experimental Stretch Neuropathy: Changes in Nerve Conduction under Tension." *Journal of Bone and Joint Surgery - Series B* 74 (1): 126–29. https://doi.org/10.1302/0301-620x.74b1.1732240.

Wallenius, V, and Almantas Maleckas. 2015. "Surgery in the Treatment of Type 2 Diabetes Mellitus." *Scandinavian Journal of Surgery* 104: 40–47. https://doi.org/10.1177/1457496914561140Surgery.

Wallia, Amisha, and Mark E Molitch. 2014. "Insulin Therapy for Type 2 Diabetes Mellitus." *JAMA, the Journal of the American Medical Association* 311 (22): 2315–25. https://doi.org/10.1001/jama.2014.5951.

Walter, S J, T Zewde, and D G Shirley. 1989. "The Effect of Anaesthesia and Standard Clearance Procedures on Renal Function in the Rat." *Q J Exp Physiol* 74: 805–12.

Ward, Matthew P., Kurt Y. Qing, Kevin J. Otto, Robert M. Worth, Simon W.M. John, and Pedro P. Irazoqui. 2015. "A Flexible Platform for Biofeedback-Driven Control and Personalization of Electrical Nerve Stimulation Therapy." *IEEE Transactions on Neural Systems and Rehabilitation Engineering* 23 (3): 475–84. https://doi.org/10.1109/TNSRE.2014.2351271.

Wark, H. A.C., R. Sharma, K. S. Mathews, E. Fernandez, J. Yoo, B. Christensen, P. Tresco, et al. 2013. "A New High-Density (25 Electrodes/Mm2) Penetrating Microelectrode Array for Recording and Stimulating Sub-Millimeter Neuroanatomical Structures." *Journal of Neural Engineering* 10 (4). https://doi.org/10.1088/1741-2560/10/4/045003.

Wark, H A C, K S Mathews, R A Normann, and E Fernandez. 2014. "Behavioral and Cellular Consequences of High-Electrode Count Utah Arrays Chronically Implanted in Rat Sciatic Nerve." *Journal of Neural Engineering* 11 (August). https://doi.org/10.1088/1741-2560/11/4/046027.

Watts, Alan G., and Casey M. Donovan. 2010. "Sweet Talk in the Brain: Glucosensing, Neural Networks, and Hypoglycemic Counterregulation." *Frontiers in Neuroendocrinology* 31 (1): 32–43. https://doi.org/10.1016/j.yfrne.2009.10.006.

Weerasuriya, A., R. A. Spangler, S. I. Rapoport, and R. E. Taylor. 1984. "AC Impedance of the Perineurium of the Frog Sciatic Nerve." *Biophysical Journal* 46 (2): 167–74. https://doi.org/10.1016/S0006-3495(84)84009-6.

Wei, Michael, Leslie Ong, Maree T. Smith, Fraser B. Ross, Katrina Schmid, Andrew J. Hoey, Darryl Burstow, and Lindsay Brown. 2003. "The Streptozotocin-Diabetic Rat as a Model of the Chronic Complications of Human Diabetes." *Heart Lung and Circulation* 12: 44–50. https://doi.org/10.1046/j.1444-2892.2003.00160.x.

Welle, Elissa J., Paras R. Patel, Joshua E. Woods, Artin Petrossians, Elena della Valle, Alexis Vega-Medina, Julianna M. Richie, Dawen Cai, James D. Weiland, and Cynthia A. Chestek. 2020. "Ultra-Small Carbon Fiber Electrode Recording Site Optimization and Improved in-Vivo Chronic Recording Yield." *Journal of Neural Engineering*.

Wilding, John P H. 2014. "The Role of the Kidneys in Glucose Homeostasis in Type 2 Diabetes: Clinical Implications and Therapeutic Significance through Sodium Glucose Co-Transporter 2 Inhibitors." *Metabolism: Clinical and Experimental* 63 (10): 1228–37. https://doi.org/10.1016/j.metabol.2014.06.018.

Witkowski, Adam, Aleksander Prejbisz, Elzbieta Florczak, Jacek Kądziela, Paweł Śliwiński, Przemysław Bieleń, Ilona Michałowska, et al. 2011. "Effects of Renal Sympathetic Denervation on Blood Pressure, Sleep Apnea Course, and Glycemic Control in Patients with Resistant Hypertension and Sleep Apnea." *Hypertension* 58: 559–65. https://doi.org/10.1161/HYPERTENSIONAHA.111.173799.

Woodbury, D M, and J W Woodbury. 1990. "Effects of Vagal Stimulation on Experimentally Induced Seizures in Rats." *Epilepsia* 31 ((Suppl 2)): S7–19.

World Health Organization. 2016. "Global Report on Diabetes." https://doi.org/ISBN 978 92 4 156525 7.

Wurth, S., M. Capogrosso, S. Raspopovic, J. Gandar, G. Federici, N. Kinany, A. Cutrone, et al. 2017. "Long-Term Usability and Bio-Integration of Polyimide-Based Intra-Neural Stimulating Electrodes." *Biomaterials* 122: 114–29. https://doi.org/10.1016/j.biomaterials.2017.01.014.

Yan, Dongxiao, Ahmad Jiman, David Ratze, Shuo Huang, Saman Parizi, Elissa Welle, Zhonghua Ouyang, et al. 2019. "Microneedle Penetrating Array with Axon-Sized Dimensions for Cuff-Less Peripheral Nerve Interfacing." *Proceedings of the 9th International IEEE EMBS Conference on Neural Engineering*, 827–30.

Yan, Liwei, Jian Qi, Shuang Zhu, Tao Lin, Xiang Zhou, and Xiao Lin Liu. 2017. "3D Micro CT Imaging of the Human Peripheral Nerve Fascicle." *International Journal of Clinical and Experimental Medicine* 10 (7): 10315–23.

Yao, Y., I. C. Fomison-Nurse, J. C. Harrison, R. J. Walker, G. Davis, and I. A. Sammut. 2014. "Chronic Bilateral Renal Denervation Attenuates Renal Injury in a Transgenic Rat Model of Diabetic Nephropathy." *AJP: Renal Physiology* 307 (3): F251–62. https://doi.org/10.1152/ajprenal.00578.2013.

Yi, Chun Xia, Susanne E. la Fleur, Eric Fliers, and Andries Kalsbeek. 2010. "The Role of the Autonomic Nervous Liver Innervation in the Control of Energy Metabolism." *Biochimica et Biophysica Acta - Molecular Basis of Disease* 1802 (4): 416–31. https://doi.org/10.1016/j.bbadis.2010.01.006.

Zanchetti, A., A. Stella, R. Golin, and S. Genovesi. 1984. "Neural Control of the Kidney - Are There Reno-Renal Reflexes?" *Clinical and Experimental Hypertension* 6: 275–86.

Zanos, Theodoros, Harold A Silverman, Todd Levy, Tea Tsaava, Emily Battinelli, Peter Lorraine, Jeffrey Ashe, Sangeeta S Chavan, Kevin J Tracey, and Chad Bouton. 2018. "Identification of Cytokine-Specific Sensory Neural Signals by Decoding Murine Vagus Nerve Activity." *Proceedings of the National Academy of Sciences*, in press. https://doi.org/10.1073/pnas.1719083115.